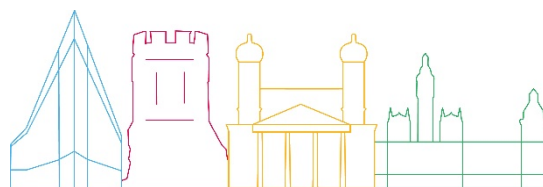




ARCH D4.1

Sensing and Repositories



Deliverable No.	D4.1
Work Package	WP4
Dissemination Level	PU
Author(s)	Artur Krukowski and Emmanouela Vogiatzaki (RFSAT)
Co-Author(s)	Antonio Costanzo, Fabrizia Buongiorno, Christian Bignami, Antonino D'Alessandro, Sergio Falcone, Massimo Musacchio, Malvina Silvestri, Giovanni Vitale (INGV), Michele Morici , Andrea Dall'Asta and Alessandro Zona (UNICAM), Sonia Giovinazzi (ENEA)
Contributor(s)	Quintilio Piattoni (Camerino) and Camerino Team
Due date	2021-05-31
Actual submission date	2021-07-02
Status	Final (post internal peer review)
Revision	1.0
Reviewed by	Katharina Milde and Daniel Lückerath (Fraunhofer) Emilio Servera (Las Naves)

This document has been prepared in the framework of the European project ARCH – Advancing Resilience of historic areas against Climate-related and other Hazards. This project has received funding from the European Union’s Horizon 2020 research and innovation programme under grant agreement no. 820999.

The sole responsibility for the content of this publication lies with the authors. It does not necessarily represent the opinion of the European Union. Neither the EASME nor the European Commission are responsible for any use that may be made of the information contained therein.

Contact

arch@iais.fraunhofer.de

www.savingculturalheritage.eu



This project has received funding from the European Union’s Horizon 2020 research and innovation programme under Grant Agreement no. 820999.

Executive Summary

This deliverable has been prepared for the European Commission-funded research project ARCH: Advancing Resilience of historic areas against Climate-related and other Hazards. It is the key output of task 4.1 “Sensing and Data Repositories” within work package 4 “Hazard & Object Information Management System”. The aim of Task 4.1 was the development and application of technological means for determining the current condition of heritage assets and for the characterization of historic areas. This document outlines the research and development concepts related to task 4.1, together comprising the overall repository of sensor data about heritage assets and their environmental conditions, ready for passing its data on the historic areas and hazards to the information management systems (task 4.2 and task 4.3).

The work describes in this deliverable focused on:

- the provision of a range of custom sensor deployments offering a variety of options for detecting weather/climatic conditions and air quality parameters that have direct potential effect on the level of degradation of heritage assets (HA), those being objects and structures, and historical areas when referring to sites. A range of wireless sensing solutions have been developed, ranging from collection of data of 3rd-party global-coverage weather services to custom sensors for local deployment at ARCH pilot sites. Furthermore, different Internet-of-Things (IoT) service options have been produced to ease the collection, processing and transmission of sensor information to the Threats and Hazards Information System (THIS) server deployed for ARCH.
- the development and implementation of technological systems for the structural monitoring of selected buildings that allow to assess static and their dynamic behaviour over time, specifically addressing the needs of Bratislava to monitor a bedrock under Devin castle, Camerino in assessing post-seismic damages to heritage assets as well as Hamburg long term damage caused by varying canal water levels to safety of structures around canals
- the development of a custom dense seismic monitoring network with low-cost sensors deployed on and around the hill where the historic centre of Camerino was edified
- the collection and processing of Earth Observation data providing climate and pollution data for all ARCH pilot areas required for assessing immediate and long-term risks:
 - 1) from middle-high resolution satellite images - optical, thermal, radar – to produce land use and land cover maps, information on the thermal situation and change detection
 - 2) from high-resolution Light Detection and Ranging (LiDAR) data to obtain digital elevation models of historic areas
 - 3) from low-resolution satellite data about climate and atmospheric conditions, both current and historic
- the collection of historic information about heritage assets, both constructions and objects, to characterize position, geometry, structural composition, materials, previous damages, and other information useful to support the assessment of the current state of heritage assets and historical area, thus applicable to ALL pilot sites in the ARCH project

Table of contents

Executive Summary	3
Table of contents.....	4
Table of Abbreviations.....	7
1. Introduction.....	10
1.1. Purpose of this report and relation to other deliverables.....	10
1.2. Gender statement	12
1.3. Structure of this report.....	12
2. Environmental Sensors.....	15
2.1. Relevance to end-user needs from ARCH pilot sites.....	15
2.2. Overview of the environmental monitoring system	16
2.1. On-Premise Weather / Climate and Air Quality Sensing.....	18
2.1.1. Libelium waspmotes and Meshlium IoT server.....	19
2.1.2. Analog Devices MVP based custom sensor node	22
2.1.3. Multi-gas based on M5Stack/M5Stick	23
2.1.4. Raspberry-PI based sensors with Turta IoT HATs.....	24
2.1.5. Mobile environmental sensors	26
2.2. Cloud and on-premise IoT Platform deployments.....	27
2.2.1. RFSAT repository on ThingSpeak cloud IoT platform.....	27
2.2.2. Thingier.io IoT platform	28
2.3. Open Data Platform Integration	29
2.3.1. NetAtmo WeatherMap.....	33
2.3.2. Environmental WEB service of the THIS server	34
2.3.3. Open WeatherMap.....	36
2.3.4. Air Quality Open Data.....	36
2.3.5. Air Pollution WEB service.....	37
2.4. Geometry (3D) scanning technologies.....	38
2.5. Common 3D model representation for ARCH	40
2.5.1. Long-Medium Range 3D Scanners (LiDAR).....	41
2.5.2. Overview of 3D Modelling Software	41
2.6. RFSAT implementation of automatic 3D scanning system	42
2.6.2. Communication interfaces	46
2.7. Autonomous 3D aerial scanning.....	53
2.7.1. Development and Test Conditions	58

2.7.2.	Features supported	59
2.7.3.	Planned future developments	59
2.8.	Multispectral surveillance technologies	60
2.8.1.	Experiments with land monitoring using UAVs	61
2.8.2.	3D Area Mapping	63
2.8.3.	Crops Conditions Estimation.....	63
2.9.	Conclusions	64
3.	Monitoring of heritage assets	66
3.1.	Seismic structural monitoring.....	69
3.1.1.	The Ducal Palace in Camerino	69
3.1.2.	The Santa Maria in Via Church in Camerino	75
3.1.3.	Monitoring system and preliminary dynamic characterization	78
3.2.	Analysis of the data collected via monitoring.....	82
3.2.1.	The Ducal Palace	82
3.2.2.	The Santa Maria in Via Church.....	83
4.	The Real-Time Urban Seismic Network.....	85
4.1.	The seismic station	86
4.1.1.	POWER	87
4.1.2.	UPS	87
4.1.3.	GPS	88
4.1.4.	SENSOR.....	88
4.1.5.	NETWORK.....	88
4.1.6.	SBC	88
4.2.	Software upgrade.....	88
4.2.1.	Native software structure.....	88
4.2.2.	Latest software updates.....	90
4.3.	LTE and SIM transmission equipment	91
4.4.	Installation scenarios.....	92
4.4.1.	Indoor installations with local connectivity and permanent electricity network	92
4.4.2.	Indoor installations without local connection and unstable power grid.....	93
4.4.3.	Outdoor installations in a cabin on the road	92
4.5.	Network and data acquisition.....	94
5.	Earth Observation Data	99
5.1.	Ground motion by interferometry	100
5.2.	Thermal maps and Heat Islands.....	103
5.2.1.	Methodology	104
5.2.2.	Comparison between LST and weather station.....	106

5.2.3. Urban Heat Islands.....	107
5.3. Land classification.....	108
5.3.1. Land cover classification.....	109
5.3.2. LULC by Copernicus Land Monitoring Service.....	113
5.4. Digital Elevation Models by LIDAR data.....	113
5.5. Copernicus Atmosphere Monitoring Service (CAMS) integration.....	115
5.5.1. MapUpload WEB service from INGV.....	118
5.6. Conclusions.....	119
6. Summary of outcomes.....	120
7. References.....	122
8. Annex.....	127
8.1. Installation report of the accelerometric stations of the RUSN.....	127
8.1.1. Accelerometric station CAM00.....	128
8.1.2. Accelerometric station CAM01.....	129
8.1.3. Accelerometric station CAM02.....	130
8.1.4. Accelerometric station CAM03.....	131
8.1.5. Accelerometric station CAM04.....	132
8.1.6. Accelerometric station CAM05.....	133
8.1.7. Accelerometric station CAM06.....	134
8.1.8. Accelerometric station CAM07.....	135
8.1.9. Accelerometric station CAM08.....	136
8.1.10. Accelerometric station CAM09.....	137
8.1.11. Accelerometric station CAM10.....	138
8.1.12. Accelerometric station CAM11.....	139
8.1.13. Accelerometric station CAM12.....	140
8.1.14. Accelerometric station CAM13.....	141

Table of Abbreviations

Abbreviation	Explanation
AC	Alternating Current
AD	Analog Devices
ADS	Atmospheric Data Store
API	Application Programming Interface
ASTER	Advanced Spaceborne Thermal Emission and Reflection Radiometer
C3S	Copernicus Climate Change Service
CAMS	Copernicus Atmospheric Monitoring Service
CDS	Climate Change Service
COTS	Commercial Off the Shelf
CSV	Comma Separated Values
DC	Direct Current
DSP	Digital Signal Processing
DSS	Decision Support System
DTM	Digital Terrain Model
ECOSTRESS	Ecosystem Spaceborne Thermal Radiometer Experiment on Space Station
EO	Earth Observation
GCC	Ground Control Centre
GNSS	Global Navigation Satellite System
GPRS	General Packet Radio Service
GPS	Global Positioning System
GSD	Ground Sampling Distance
GUI	Graphical User Interface
HA	Heritage Asset (Historic Area ?)
HAris	Historic Areas Information System

HDF	Hierarchical Data Format
InSAR	Interferometric Synthetic Aperture Radar
IP	Internet Protocol
JSON	JavaScript Object Notation
LiDAR	Light Detection and Ranging
LSE	Land Surface Emissivity
LST	Land Surface Temperature
LTE	Long-Term Evolution
LULC	Land Use and Land Cover
M2M	Machine to Machine
MEMS	Micro-Electro-Mechanical System
ML	Machine Learning
NDVI	Normalized Difference Vegetation Index
NO₂	Nitric Dioxide
NTP	Network Time Protocol
O₃	Ozone
OE	Open Edge
PCA	Principal Component Analysis
PM	Particulate Matter
PPS	Packets Per Second
PS	Phase Screen (correction technique)
RAM	Random Access Memory
ROM	Read Only Memory
REST	Representational State Transfer
RUSN	Real-time Urban Seismic Network
SAR	Synthetic Aperture Radar

SBC	Session Border Controller
SBC	Single Board Computer
SCA	Single-channel algorithms
SCP	Secure Copy Protocol
SD	Secure Digital (card)
SDK	Software Development Kit
SFTP	SSH File Transfer Protocol
SHM	Structural Health Monitoring
SIM	Subscriber Identification Module
SO₂	Sulphuric Dioxide
SSH	Secure Shell Protocol
SVM	Support Vector Machine (algorithm in Machine Learning)
SWIR	Short-Wave InfraRed
TCP/IP	Transmission Control Protocol (TCP) and Internet Protocol (IP)
TES	Temperature and Emissivity Separation
THIS	Threats and Hazard Information System
TIR	Thermal Infra-Red
UAV	Unmanned Aerial Vehicle
UAS	Unmanned Aerial System
UHI	Urban Heat Islands
UPS	Uninterruptable Power Supply
USB	Universal Serial Bus
USGS	United States Geological Survey
UTC	Coordinated Universal Time
VNIR	Visible and Near-Infra-Red
VPU	Vision Processing Unit

1. Introduction

This deliverable has been prepared for the European Commission-funded research project ARCH: Advancing Resilience of historic areas against Climate-related and other Hazards. ARCH will develop decision support tools and methodologies to improve the resilience of historic areas to climate change-related and other hazards. These tools and methodologies are developed with the pilot cities of Bratislava (Slovakia), Camerino (Italy), Hamburg (Germany), and Valencia (Spain), in a co-creative approach, including local policy makers, practitioners, and community members. The resulting solutions have been combined into a collaborative disaster risk management platform for guided resilience building, and including:

- information management system for relevant geo-referenced properties of historic areas
- information management system for geo-referenced data regarding hazards and risks relevant for historic areas
- Decision Support System (DSS) for risk and impact analysis of historic areas
- inventory of resilience building measures and appropriate financing sources
- visual planning tool for resilience pathways
- resilience assessment framework to identify resilience weak points and formulate resilience action plans

1.1. Purpose of this report and relation to other deliverables

This report (D4.1) is the accompanying document to the demonstrator for activity 4.1 "Data collection and storage" within Work Package 4 (WP4) "Hazard and Object Information Management System". The objectives of WP4 are the development and implementation of two information systems:

- Historic Areas Information System (HARIS) for archiving the properties of the heritage and the characteristics of the historic area as a whole, interacting with the surrounding urban and natural systems;
- Threats and Hazard Information System (THIS) to "combine" data from different sources to obtain measurable indicators to characterize the hazards that potentially affect the historic area and to collect historic and real-time data produced by climate services and / or through specific monitoring.

In the framework of WP4, datasets are structured and tools are developed to support:

- the DSS (WP5) in the production of hazard models and vulnerability analyses, with the main purpose of evaluating the impact scenarios and quantifying potential effects on the historic area and heritage assets, and consequently to support formulation and assessment of resilience measures;
- the ARCH Hub in giving end-users direct access to the datasets and information relevant to their historic area.

Accordingly, the contents of this document and the systems described therein are mainly linked to: (1) the technological solutions provided by WP4; (2) the needs arising from the co-creation processes with the cities and the technical partners; and (3) the consequent analyses performed by the other work packages.

Therefore, D4.1 is directly related to the following deliverables:

- **D3.4** Report on co-creating the information system
- **D4.2** Historic Area Information Management System (HArIS)
- **D4.3** Threats and Hazard Information Management System (THIS)
- **D5.1** Hazard models for impact assessment
- **D5.2** Handbook on heritage asset vulnerability
- **D7.4** Requirements description
- **D7.5** Interface specification and system architecture
- **D7.6** System design, realisation, and integration

The chart in **Figure 1** is a graphical representation of the interaction between D4.1 and the before mentioned deliverables with their related tasks.

It is worth pointing out that the developments described in this document support dynamic information systems and can themselves undergo improvements, so they can be updated even after their delivery. Likewise, any new datasets and information collected by technological systems within the ARCH project will feed the information systems, even if they are obtained after the drafting of this document.

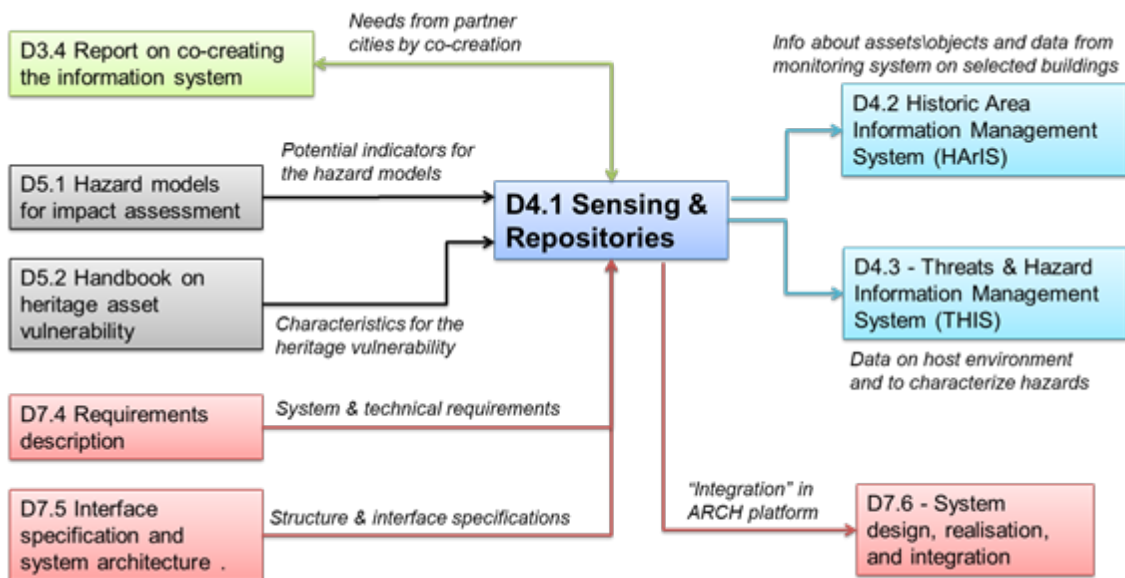


Figure 1: Representation of the main interactions between D4.1 and the other ARCH deliverables.

1.2. Gender statement

This document has been developed taking into consideration the guidance on gender in research provided in the *Project Handbook* (D1.2)¹ as well as State-of-the-Art report number 5 of deliverable D7.1² on “*Gender aspects in conservation and regulation of historic areas, disaster risk management, emergency protocols, post-disaster response techniques, and techniques for building back better*”.

1.3. Structure of this report

The report is divided in eight sections:

- Following this introduction, **Section 2** describes the custom sensor deployments for detecting weather/climatic conditions and air quality parameters, the wireless sensing solutions ranging from collection of data of 3rd-party to custom sensors, and the related IoT service options.
- **Section 3** reports on the design and installation of the structural and environmental sensors to monitor the behaviour of the selected constructions of CH.
- **Section 4** focuses on the technological development of low-cost Micro-Electro-Mechanical System (MEMS) seismic stations and their configuration to implement an accelerometric network. The server-side systems for the control and acquisition of data in real time are also illustrated.
- **Section 5** describes the system of controlling swarms of autonomously operating Unmanned Aerial Systems / Unmanned Aerial Vehicles (UAS/UAV) equipped with micro-sensors.
- **Section 6** gives an overview on the products obtained by processing of Earth Observation (EO) data to obtain: land use and land cover classification, thermal maps and urban heat Islands, digital elevation models and information about atmospheric conditions, including detection of changes to those.
- Finally, in **Section 7** the main findings related to task 4.1 are summarized.

Bibliographic references (**Section 8**) and annexes (**Section 9**) are reported at the end of the document.

In addition, surveys and monitoring systems, developed within the task 4.1, are summarized in Table 1.

¹ D. Lückerath, "ARCH D1.2 *Project Handbook*," H2020 ARCH, GA no. 820999, 2019.

² V. Rebollo, T. Rangil-Escribano and E. Chapman, “*ARCH D7.1 State-of-the-Art report no. 5: Gender aspects in conservation and regulation of historic areas, disaster risk management, emergency protocols, post-disaster response techniques, and techniques for building back better*,” H2020 ARCH, GA no. 820999, 2019.

Table 1: Surveys and monitoring systems, application sites and data storage\availability

Survey or Monitoring	Description	City or Laboratory	Purpose	Data storage	Data Availability
Weather/climatic monitoring	Monitoring of the environmental conditions (e.g. temperature, rain, humidity, wind) by means of crowd-sensing	All cities	Provide data in near real-time to characterize current situation and inform the users	THIS database managed by INGV (details in D4.3).	Data available via GIS web-service (details in D4.4)
Air quality monitoring	Monitoring of the pollutants combining data from crowd-sensing and official sensors (data provided by the European Environment Agency)	All cities	Provide data: (1) in near real-time to characterize current situation and inform the users; (2) in aggregate form to support analyses in WP5 (e.g. degradation materials)	THIS database managed by INGV (details in D4.3).	Data available via GIS web-service (details in D4.4).
Copernicus EO from CAMS (Atmospheric) service	Copernicus CAMS maps for the whole Earth and sensor values for ARCH pilot sites.	All cities	Large area air quality and climate data at 12hrs intervals (resolution of 0.125deg/pixel) for 60 available parameters	Local database managed by RFSAT with upload of all data to THIS by INGV (details in D4.3)	Data available via GIS web-service (details in D4.4).
Copernicus EO from C3S (Climate) service	Copernicus C3S maps for pilot cities	All cities	Large scale overview of climate conditions & temporal changes	THIS repository managed by INGV (details in D4.3).	Data available via GIS web-service (details in D4.4).
Structural and environmental monitoring	Monitoring by sensors deployed in ARCH project	Selected buildings in Camerino	Keep under control the structural behaviour of already damaged heritage assets, also taking into account influence due to the change of the environmental parameters, and inform the decision makers	Repository managed by UNICAM	Files downloadable (details in D4.4)

Survey or Monitoring	Description	City or Laboratory	Purpose	Data storage	Data Availability
Seismic monitoring (RUSN)	Monitoring by accelerometric network deployed in ARCH project	Camerino	Record ground motion in (and around) the historic areas at the occurrence of an moderate/severe earthquake and produce synthetic parameters to improve the impact scenario	THIS Repository managed by INGV	- Time-histories - Parameters (extracted in case of earthquake) available via GIS web-service (details in D4.4)
Unmanned Aerial Systems / Unmanned Aerial Vehicles (UAS/UAV) equipped with micro-sensors	Automated system for 3D scanning heritage assets and historical areas	Laboratory, currently self-contained with capability for integration with THIS	Automated 3D photogrammetric scanning of chosen areas and heritage assets for subsequent geometric erosion analysis	Local server at RFSAT, pending upload to THIS by INGV	3D models in FBX format, API available
Earth Observation surveys and service from CLMS	Surveys to characterize the sites by means of remote sensors (satellite and airborne)	InSAR – Hamburg and Valencia	Analyse any deformation process	THIS repository managed by INGV	Vector files via GIS web-service or downloadable (details in D4.4)
		Thermal maps – Bratislava and Valencia	Detect persistent differences of temperature and UHI	THIS repository managed by INGV	Vector and Raster files via GIS web-service or downloadable (details in D4.4)
		LULC – All cities	Classify large areas in terms of use/coverage or analyse the presence of a specific component in the area (e.g. water, vegetation)	HArIS service and repository managed by INGV	Raster files via GIS web-service or downloadable (details in D4.4)
		DEM – Bratislava, Camerino and Valencia	Produce 3D models	HArIS repository managed by INGV	Vector files downloadable (details in D4.4)

2. Environmental Sensors

This section describes the architecture design of the RFSAT contribution to THIS (Figure 2). The system combines acquisition of information about the environment (weather, climate and pollution) from variety of cloud participatory IoT networks complemented with custom developments of in-situ deployable (or fully mobile) sensors nodes, in response to expressed needs and requirements of end-users from ARCH pilot sites.

2.1. Relevance to end-user needs from ARCH pilot sites

The reference information and guidelines for developing environmental sensing subsystem has been from one side deliverable D7.4 providing focussed information about user requirements, while workshops with cities (initially physical and later depending on teleconferencing as the COVID outbreak has made local visits impossible). In all pilot cases end users requested Current and historical weather and climate information. since periodicity has varied among pilots, decision was made to provide such information as often as every half hour. Such information included standard data like temperature, humidity and pressure as ground level as well as info about wind (speed, direction and types) and rainfall (current and accumulated over different periods of time). In cases of Hamburg and Bratislava, where risks of floods and excessive water level changes were important, the latter data become an essential source of data for detection of various types of flood risks as part of HARIS.

Since large area coverage has become immediately indicated as essential factor, original focus on deployments of in-situ sensors has moved to collection of data from all available cloud 3rd-party data sources that offered large coverage areas, those including and not limited to European Environmental Agency (EEA), National Weather monitoring networks, private cloud Weathermap such as from NetAtmo and many others. Agents collecting data for ARCH pilot sites have been developed (described in section 2.3). Since coverage density was beyond ARCH control, custom sensors have been developed by RFSAT (described in section 2.1) to supplement data available at specific locations with local deployments at carefully selected locations. Ground level sensing has been further complemented with Earth Observation (EO) data to offer even larger scale view of the climate and environmental conditions beyond pilot areas to be able to easier determine inherent effects from conditions at more distant areas, such as sea level variations on water level changes in Hamburg or rainfalls in surrounding areas of Bratislava on floods in the city. Similarly, EO data offers an insight into climate changes causing draughts and floods in Valencia as well as possible influence on occurrence of earthquakes in Camerino.

An important factor to erosion of heritage assets as well as historical areas have been raising pollution levels and their monitoring has been indicated by all pilots as important source of data. Since the number of public and private cloud IoT networks offering pollution data beyond common SO₂, NO₂, CO and CO₂ have been very sparse, focus on EO originated data from CAMS service (offering over 60 types of parameters regularly every 12 hours with up to 5493³

³ CAMS sensor selection: <https://apps.ecmwf.int/codes/grib/param-db/?filter=All>

in total as off the 15th June 2021 as part of historical processed data via Copernicus Meteorological Archival and Retrieval System (MARS)⁴ this source of data has become one of the most important (in addition to EEA data that collects yearly reports from national authorities). Considering that both CAMS and EEA data do not offer localised (in-situ) coverage, work on custom sensors by RFSAT has become a necessity, leading to a variety of sensing approaches developed in the frame of ARCH project, which have been described in section 2. All of those offer a high level. of customisation in terms of pollution and weather sensing. Being generally highly integrated into a very small form factor, they are suitable equally for fixed in-situ deployment, attaching to micro-UAVs as well as for wearable and on-vehicle applications. They can be powered from mains, as well as using embedded and solar batteries, as required for any specific indoor or outdoor application.

2.2. Overview of the environmental monitoring system

From one side the system developed by RFSAT acquires relevant information from 3rd-party cloud services, such as Netatmo Weathermap⁵, Open Weathermap⁶, global natural disaster monitoring services and similar ones, for subsequent upload of processed data for each of the sites supported in ARCH to the THIS server deployed by INGV. On the other hand, in-situ deployed sensors (such as those described in Section 2) can offer supplementary monitoring data and information in areas not covered by pre-existing sensor networks. Although in the frame of ARCH only data for selected pilot sites are gathered and provided via THIS and HARiS, they can be flexibly extended to cover any other site and the whole Earth, if such a need arises.

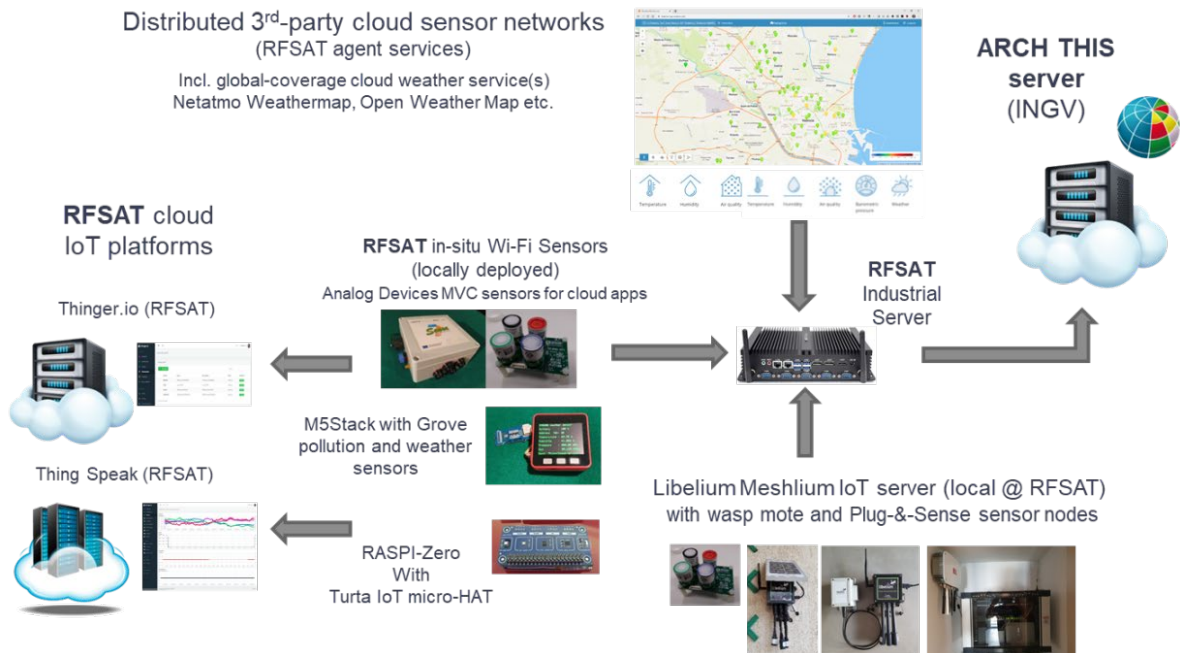


Figure 2: Concept architecture of the RFSAT IoT sensor acquisition and processing system

⁴ MARS: <https://confluence.ecmwf.int/display/COPSRV/EFAS+data+services>

⁵ NetAtmo Weathermap: <https://weathermap.netatmo.com/>

⁶ Open Weathermap: <https://openweathermap.org/>

For collection of sensor data from existing IoT cloud environmental sensor repositories, micro agents have been deployed on the RFSAT cloud server that gather and process only relevant (required) information from other IoT platforms for pre-defined geographical areas of interest (in case of ARCH the boundaries of pilot sites), which is then processed and, on the server, deployed at RFSAT offices and repackages into the format accepted by THIS platform. Additionally, the RFSAT server collates and combined sensor information from such cloud repositories with data coming from custom sensor deployed in-situ at each CH pilot site.

The physical architecture of the RFSAT sensor acquisition sub-system is shown in Figure 3. It indicates location and role of different components as well as servers deployed by RFSAT, both in the cloud and on premises. Notice the central role of the RFSAT Industrial server, deployed at RFSAT offices that performs both the collection of relevant sensor information from open-access 3rd-party sensor networks and servers dedicated to collection of specific sensor data from individual networks, intended to be deployed by RFSAT at CH sites.

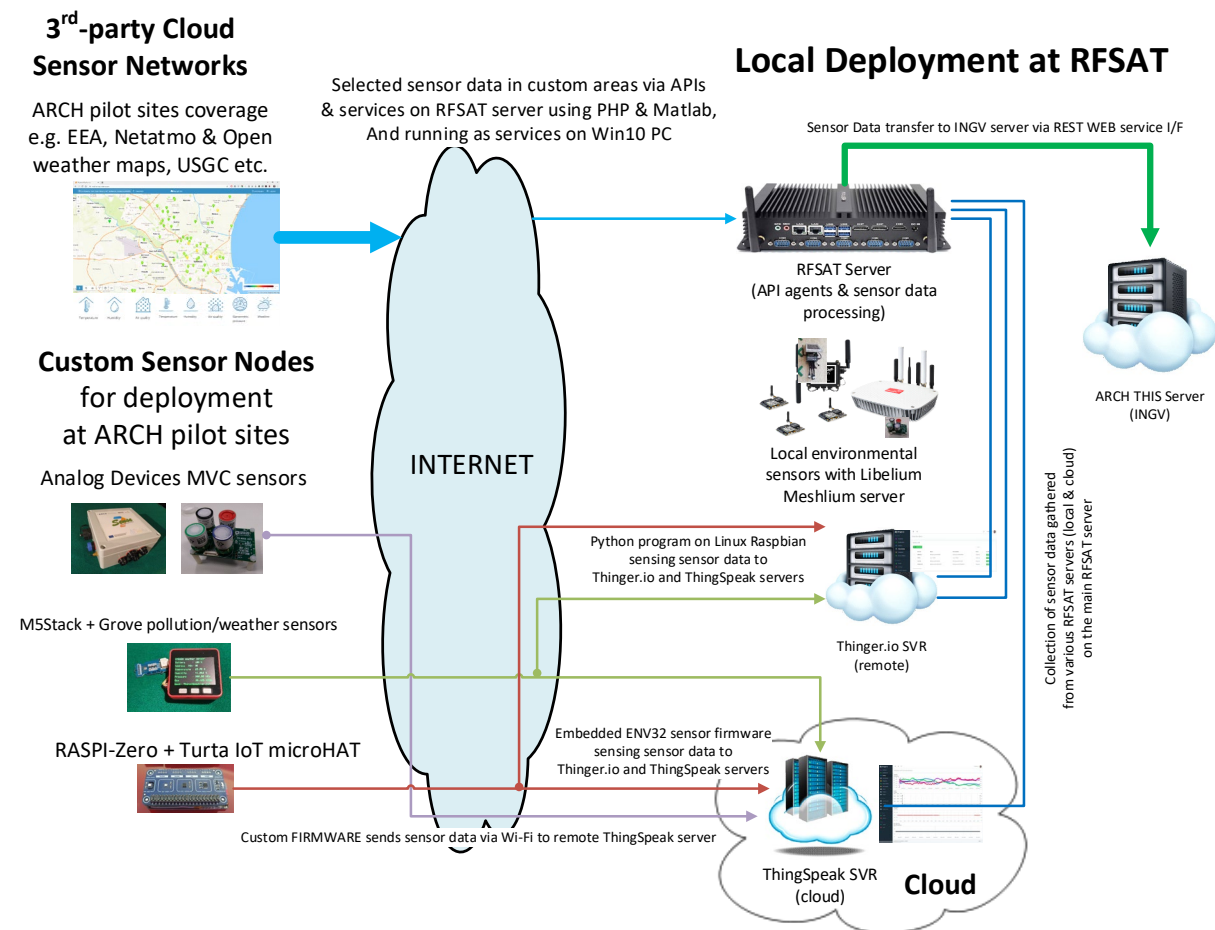


Figure 3: Integration of RFSAT IoT sensors with THIS server

Each of such sensor networks uses different sensor nodes (from high-quality embedded sensors from Analog Devices⁷ (AD) to simplest/cheapest Raspberry-PI with sensor connected via Grove I/F) and types of sensors (high-quality calibrated and/or low-precision detectors). In

⁷ Analog Devices sensors: <https://www.analog.com/en/products/sensors-mems.html>

all cases, sensors communicate using TCP-IP network protocol and Representational State Transfer (REST) WEB service interface with local/remote IoT platforms. To offer higher diversity and customisation, RFSAT has investigated and deployed a number of IoT platform types, from Meshlium IoT gateway⁸, through cloud and/or local Thinger.io IoT platforms to fully cloud based Thing Speak IoT platforms from MathWorks. They all allow collection of sensor data in batches and distribution to other ARCH solutions through a secure REST WEB interface, currently used for sending RFSAT sensor data to the INGV server.

2.1. On-Premise Weather / Climate and Air Quality Sensing

To address the needs of ARCH pilot cities, RFSAT has pursued integration of dedicated sensors both based on Commercial off-the-shelf (COTS) technologies (e.g. wasp-mote sensor platform⁹ and Meshlium IoT gateway from Libelium, M5Stack and M5Stick¹⁰, Raspberry PI v4¹¹ and PI-Zero¹² embedded computer boards, and many other ones), as well as proprietary developments of own embedded sensors and in collaboration with other companies, such as Analog Devices (Ireland) and Turta¹³ (Turkey). Those sensors were initially intended as dedicated ones for measuring accurately levels of climate and pollution parameters at sites in pilot cities, to complement wider-area data coming from local, national and global observation platforms. Sensors purposely developed by RFSAT offer added value in providing more sensing elements (temperature, humidity, pressure and four more custom sensors) as compared to similar nodes such as Libelium Plug & Sense¹⁴ offering six custom sensors. Sensors built by RFSAT can operate both in fixed position (mounted at specific location) for constant monitoring of important environmental parameters and in mobile manner (wearable and/or installed in vehicles) to leverage a smaller number of sensors that can span larger geographical areas, though at less temporal density of measurements.

In terms of sensor coverage, the number of sensors that need to be deployed to offer meaningful results varies depending on the location: indoor versus outdoor, rural versus urban as well as the accuracy required. The rule of thumb says that sensors should be deployed one at each of the “self-contained area”, such as indoors at each room that can be isolated by closing e.g. the doors/windows, or outdoors one per area that has local; micro-climate characteristics such as narrow roads without many crossings, etc. Larger distances among sensors dilute results that may vary dramatically especially in case of air movements, sun radiations etc. In practice sensor deployment is strongly dependent on the floorplan and requires custom placements. Communication and power supply is often one of the important factors, such as Wi-Fi availability within no more than 300 meters is usually a restriction, unless long-range mesh networking that may reach even few kilometres can be used at a cost of higher power consumption and hence need for larger (solar) batteries of fixed power. In terms of pollution data, sensors need to be deployed close to immediate sources of expected

⁸ Libelium Meshlium IoT gateway: <https://www.libelium.com/iot-products/meshlium/>

⁹ Libelium waspmote: <https://www.libelium.com/iot-products/waspmote/>

¹⁰ M5Stack and M5Stick: <https://m5stack.com/>

¹¹ Raspberry PI v4: <https://www.raspberrypi.org/products/raspberry-pi-4-model-b/>

¹² Raspberry PI zero: <https://www.raspberrypi.org/products/raspberry-pi-zero/>

¹³ Turta: <https://docs.turta.io/>

¹⁴ Libelium Plug & Sense: <https://www.libelium.com/iot-products/plug-sense/>

pollutions and in the vicinity of monitored heritage assets, such that effects from combined climate and pollution conditions can be more precisely anticipated. As an example, in urban areas of Bratislava and Hamburg weather sensors are practically over-populated with usual spacing among them within few hundred meters. Nevertheless, such close proximity offers an opportunity for local-scale modelling of micro-climate conditions at road levels, which would not be possible in case of usual deployment of single high-precision sensor stations by local authorities per municipality.

The costs of sensors are also a highly differentiating factor. Although the cost of sensor collection and communication boards like Libelium waspmote, Analog Devices MVP or M5Stack are reasonably low and can reach 150-250 euros in the extreme cases, the costs of sensing elements can be significant, especially when calibration at manufacturing factory is required for accurate measurements. Such sensors may reach even 1500 euros in the case of Libelium Particulate Matter sensor with average costs of more “classical” gas sensors like NO₂, SO₂, CO₂, NH₄, CO and similar ranging between 60 euros and 250 Euros. As a result, the costs of complete integrated sensor nodes, including ambient power with battery, waterproof casing etc, may well exceed few thousand euros, example being a Libelium P&S with six calibrated sensors (T/M/P, CO, CO₂, NO₂, SO₂ and PM) priced at 3000 euros each. As such it becomes non-economic to deploy many such sensors. An alternative approach would be to leverage a higher number of lower-quality and hence significantly cheaper sensors for higher coverage. By using oversampling algorithms from Digital Signal Processing (DSP) domain, a large number of low-precision sensors can be used to calculate the real sensor value to a much higher precision [43]. Furthermore, leveraging spatial versus temporal coverage by using lower number of precision sensors in mobile application allows covering large (mostly populated and commonly accessible) areas when sensors are mounted on e.g. bicycles, motorbikes or even public transport/utility vehicles by city/local authorities (examples are mentioned in section 2.1.5). Various types of sensors built for diverse applications in ARCH pilot cities are presented in the follow up sections.

2.1.1. Libelium waspmote(s) and Meshlium IoT server

The Libelium waspmote boards are well known types of IoT sensors specially designed to work with extremely low power consumption. The latest gas sensor board from Libelium allows to selectively switch on and off sensors, thus contributing to even lower energy usage. The whole system can be also put to different sleep modes, even further reducing its power needs. There is a vast number of sensor add-on boards that can be connected to waspmote. In ARCH we have used the gas sensor board 2, offering the capability to measure up to six custom parameters. The advantage of this board is that high precision and calibrated sensors can be flexibly connected. The disadvantage is that not all combinations of sensors are possible e.g., measuring all three common climate parameters i.e., temperature, humidity and pressure, might prevent connecting some air quality sensors such as NO₂ or O₃. This may be in some cases an obstacle in using such sensors.



Figure 4: Libelium based sensors for ARCH on-premise installation from RFSAT

In the test deployment aimed for ARCH (Figure 4), the waspmote board was integrated with a Wi-Fi communication interface, gases PRO¹⁵ add-on board and solar panel. The complete setup thus allowed fully wireless and power autonomous setup, hence flexibly deployable in any external environment. With use of a range of power saving modes, such a sensor has been proven to operate autonomously for several months, sending its measurements to Libelium Meshlium scanner, the IoT gateway that allows the detection of smart devices which works with Wi-Fi or Bluetooth interfaces (phones, tablets, hands-free and wearables).

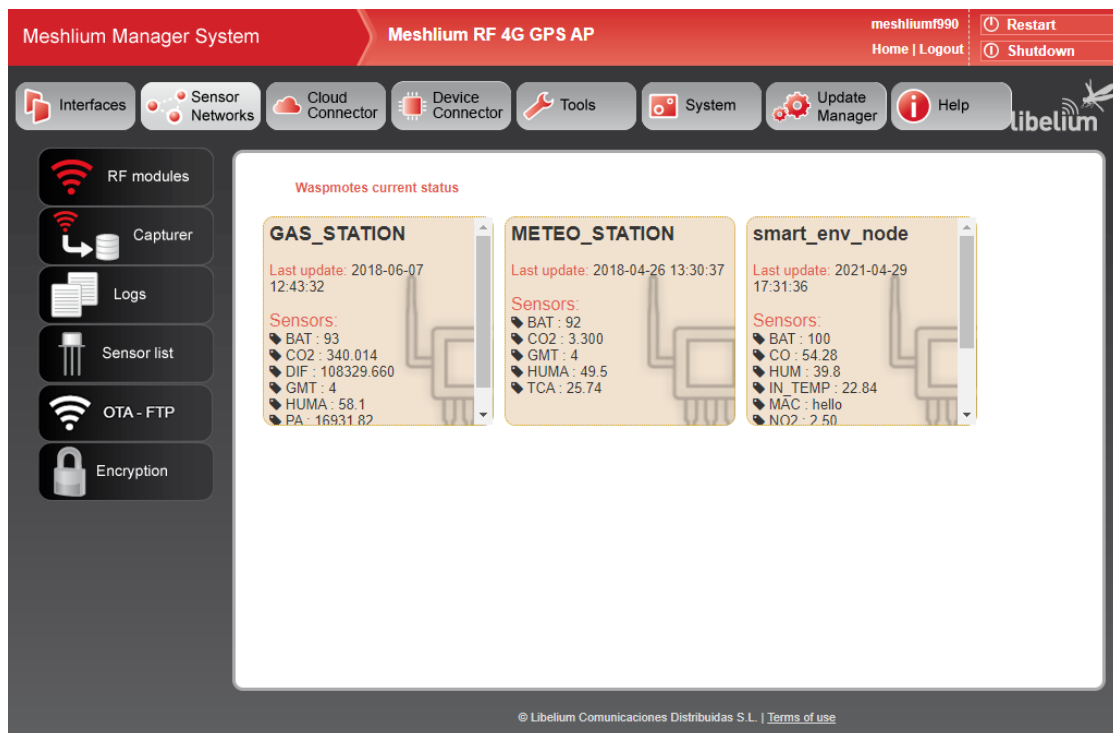


Figure 5: Sensor management on RFAT Meshlium server

¹⁵ <https://www.libelium.com/libeliumworld/calibrated-air-quality-gas-dust-particle-matter-pm10-smart-cities/>

The instance deployed by RFSAT enables connectivity of sensors via 802.14, 802.11, 3G/4G wireless interfaces. An example screenshot from the Meshlium embedded WEB server is shown in Figure 5. Such an IoT server has an advantage of enabling connectivity not only to Libelium sensors but can serve as a generic IoT server to gather data from other types of sensors via flexible APIs as long as they communicate via an over-the-air interface supported by Meshlium. The figure shows also two more sensors that have been connected to it earlier, one being a raspberry-PI based custom sensor built by RFSAT, which has been later moved to ThingSpeak IoT online platform¹⁶ described in a later section. The custom sensor can be seen to measure the following parameters.

Table 2: Range of parameters captured by local RFSAT Plug & Sense sensor node on Meshlium IoT server

ID	Date	ID Wasp	ID Secret	Sensor	Value
1324809	2021-06-22 16:12:14	smart_env_node	2D0767057C105494	NO2	0.00
1324808	2021-06-22 16:12:14	smart_env_node	2D0767057C105494	BAT	100
1324807	2021-06-22 16:12:02	smart_env_node	2D0767057C105494	SO2	0.29
1324806	2021-06-22 16:12:02	smart_env_node	2D0767057C105494	O3	0.00
1324805	2021-06-22 16:12:02	smart_env_node	2D0767057C105494	CO	3.50
1324804	2021-06-22 16:10:02	smart_env_node	2D0767057C105494	PRES	99491.11
1324803	2021-06-22 16:10:02	smart_env_node	2D0767057C105494	HUM	30.2
1324802	2021-06-22 16:10:02	smart_env_node	2D0767057C105494	IN_TEMP	27.84
1324801	2021-06-22 16:09:50	smart_env_node	2D0767057C105494	MAC	hello
1324800	2021-06-22 16:09:50	smart_env_node	2D0767057C105494	PM10	5.25
1324799	2021-06-22 16:09:50	smart_env_node	2D0767057C105494	PM2_5	4.23
1324798	2021-06-22 16:09:50	smart_env_node	2D0767057C105494	PM1	3.06
1324797	2021-06-22 16:09:16	smart_env_node	2D0767057C105494	NO2	0.00
1324796	2021-06-22 16:09:16	smart_env_node	2D0767057C105494	BAT	100
1324795	2021-06-22 16:09:04	smart_env_node	2D0767057C105494	SO2	0.37
1324794	2021-06-22 16:09:04	smart_env_node	2D0767057C105494	O3	0.00
1324793	2021-06-22 16:09:04	smart_env_node	2D0767057C105494	CO	3.45
1324792	2021-06-22 16:07:04	smart_env_node	2D0767057C105494	PRES	99490.75
1324791	2021-06-22 16:07:04	smart_env_node	2D0767057C105494	HUM	30.9
1324790	2021-06-22 16:07:04	smart_env_node	2D0767057C105494	IN_TEMP	27.90

Note that all particulate matter values are provided by one custom sensor, while weather conditions (temperature, humidity, and pressure) are embedded into a gas PRO add-on board. The sensor node can be also seen to provide battery level in case of battery/solar operation. In our case it has been connected to mains power and so battery can be seen to have a maximum level. When using solar power in well-lit area, the sensor node is capable to operate in power autonomous mode when transmitting data once every three hours, being acceptably sufficient for most environmental monitoring applications in smart cities.

¹⁶ Mathworks™ Thing Speak IoT platform: <https://thingspeak.com/>

2.1.2. Analog Devices MVP based custom sensor node

The ongoing collaboration with Analog Devices (Limerick, Ireland)¹⁷, the world renowned semiconductor chip manufacturer, has resulted in the joint development of a novel sensor node based on a new AD MVP sensor board (Figure 6). RFSAT has been a proud first tester of this board offered on complimentary bases for testing in the ARCH project.

This board uses a generic AduCM355 EC sensor board suitable for cloud IoT applications. In the context of ARCH, a sensor was built for measuring standard local climate parameters (temperature, humidity, and pressure) in addition to HS₄, CO, SO₂ and NO₂. Such pollutants have been initially indicated by ARCH pilot cities as important not only for health of citizens, but also as responsible for erosion of materials used for historic objects and buildings. All sensor elements are “calibrated”, i.e. their accuracy has been verified by manufacturers and certified to be within 1PPM for at least two years.

The MVP sensor offers wireless transmission capabilities and power autonomy with solar panels. As such, it is comparable to Libelium waspmote. However, the MVP offers better power optimisation and hence has proven to be more reliable during high overcast periods, e.g. during last autumn and winter period, when Libelium had to be ultimately plugged into mains. The additional advantage of such a solution is a smaller form factor, thus less visually obstructive when placed either indoors or outdoors on historic buildings.

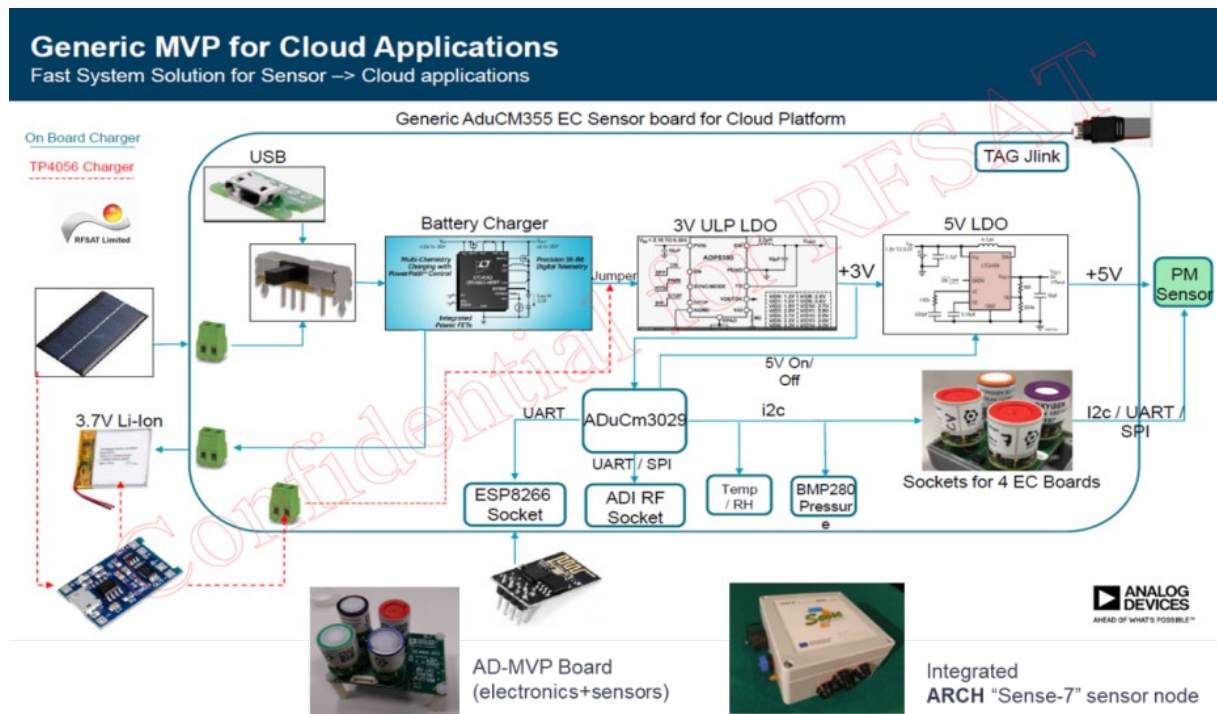


Figure 6: Sensor node based on Analog Device MVP board

¹⁷ Analog Devices Ireland: <https://www.analog.com/en/about-adi/corporate-information/regional-headquarters/directions-to-analog-devices-international.html>

2.1.3. Multi-gas based on M5Stack/M5Stick

An interesting development made for ARCH was made using generic M5Stack/M5Stick¹⁸ (Figure 7) embedded devices. Those devices are ESP32-based boards and can be easily programmed and flexibly reconfigured to custom needs using Arduino Studio.

The most important advantages of those devices over their predecessors above are:

- Very small form factor with long battery life for mobile sensing
- Embedded screen for simultaneous graphics and text display
- Grove connectivity for I2C and SPI sensor boards

The custom development for ARCH focussed on building a universal plug-and-play sensor board, considering a vast range of interests from pilot cities in ARCH for different types of sensors. As such the board has been programmed to automatically detect connected sensors as well as chose from the range of pre-configured wireless networks to send its data to cloud IoT platforms. For testing purposes support for BME680 (temperature, humidity, and pressure), particulate matter (PM1.0, PM2.5, PM10), SI1145 (visible light with UV index), VEML6070 (UV light sensor) has been implemented. Note that Figure 7 shows the M5Stack version with BME 680 sensor, displaying measured parameters with gas resistance corresponding to CO₂ levels as added value. Similar developments were pursued that took advantage of even smaller M5Stick device and similar plug-and-play capabilities connected to the SI1145 sun light sensor as well as the BME280 environmental sensor, the white box plugged on the right to its proprietary port.



Figure 7: Gas sensor nodes based on M5Stick/M5Stack embedded platforms

¹⁸ M5Stack and M5Stick: <https://m5stack.com/>

Note that except for M5Stick special port, multiple sensor elements can be connected through Grove connectors (both I2C and SPI interfaces are supported). By using Grove HUB one port can be populated with three other sensors, thus extending the range of parameter value that can be measured simultaneously.

The firmware built by RFSAT offers an added-value of automatically adapting to the type(s) of sensor(s) connected, also permitting dynamic exchange of sensors connected to its I2C and SPI ports. The node senses removal of a sensor element and after few seconds waiting time it switched to a search mode. Once sensor is identified and communication re-established, the periodic acquisition and upload of sensor values to cloud IoT servers is resumed. In similar manner change of communication interfaces is accomplished, allowing dynamic switching among pre-configured Wi-Fi networks.

2.1.4. Raspberry-PI based sensors with Turta IoT HATs

In order to increase the number of connected sensors the Raspberry-PI embedded computer has been investigated. However, this meant higher power consumption and hence a need to remove the display as a way to reduce high power consumption of the RASPI board. The use of Grove HATs enables up to 15 simultaneously connected sensors (with some compromise regarding I2C and SPI connectivity), which may be beneficial for applications requiring a large number of parameters to be monitored simultaneously. Figure 8 shows a smaller version of the Grove HAT board with only eight ports built in collaboration with Turta.io, but with additional sensors embedded directly onto the board. Initially, the latest standard-size RASPI-4 was selected for testing (left), which has proven to work well in mains powered mode. However, its power consumption has proven too high to be powered from a battery of the same size as the computer itself, even in shall mode (i.e. without X-Windows GUI).

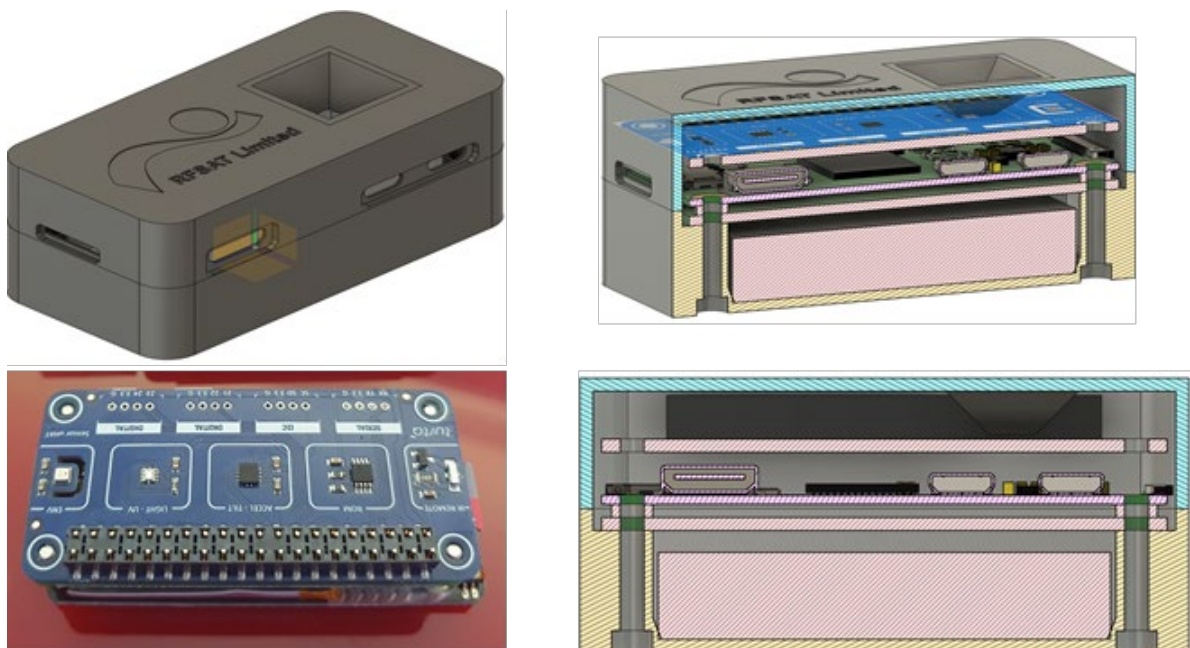


Figure 8: Sensor nodes based on Raspberry-PI and Turta-IoT2 HAT

The figure shows both the real hardware and the design of the case built for deployment at selected ARCH pilot sites. With embedded UPS battery HAT, main power option as well as

mount option for bicycle/motorbike handles, it can be used both for fixed deployment as well as for mobility application. In the former case it offers a capability to directly link with pre-configured Wi-Fi access points. In the latter case, communication can be done either to the smartphone via Bluetooth, Wi-Fi direct or USB cable (incl. charging) using it as a long-haul communication interface to the remote IoT server, such as ThingSpeak IoT server (shown in Figure 9), and for direct access to displaying acquired sensor data. An option is also possible to connect the mobile GPRS and GNSS add-on card thus it becoming a self-contained mobile sensor node for deployment on e.g. public transport or utility vehicles as shown in Figure 10.

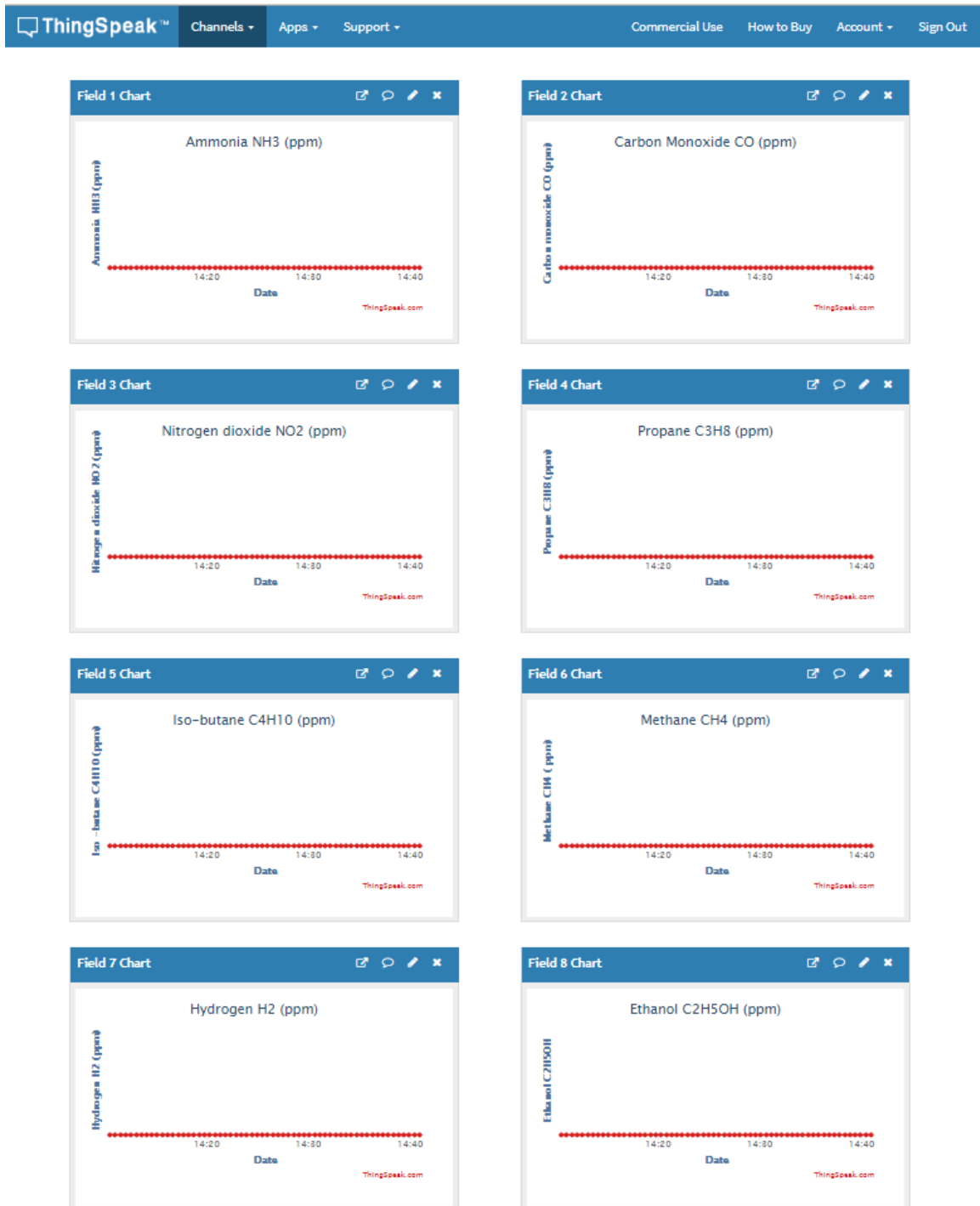


Figure 9: Sensor values from RASPI-Zero sensor as recorded by ThingSpeak IoT platform

In order to push the RASPI technology capabilities to its limits, the RASPI-Zero-W has been investigated. Due to its significantly smaller size, the number of Grove connected sensors had to be reduced to four (4), though at a benefit of much lower power consumption of the board itself, making it a promising choice for mobile application. With addition of the UPS-HAT¹⁹ and a 1200mAh battery, the integrated sensor was able to work for several hours on battery.

The collaboration between RFSAT and Turta.IO from Turkey has led to the development of the Turta IoT HAT²⁰, which has been evaluated by RFSAT for possible evaluation by pilot cities. The latest version is an upgrade following evaluations by RFSAT and contains four Grove-type connectors for connecting I2C, SPI and serial connected sensors. At the same time, it contains light-UV and BM280 environmental sensors, as well as accelerometers for possible use as shake/earthquake sensor. The resulting sensor node has a very small form factor of only 65mm x 30mm x 20 mm, including the uHAT and UPS boards. The sensor can be easily programmed under Linux using Python using provided libraries. This device is currently tested sending sensor data to RFSAT cloud IoT repositories on Thing Speak and Thinger.io platforms. Both are described in later sections.

2.1.5. Mobile environmental sensors

Following up on the sensor described in the previous section, it is very attractive for operating in a mobile scenario for collecting data from large areas, especially in populated areas. Therefore, simultaneous developments have been made by RFSAT and ENEA of such sensors, as shown in Figure 10.

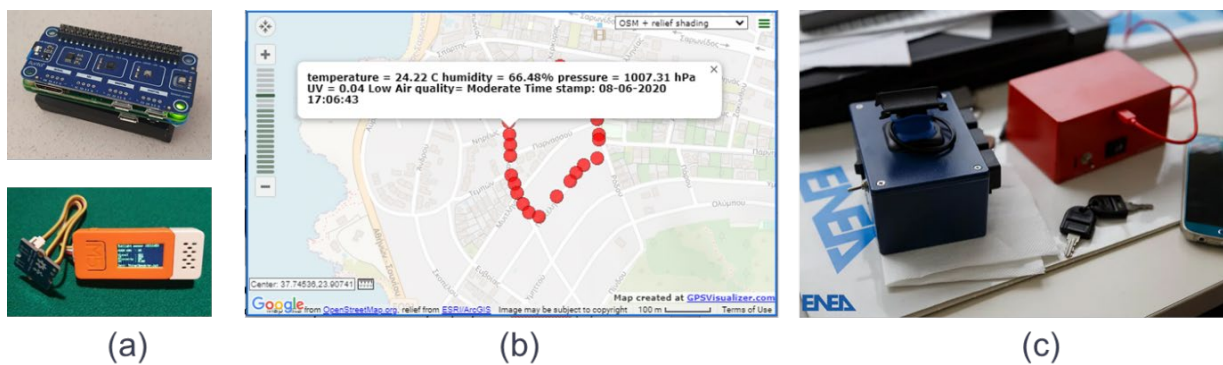


Figure 10: Mobile environmental sensors: (a) RASPI and M5Stick versions, (b) tracking RASPI-Zero-based sensor via Web application, (c) MONICA sensor from ENEA

The MONICA²¹ system of ENEA has been already used in Camerino for crowd sensing applications. It is a result from the “MONItoraggio Cooperativo della qualità dell’Aria” project, built as a crowd-funded Smog Tracker²² by ENEA and already deployed in Camerino (IT). It can be deployed on vehicles (e.g. bikes) and leverages the coverage for the number of sensors. Sensor box is capable of measuring various pollutants and can be paired with a

¹⁹ https://www.amazon.de/gp/product/B07RDNT8CY/ref=ppx_yo_dt_b_asin_title_o08_s00?ie=UTF8&psc=1

²⁰ Turta sensor uHAT: <https://docs.turta.io/raspberry-pi-hats/sensor-uhat>

²¹ <https://www.enea.it/en/news-enea/news/environment-project-for-cooperative-air-quality-monitoring-begins>

²² Smog Tracker by ENEA: <https://www.eppela.com/en/projects/9652-monica-your-personal-anti-smog-gps>

smartphone application. Equipped with GPS receiver and the ability to be mounted on vehicles and bicycles, the devices send their data to the central IoT platform for processing.

A similar sensor has been developed by RFSAT, but adding a Global Navigation Satellite System (GNSS) position sensing with General Packet Radio Service (GPRS) mobile data communication capabilities to send data to the IoT platform deployed by RFSAT. A screenshot from RFSAT server showing the route and collected sensor data is shown in Figure 10. This prototype combines Battery/UPS (8hrs+operation) with high-precision GNSS (1.2m accuracy) s. Alternative design uses M5Stack (incl. display) with embedded GPS and up to 3 simultaneously connected Grove sensors.

2.2. Cloud and on-premise IoT Platform deployments

Further to the Libelium Meshlium IoT server platform, RFSAT has investigated in ARCH two types of IoT platforms for both the cloud and on-premise deployment, those being the ThingSpeak from Mathworks as an example of a cloud-based platform and Thinger.io, which can be deployed either using Cloud Service Providers such as Amazon AWS as well as locally at the premises of the IoT service provider. Note that all sensors described in this document have embedded capabilities to upload their sensor data to either of these platforms, to be accessed from anywhere and on any devices, from personal computers to tablets and smartphones.

2.2.1. RFSAT repository on ThingSpeak cloud IoT platform

The ThingSpeak²³ IoT platform from Mathworks™ (Figure 11) is a powerful cloud service platform for capturing, processing, and distributing sensor information. Having the Matlab engine embedded into its core system, it offers possibilities for rapidly coding and testing scripted functions that gather and analyse sensor information.

Such capabilities have been used by RFSAT not only for working with its own sensors, but also for fast testing of gathering and processing responses received from APIs provided by Open IoT sensor platforms and repackaging received measurements into the format required by WEB services created by INGV for uploading sensor data to the THIS server of ARCH.

At a later phase (in early 2021) RFSAT has ultimately deployed its own proprietary industrial embedded fan less server for processing all sensor data prior to sending those to the THIS server. Nevertheless, ThingSpeak has remained a rapid testing and development system, not to mention having in its repository over 6 years' worth of environmental data and corresponding to more than 650.000 records that started being collected before the ARCH project has started.

²³ ThingSpeak: <https://thingspeak.com/channels>

Mathworks ThingSpeak : <https://thingspeak.com/>

Functionalities useful for ARCH:

- Diverse sensors and data sources
- Matlab-based data processing
- Embedded visualisation (WEB, Android etc)

Data sources can be accessed from (operational):

- [Analog Devices MVP Sensor node #1](#) (Athens):
Read key / Channel ID :OIIQ4SUA1TXAEBG2 / 894669
- [Analog Devices MVP Sensor node # 2](#) in (Athens):
Read key / Channel ID :4JG854BI0SRM5OCD / 895045
- [RASPI-4 Station in Athens:](#)
Read key / Channel ID :L0OBDMLKE5OASFP9 / 899967
- [RASPI-Zero-W Station in Athens:](#)
Read key / Channel ID :PRLE98VJBQQZLO7B / 902892
- [Netatmo Weather Station #1 in Athens:](#)
Read key / Channel ID: I60SV2BK0SD0BSDW / 905019
- [Netatmo Weather Station #2 in Athens:](#)
Read key / Channel ID :LPXUKCQC2NP9F67J / 905675
- [Weather \(BME680\) in Athens:](#)
Read key / Channel ID :R8FA7BOEC41E79JV / 1025518
- [Sunlight \(SI1145\) in Athens:](#)
Read key / Channel ID :MYETBXLJFJB7SP1O / 1025554
- [UV \(VEML6070\) in Athens:](#)
Read key / Channel ID :B5RKMY7UHFKV1738 / 1025557
- [PM 2.5 \(HM3301\) in Athens:](#)
Read key / Channel ID :ES301V6N9Z0VVHFF / 1025559



Figure 11: RFSAT repository of sensor data on ThingSpeak IoT platform

2.2.2. Thinger.io IoT platform

Thinger.io²⁴ is an Open Source IoT platform development project, offering IoT platforms to be co-developed and deployed either in Cloud on on-premises. The advantage of this system is the low computing requirements, allowing it to be deployed even on a Raspberry-PI. Figure 12 shows such a deployment on a Raspberry-PI v4 for collecting sensor information from custom sensors described earlier.

The figure shows data sources collected by the platform and on the platform WEB interface. Note that all the custom RFSAT sensors are capable of sending their data simultaneously to the ThinkSpeak platform and the THIS server as well.

The specific functionalities that have been identified as useful for ARCH pilots are:

- On-premise server deployment by RFSAT with option of replicating it at pilot sites
- Support for range of sensors and data sources, practically any one shown earlier
- Tested on: M5Stack/M5Stick, Raspberry PI and Zero etc
- Offers embedded WEB-based visualisation and online data analytics
- Supports API based access for integrating into own applications

²⁴ Thinger.io: <https://thinger.io/>

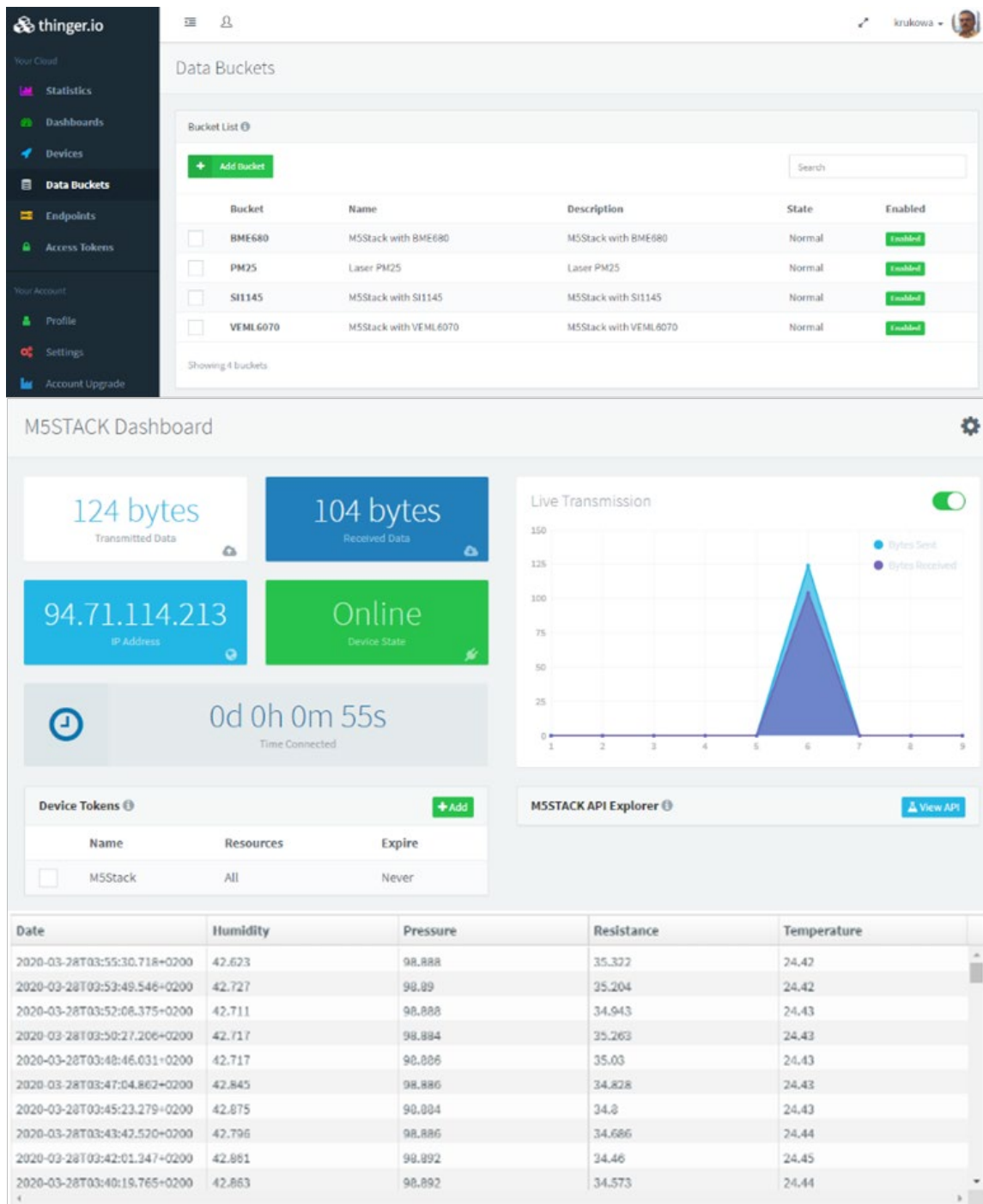


Figure 12: RFSAT repository of sensor data on the Thinger.io IoT platform

2.3. Open Data Platform Integration

Since deployment of new sensors over large areas of the ARCH pilot cities has not been feasible, both in terms of associated costs, technological manufacturing capabilities of technical partners, and logistic issues especially due to the COVID-19 outbreak, data from available Open Data platforms that collect sensor data from terrestrial sensors through a citizen observatories approach have been considered and integrated into the ARCH system. Services integrated into THIS with a list of parameters captured are shown in Table 3.

	<u>Humidity (outdoor)</u> current measure, min, max [%] <u>Wind:</u> current speed, min, max [m/s]	~1% ~1m/s	
<u>Weatherbit.io IoT platform</u> ²⁸	<u>Sunrise time</u> [HH:MM] <u>Sunset time</u> [HH:MM] <u>Pressure</u> [mb] <u>Sea level pressure</u> [mb] <u>Wind speed</u> [m/s] <u>Wind direction</u> [deg] <u>Temperature</u> [°C] "Feels Like" temperature [°C] <u>Relative humidity</u> [%] <u>Dew point</u> [°C] <u>Cloud coverage</u> [%] <u>Visibility</u> [km] <u>Precipitation rate</u> [mm/hr] <u>Snowfall</u> [mm/hr] <u>UV Index</u> [0-11+] <u>Air Quality Index</u> [US-EPA: 0 - +500] <u>Diffuse hor. solar irradiance</u> [W/m ²] <u>Direct normal solar irradiance</u> [W/m ²] <u>Global hor. solar irradiance</u> [W/m ²] <u>Estimated Solar Radiation</u> [W/m ²] <u>Solar elevation angle</u> [deg] <u>Solar hour angle</u> [deg]	<u>Sources:</u> METAR stations NOAA Meteorological Assimilation Data Ingest System (MADIS) MAE < 0.5° RMSE < 2°	Pilot areas defined by end users
<u>Smart Citizen open data IoT platform</u> ²⁹	<u>Noise</u> [dBA] <u>Air temperature</u> [°C] <u>Humidity</u> [%] <u>Barometric pressure</u> [kPa] <u>Light</u> [lux] <u>NO₂</u> [kOhm] <u>PM1.0, PM2.5, PM10</u> [µg/m ³] <u>eCO₂</u> [ppm] <u>CO</u> [kOhm] <u>TVOC</u> [ppb]	±1 dB ±0.3 °C ±2% ±1 hPa 15% ±20µg/m ³ ±3% MV	Pilot areas defined by end users
<u>Citizen Weather Observer Program</u> ³⁰	<u>Barometric pressure</u> [millibars] measures + error + standard deviation <u>Temperature</u> [°C] measures + error + standard deviation <u>Temperature Dewpoint</u> [°C] measures + error + standard deviation <u>Relative humidity</u> [%] measures + error + standard deviation	Accuracy compliant with MADIS & NOAA	Pilot areas defined by end users

²⁸ Weatherbit.io platform: <https://www.weatherbit.io/features> and API: <https://www.weatherbit.io/api>

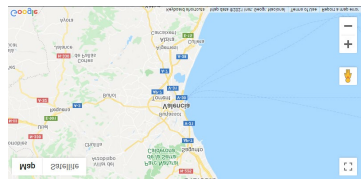
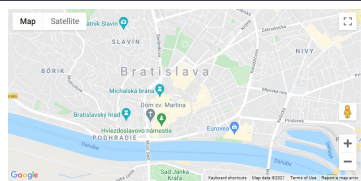
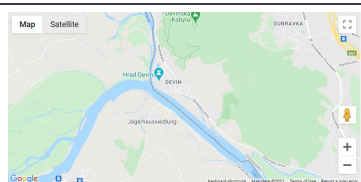
²⁹ Smart Citizen platform: <https://smartcitizen.me/> and API: <https://developer.smartcitizen.me/>

³⁰ Citizen Weather Observer Program: <http://wxqa.com/>

	Wind vector: Speed [knots], angle [deg]		
<u>European Environmental Agency</u> ³¹	Air quality from national reports: <u>Arsenic</u> As [ng/m ³] <u>Benzene</u> C6H6 [µg/m ³] <u>Benzo(a)pyrene</u> BaP [ng/m ³] <u>Cadmium</u> Cd [ng/m ³] <u>Carbon monoxide</u> CO [µg/m ³] <u>Lead</u> Pb [µg/m ³] <u>Nickel</u> Ni [ng/m ³] <u>Nitrogen dioxide</u> NO ₂ [µg/m ³] <u>Ozone</u> O3 [µg/m ³] <u>Particulate matter</u> PM2.5, PM10 [µg/m ³] <u>Sulphur dioxide</u> SO ₂ [µg/m ³]	STD < 2% (country specific)	Pilot areas defined by end users

Definitions of observed pilot areas for all ARCH pilot cities were as in .

Table 4: Observable areas of pilot sites defined by end users

Pilot city	Observable area [north, west, south, east]	Orientation map
Hamburg Canals	[53.553045, 10.010375, 53.537913, 9.944591]	
Camerino Centre	[43.190177, 13.136211, 43.083472, 12.995326]	
Valencia Huerta	[39.718700, 0.157300, 39.091800, -0.807500]	
Bratislava Old Town	[48.151858, 17.120197, 48.139325, 17.103021]	
Bratislava Castle	[48.181925, 17.006773, 48.157317, 16.970385]	

³¹ European Environmental Agency API: : <https://www.eea.europa.eu/code/api>

<p>Dublin Centre</p>	<p>[53.347545, -6.251679, 53.337019, -6.270585]</p>	
<p>Athens Centre</p>	<p>[37.988472, 23.751141, 37.964406, 23.713826]</p>	

2.3.1. NetAtmo WeatherMap

NetAtmo is a manufacturer of weather stations permitting users to monitor their weather conditions, including temperature, humidity, pressure for both indoor and outdoor, as well as rain and wind (with optional modules). Data collected from user devices is uploaded to a cloud, hosted by the manufacturer, that offers access to geocoded outdoor conditions, excluding user identifiable information. Data can be displayed on a map via a WEB GUI (Figure 13) for the wide area surrounding Valencia and including Huerta, being an example of a high density of available sensors contributed by community of users of such sensors.

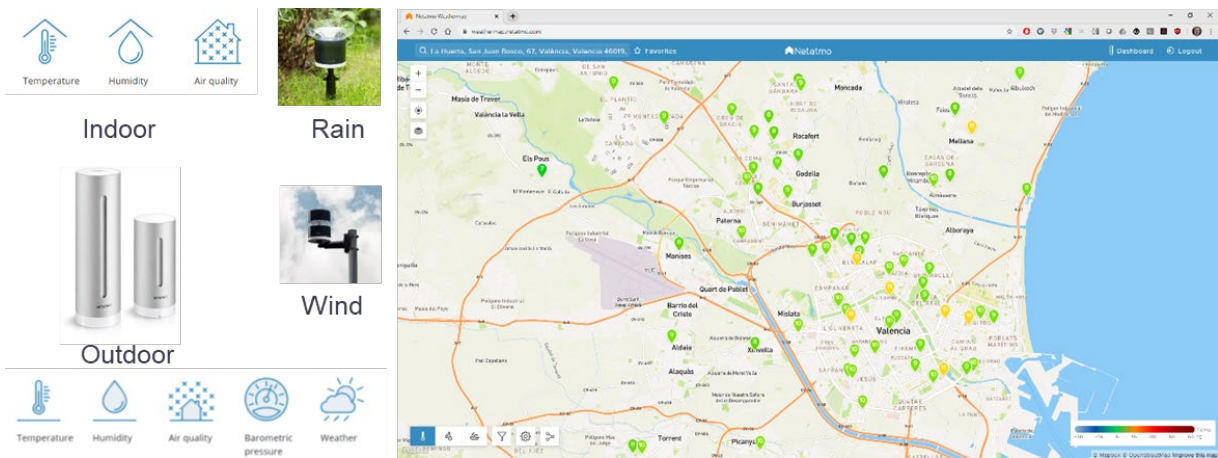


Figure 13: Integration of sensor data from NetAtmo WeatherMap

Considering thousands of devices already sold, such a global map offers an invaluable source of real-time information at any location where such stations are located. The company also offers an API allowing downloading of data for specific locations and individual weather stations³². In ARCH we have taken advantage of this opportunity and a service has been set-up by RFSAT to periodically (every hour) collect data from stations located within the expressed interest areas of ARCH pilot cities.

A full list of available parameters is shown in Figure 14.

³² NetAtmo API: <https://dev.netatmo.com/apidocumentation/weather#product-details>

- <https://160.97.1.28/archportal/api/envdata/list>

It accepts a JavaScript Object Notation (JSON) object containing a list of measures as the body of a POST request, e.g.:

```
[{
  "Timestamp": "",
  "Latitude": "10",
  "Longitude": "10",
  "Altitude": "10",
  "Temperature": "1",
  "Humidity": "10",
  "Pressure": "1",
  "TMRainUTC": "",
  "RainLive": "1",
  "Rain60min": "1",
  "Rain24hrs": "1",
  "TMWindTimeUTC": "",
  "WindStrength": "1",
  "WindAngle": "1",
  "GustStrength": "1",
  "GustAngle": "1"
},
{
  "Timestamp": "",
  "Latitude": "10",
  "Longitude": "10",
  "Altitude": "10",
  "Temperature": "1",
  "Humidity": "10",
  "Pressure": "1",
  "TSRainUTC": "",
  "RainLive": "1",
  "Rain60min": "1",
  "Rain24hrs": "1",
  "TSWindTimeUTC": "",
  "WindStrength": "1",
  "WindAngle": "1",
  "GustStrength": "1",
  "GustAngle": "1"
}]
```

- <https://160.97.1.28/archportal/api/envdata>

It accepts JSON object containing one measure as a body of the POST request, e.g.:

```

{"Timestamp":"","
"Latitude":"10",
"Longitude":"10",
"Altitude":"10",
"Temperature":"1",
"Humidity":"10",
"Pressure":"1",
"TSRainUTC":"","
"RainLive":"1",
"Rain60min":"1",
"Rain24hrs":"1",
"TSWindTimeUTC":"","
"WindStrength":"1",
"WindAngle":"1",
"GustStrength":"1",
"GustAngle":"1"}

```

The WEB service from INGV incorporates a check for already existing data for the same location and same acquisition time, thus allowing this type of check to be skipped when uploading data originating from various data sources.

2.3.3. Open WeatherMap

Open WeatherMap³³ is a similar platform to NetAtmo WeatherMap offering free access to weather information for various locations around the globe, both current conditions and historic data for up to 30 days. It offers various types of licensing modes, from up to 1 million API calls per month in its free mode to up to 1 billion API calls per month in commercial mode. The service offers also access to air pollution parameters, such as CO, NO, NO₂, O₃, SO₂, PM2.5, PM10 and NH₃. A service consuming the provided API has been deployed by RFSAT for collecting all available current weather and air quality parameters at pilot cities, to complement similar data obtained from other sources.

The same WEB service as described in section 2.3.2 was used for this platform.

2.3.4. Air Quality Open Data

The Air Quality Open Data platform offers air quality sensing data for the whole globe. The example map for Hamburg with available sensor parameters is shown in Figure 15. The Air Quality Open Data API³⁴ offers the ability to search for locations and download environmental and air quality data for those. In order to avoid multiple WEB service calls, the list of locations is periodically downloaded by an RFSAT service and data for locations within areas associated with pilot sites is explicitly downloaded and then uploaded to the THIS server in bulk using a dedicated “*pollutiondata*” WEB service from INGV.

³³ <https://openweathermap.org/weathermap>

³⁴ <https://aqicn.org/json-api/doc/>

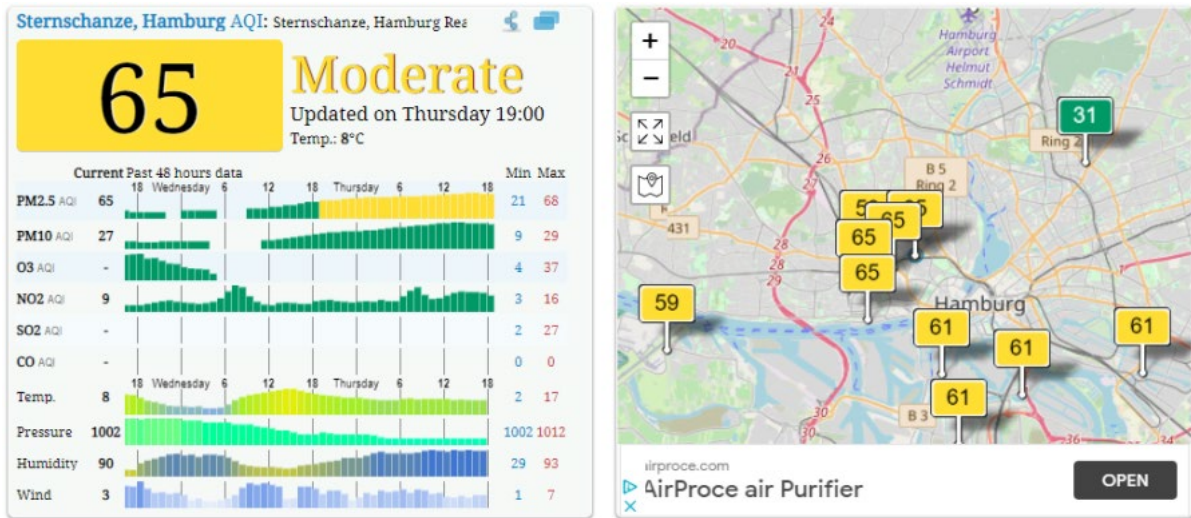


Figure 15: Map of Hamburg from Air Quality Open Data platform

2.3.5. Air Pollution WEB service

The purpose of this WEB service developed by INGV is to upload air pollution data to the THIS server. It is used by RFSAT to upload data both from its proprietary sensors and sensor data acquired from online repositories. The list of available methods includes:

- <https://160.97.1.28/archportal/api/pollutiondata/list>

It accepts a JSON object containing a list of measures as a body of POST request, e.g.:

```

[[{"date": "2015-01-13", "country": "ES",
  "city": "Valencia",
  "Notation": "co",
  "counter": "57",
  "minval": "0.1",
  "maxval": "0.1",
  "median": "0.1",
  "variance": "0.00"
},
{
  "date": "2015-01-14",
  "country": "ES",
  "city": "Valencia",
  "Notation": "co",
  "counter": "57",
  "minval": "0.1",
  "maxval": "0.1",
  "median": "0.1",
  "variance": "0.00"
}]]

```

- <https://160.97.1.28/archportal/api/pollutiondata/binary>

The method accepts as the body of the POST request a string containing one or more pollutant measurements; a single measure can be a CSV-style, while the measures will be separated from each other by the line break character, e.g.:

```
"2015-04-08,ES,Valencia,co,41,0.1,0.1,0.1,0.00"
```

- <https://160.97.1.28/archportal/api/pollutiondata>

It accepts a JSON object containing one measure as a body of the POST request, e.g.:

```
{
  "date":"2015-01-13",
  "country":"ES",
  "city":"Valencia",
  "Notation":"co",
  "counter":"57",
  "minval":"0.1",
  "maxval":"0.1",
  "median":"0.1",
  "variance":"0.00"
}
```

- <http://160.97.1.28/archportal/api/pollutiondata/count>

The method returns the total number of measures inserted (GET)

- <http://160.97.1.28/archportal/api/pollutiondata/>

The method returns the list of all measures inserted (GET)

2.4. Geometry (3D) scanning technologies

Over recent years, 3D scanning has become part of a coherent and non-contact approach to the documentation of heritage assets and its long-term preservation. From one side high-resolution 3D recordings of heritage assets and historical areas allow us to monitor, study, disseminate and understand our shared cultural history. On the other hand digital models offer also the ability to re-materialise data as physical 3D objects is demanding new explorations into the types of information the data contains from data-driven shape analysis³⁵, semantic object understanding³⁶ to complete 3D scene recognition³⁷. The levels of damage and

³⁵ https://people.cs.umass.edu/~kalo/datadrivenshape/data_driven_shape.pdf

³⁶ https://www.ecva.net/papers/eccv_2020/papers_ECCV/papers/123670494.pdf

³⁷ <https://arxiv.org/abs/1411.5935>

destruction of heritage sites caused by mass tourism, wars, iconoclastic acts, the ravages of time, commercial imperatives, imperfect restoration, and natural disasters has led to a re-evaluation of the importance of high-resolution facsimiles.

A number of different 3D scanning methods exist, each with their own advantages and limitations, including time of flight (laser scanning), triangulation and 3D photogrammetry. The 3D data can now vary dramatically, from recording the topography of a landscape from large distances and altitudes (aerial scanning as in the FP7-AF3 projects of RFSAT) to at close range and accurate enough to document the surface of a carving, marks that are not easily visible to the human eye can be visualized for reconstruction study or condition monitoring (as demonstrated by RFSAT in the H2020-SCAN4RECO project). While some systems can obtain colour data as well as 3D information, currently no 3D scanner is able to record colour to the standard required for the production of an exact replica [1]. All 3D recording is based on metrology. Outlined below are the main techniques and scanners that are commonly used and the reasons they are used in the way they are. Both of the mentioned earlier projects as well as other running in parallel to them, such as H2020-DiGiArt³⁸ (capturing objects from air with drones) or H2020-Gravitate³⁹ (aimed at geometric object reconstruction) have shown the potential behind use of 3D model capture for preservation of European cultural heritage.

The needs in the ARCH project and as a result a further advancement beyond the results of the previously mentioned projects have been twofold. From one side there was a need to improve correct and accurate representation of the model geometry from images taken at non-perfectly accurate positions (caused by errors in GNSS position, drone movements due to wind, issues with geometrical matching etc) thus diluting the range estimates for the same feature in different images. On the other one dealing correctly with difficult and complicated objects necessitating carefully designed image capturing schemes, not to mention difficulties in dealing with different materials to capture their correct colour and appearance. The focus of this chapter is capturing the global shape, whereby some of the presented commercial technologies show potential for correct representation of object appearance as well.

Practically the 3D photogrammetry, despite being a conceptually simple enough, it often becomes tiresome for many of those who are non-familiar with such technology, thus preventing its use by most of the hosts of heritage sites. The automated system that is being developed by RFSAT since the AF3 project through to ARCH, has an aim to offer user-friendly approach to such 3D scanning with high-accuracy and precision of object representation, suitable for e.g. quick differential assessment of changes such as ageing caused by climatic changes and weather conditions, natural disasters etc.

³⁸ DigiArt project: <https://cordis.europa.eu/project/id/665066>

³⁹ Gravitate project: <https://cordis.europa.eu/project/id/665155>

2.5. Common 3D model representation for ARCH

The formats suggested for use in ARCH have been OBJ⁴⁰ and FBX⁴¹ as well as 3MF⁴², in addition to all point cloud formats accepted already by THIS platform. The first one is from one side the most commonly used, while being resistant to inconsistencies among various software than other formats, while FBX is easier in processing models and less prone to losing link with textures among common 3D editing commercial software (presented briefly in section 2.5.2). The 3MF format, even that still under development, shows a potential to become very flexible and future proof, especially that the 3MF consortium is willing to accept our suggestions for extensions to it.

A comprehensive review of existing 3D model formats with analysis of their suitability for representing historical objects and their spatial-temporal analysis has been performed by RFSAT in an earlier SCAN4RECO project⁴³ from the perspective of universality (ability to be used without conversions among vast number of software applications), interoperability (ability to be imported and used without loss of information) and flexibility for extensions (ability to add more features) to fit the needs of the ARCH project. The analysis in SCAN4RECO combined with needs arising from ARCH pilot sites has led to the following conclusions:

- Common 3D model format: the same 3D format should be used among project components such that to avoid translations, that might potentially lead to changed model representations and hence losses of information. Initially, the OBJ and FBX formats are most universal and flexible for extension to fit the needs of ARCH project.
- Water-proof 3D models are essential i.e., without holes and undefined spaces/areas. This is a necessary condition for 3D models to be 3D printed correctly. This is also a condition for being able to perform integration from multiple 3D scans and then additional processing e.g., for simulated future deteriorations, etc.
- Integration of 3D scans may face problems when areas are overlapping, especially in cases when GPS coordinates and/or geometrical positioning is not accurate. In such cases shifts between parts of the objects scanned individually may be observed. The practical approach is to establish a common boundary between such parts of the object and align those boundaries, adding extra triangles to connect them together, thus producing a smooth surface of the model. Nevertheless, the best results are always achieved when 3D photogrammetry and/or laser scans are performed on the whole model.

A common model-based supports both commonly used 3D object geometry and material definitions, with extra support for new features related to new optical surface characteristics, dynamic object properties and their subsequent printing. It describes the set of elements which define the content and structure of XML documents for storing the ARCH results, namely global and local scanning of a heritage asset, as well as metadata about physical object's features.

⁴⁰ <http://www.martinreddy.net/gfx/3d/OBJ.spec>

⁴¹ <https://code.blender.org/2013/08/fbx-binary-file-format-specification>

⁴² <http://3mf.io/specification/>

⁴³ <https://ec.europa.eu/research/participants/documents/downloadPublic?documentIds=080166e5b9e747ff&appId=PPGMS>

2.5.1. Long-Medium Range 3D Scanners (LiDAR)

The long and medium range 3D scanners have been used until now to record only the general shape of large objects and surfaces with the aim of getting accurate metrological information. This has been commonly used for topography and the recording of buildings. Such scanners use time-of-flight or laser-pulse based systems where a laser light is bounced off the target at a distance. A laser range finder calculates the distance to a surface by timing the round trip of a pulse of light using the known value for the speed of light. Advanced in microelectronics and chip-based lasers have led to both decreasing the size and increasing achievable accuracies of such scanners, while lowering their price as well.



Figure 16: Indoors 3D scanning with Structure Mark 2 sensor on iPad Air 2 (a) using Canvas application (b)

The LiDAR technology becomes one of the attractive ones for ARCH, especially in COVID-19 lockdown conditions, as LiDAR sensors started to become integrated even into the latest Apple iPhone 12 Pro, the iPhone 12 Pro Max, and the iPad Pro, thus making such scanners available to end-users. Other sensor devices, such as Occipital's Structure Sensor Mark II⁴⁴ sensor (shown in Figure 16a), enable any other consumer computer, tablet, and smartphone devices to take advantage of such novel 3D scanning capabilities. The latter one, which has been released only recently, is currently being integrated into the 3D scanning and modelling SDK from RFSAT. The 3D scan from the "Scanner" application⁴⁵ or a 3rd-party "Canvas" (example 3D scan shown in Figure 16b) can be saved locally in OBJ format and/or sent by email to a monitored email account. The RFSAT implementation uses a dedicated account for receiving and parsing 3D models, to be then processed and/or sent to the THIS server via WEB service.

2.5.2. Overview of 3D Modelling Software

Since RFSAT does not have own expertise in 3D photogrammetry, it integrates 3rd-party modelling engines into its processing process. The following engines have been and/or are in process of being integrated into the processing chain, each of those suitable for different scenarios, from objects to exterior/interiors and larger areas and structures:

⁴⁴ Structure Mark 2: <https://structure.io/structure-sensor/mark-ii>

⁴⁵ Occipital "Scanner" application: <https://apps.apple.com/us/app/scanner-structure-sdk/id891169722>

- **Pix4D Mapper Pro**

Features: The software automatically converts images taken by hand, by drone, or by plane, and delivers highly precise, georeferenced 2D maps and 3D models. They're customizable, timely, and complement a wide range of applications and software.

Availability: commercial, offers discount for scientific and non-commercial use

WEB portal: <https://pix4d.com/product/pix4dmapper-pro>

- **Autodesk ReMake (NEW product under development)**

Features: It is an end-to-end solution for converting reality captured with photos or scans into high-definition 3D meshes. These meshes can be cleaned up, fixed, edited, scaled, measured, re-topologized, decimated, aligned, compared, and optimized for downstream workflows entirely in ReMake. It handles reverse engineering as support for design and engineering, for asset creation for AR/VR, film, game, art, for archiving and preserving heritage, digital fabrication or publishing interactive experiences on Web and mobile.

Availability: commercial, offered for FREE to academia

WEB portal: <https://remake.autodesk.com>

- **Agisoft Photoscan**

Features: performs photogrammetric processing of digital images & produces 3D spatial data

Availability: commercial, currently without academic discounts

WEB portal: <http://www.agisoft.com>

- **ArTec Studio**

Features: software for professional 3D scanning and data processing

Availability: commercial, currently without academic discounts

WEB portal: <https://www.artec3d.com/software/artec-studio>

2.6. RFSAT implementation of automatic 3D scanning system

Considering the inherent needs of ARCH pilot sites for 3D representations of sites and objects and considering that ongoing digitisation process is either not complete (Bratislava, Hamburg) or lacks necessary level of resolution for performing required type of analysis (example of cracks in the rock formation under the Devin castle in Bratislava or warehouse foundations in the canals of Hamburg), the high-resolution RFSAT scanning system developed originally for small objects in SCAN4RECO project has been further advanced to offer similar level of accuracies to ARCH pilot sites. Other sites are also likely to benefit, such as for modelling and surveillance of Arabic irrigation systems in Valencia or historical areas of Camerino.

The 3D photogrammetry has been developed for ARCH to offer a custom, on-demand possibility to effortlessly build 3D models of heritage assets and for historical areas, in case that such might be missing in THIS database for any of the ARCH pilot sites or in cases that those available from host organisation (such as canal areas of Hamburg, historical buildings of Camerino or historical area of Bratislava) might not be in the format required to perform analysis of cracks and/or other types of structural defects in order to assess risks to such assets

or areas. Therefore, RFSAT has adapted its 3D photogrammetry system developed in SCAN4RECO project for small tangible objects like Byzantine icons or statues to large-scale objects like buildings (for e.g., Hamburg and Camerino), natural bedrocks (for e.g., Devin castle in Bratislava) or large historical areas like Huerta in Valencia. The main difference between ARCH and SCAN4RECO systems is the replacement of the mechanical arm used in the latter project for moving the camera over the heritage asset with autonomous control of UAS over large heritage assets and historical areas [3], [6]. For specific case of Hamburg, where there is a potential need for underwater 3D scanning of stumps supporting warehouses in eth canal area, the UUV control system combining raster camera with sonar are investigated to provide both data source for 3D modelling the assets as well as the canal ground floor. Details about the autonomous drone system can be found in section 2.7 in this document.

The objective of this sub-system is to allow for a global acquisition of the entire historic asset, whether it is an object, structure/building or landscape. The sub-system consists of a depth camera setup for capturing colour and depth information, which is used by the 3D reconstruction software to generate a global coarse-resolution 3D representation of the colour and geometry of the asset, taking into consideration that this 3D representation should be “water-proof” (i.e., without holes and undefined spaces/areas, suitable for subsequent 3P printing and/or processing). This representation is used as the basis of all the local measurements performed by HARIS processing tools such as for detection of cracks and structural deformations, thus applicable to e.g., the bedrock under the Devin castle in Bratislava or buildings in Camerino.

The necessary alignment of all measurements onto the global 3D representation is performed by *Data Registration* that aligns diverse data captured from different sensors for the same physical heritage asset (for details about this process refer to Figure 19 later in this section). In the case of ARCH, it is used for combining multiple 3D scans into a single model and (where applicable) attaching metadata to 3D models (such as material composition). All the aligned representations of heritage assets are stored with the form of a single data structure in the project database and are used by the following visualization and simulation components:

- HW/VISDEPTH (depth sensor + raster camera(s))
- SW/SCAN (3D reconstruction/modelling)
- SW/REG (multi-modal data registration)

2.6.1.1. Depth scanning

The camera setup consists of a low-cost depth sensor that produces a series of colour images and depth maps. The depth measurement is based on two different approaches. In the first one, namely **structured light**, depth sensors emit a series of infrared grids onto the scene and calculate the depth information based on the distortions of patterns. The emitted light pattern has usually a wavelength in the infrared spectrum and is thus invisible for the human eye. The Intel RealSense 435i⁴⁶ device uses this approach and consists of a colour camera, an infrared light projector that projects a series of infrared light patterns onto the scene and an infrared camera which records them to compute depth information. This device offers the capability to

⁴⁶ RealSense 435i: <https://www.intel.com/content/www/us/en/architecture-and-technology/realsense-overview.html>

produce 3D point clouds as well as depth maps and transmitting those to the RFSAT processing server for production of 3D models.

2.6.1.2. Visual Stereoscopic Scanning

The role of this component is to support acquisition of raster images for visual 3D modelling using stereoscopic vision technologies to be provided by RFSAT. Images will be acquired using a still camera (CANON EOS 5DS-R 50MP) mounted on a drone (UAS) with acquisition remotely (automatically) controlled by the operational console of RFSAT using its SDK. Raster images acquired at 50 Megapixel resolutions (RAW format also supported) can embed positioning information on the 3D scanning grid using geo-tagging within the Exif data, relative to the first acquired image. If embedding such information into the image file is not possible, an alternative of producing a separate file containing positioning information of each raster image will be produced and passed together with the collection of raster images to the RFSAT processing workstation.

The key technical specifications of a commercial camera used in the visual 3D modelling are summarized in Table 5. The role of the SW/SCAN component with respect to stereoscopic visual 3D modelling technology is to perform the acquisition of images with HW/VISDEPTH for subsequent production of the 3D model through SW/REG. All three components are part of the “*Global Scanning and Registration*” sub-system. The process of the acquisition of raster images by SW/SCAN component is as follows:

1. Control drone position with camera mounted on it at the START position
2. Control system triggers a camera remotely (wirelessly)
3. Control system moves drone the next position and takes another snapshot
4. Once all photos are taken, images are transferred to the control system
5. Images are Exif 2.3 geo-tagged or a file with image locations is created (see format below)

Format of the raster image tagging file:

Filename, X [m], Y [m], Z [m], ω [deg], ϕ [deg], κ [deg], Haccuracy [m], Vaccuracy [m]

NOTE: each row corresponds to each individual raster image

Parameters:

- X, Y, Z:* image coordinates
- Accuracy horizontal:* accuracy in axis parallel to the object
- Accuracy vertical:* accuracy of distance to the object
- Omega (ω):* rotation around the X-axis.
- Phi (ϕ):* is the rotation around the Y-axis.
- Kappa (κ):* rotation around the Z-axis.

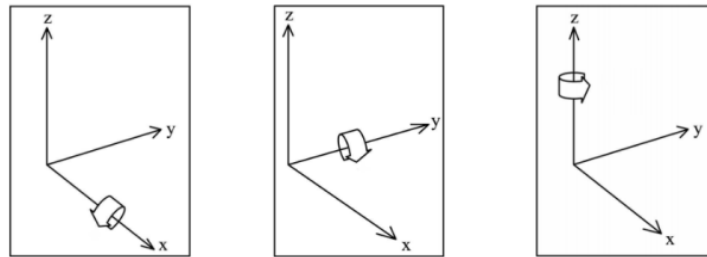


Figure 17: Interpretation of Omega (left), Phi (middle) and Kappa (right) parameters

Table 5: Technical specification of the camera used in the visual 3D modelling.

CANON EOS 5DS-R camera	
Resolution	50.6 megapixels, maximum full frame size: (L) 8688x5792
Speed	5fps
Weight	844 g
Dimensions	15.2 x 11.6 x 7.6 cm
Lenses mounting	EF (excludes EF-S / EF-M lenses)
Lenses	e.g. Canon EF-S 18-55mm f/3.5-5.6 IS II (25cm min. focus distance)
Data transfer interfaces	USB 3.0 digital terminal for fast transfer Supports Canon's WFT-E7 (Version 2) for wireless transfers Wi-Fi compatibility.
File types	JPEG: 2 compression options (Exif 2.3 compliant) RAW: RAW, M-RAW, S-RAW (14bit, Canon original RAW 2nd edition) Digital Print Order Format [DPOF] Version 1.1 compliant
Storage	CompactFlash Type I (UDMA 7 compatible), SD card, SDHC card or SDXC card. High-speed writing with UHS-I type SD cards is supported

2.6.1.3. Registration software

The function of the SW/REG component is to perform the final step of the 3D model creation that is the building of partial 3D views of the cultural assets from individual scanning modalities into a combined 3D model incorporating both outside and internal information about the historic object. Description of individual 3D modelling operations follows in sections below.

The part of the SW/REG component responsible for stereoscopic 3D modelling is hosted remotely in the RFSAT system. The reason for this is that specialised custom hardware development is required that is not easily portable for project trials. Ultimately, when ARCH system is mature for market, this component will become an integral part of a final product.

This technique is based on the principle of being able to determine relative distances among individual features of the remote object from differences in images taken some space apart, as if through human eyes. By taking advantage of high overlap among such images and the larger number of pictures seeing the same features, higher accuracy of determining distances can be achieved. Furthermore, by knowing precisely the position of the camera with relation to an object as well as by taking images at very high resolution (in excess of 50 megapixels), this allows producing 3D object exhibiting extremely high resolution and very small errors. It

has been estimated that with the camera to be used by HW/VISDEPTH, precisions reaching 50 micrometres can be realistically achieved for objects scanned at distances of 0.4-0.5 meters, alternatively 2cm accuracy can be reached from distances of nearly 40-50 meters.

Since developing software exhibiting such performance necessitates a very high amount of effort, while such software is already commercially available, the relative work in this project will focus more on integration of existing products into the processing chain in the ARCH system. Additional developments, through inter-project collaboration with the Pix4D team, explores means of achieving even higher processing accuracy for smaller historic objects exploiting additional depth information, while lowering the overall processing time through e.g., CUDA assisted parallel processing. The respective SW/REG component shall be provided as a black box with fixed data exchange interface, such that it will be possible to flexibly choose any of the COTS software packages for 3D modelling from raster images and/or a proprietary implementation that is currently pursued by RFSAT if and when it is sufficiently mature.

2.6.2. Communication interfaces

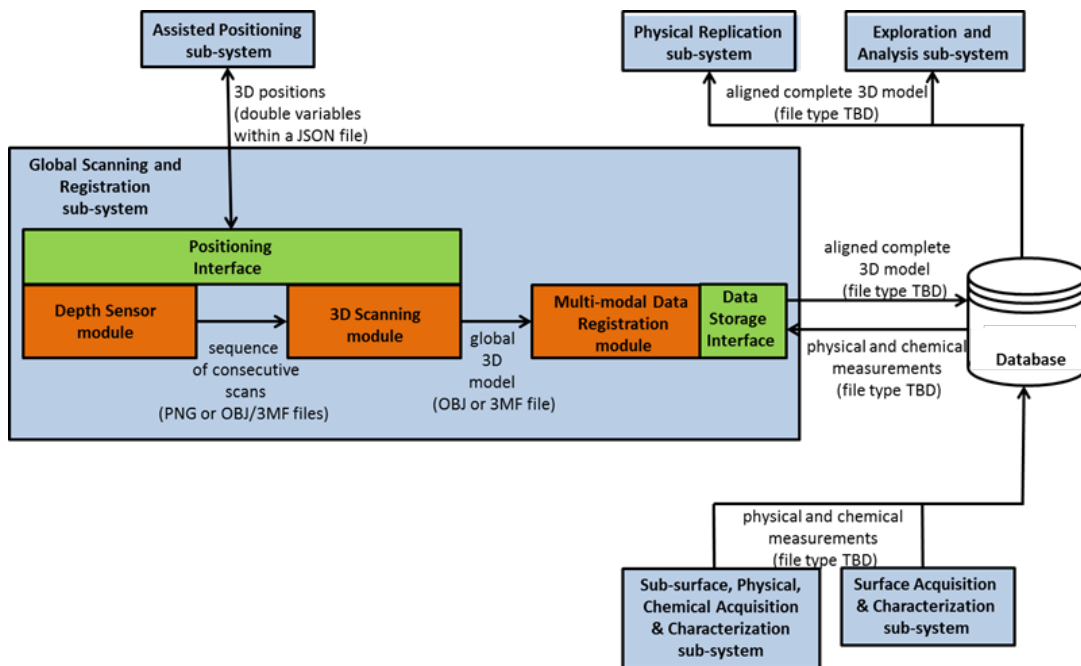


Figure 18: Communication diagram of *Global Scanning and Registration* sub-system

Figure 18 illustrates the information flow in the **Scanning and Registration** sub-system. The various modules (orange boxes) of the sub-system provide their results to another one as depicted, while the various interfaces (green boxes) enable the communication between the modules and the other sub-systems (light-blue boxes).

2.6.2.1. Control system

The RFSAT processing computer hosting a **Scanning and Registration** system has to satisfy specific SW / HW specification and communication capabilities listed below.

Depth Scanning

Operation

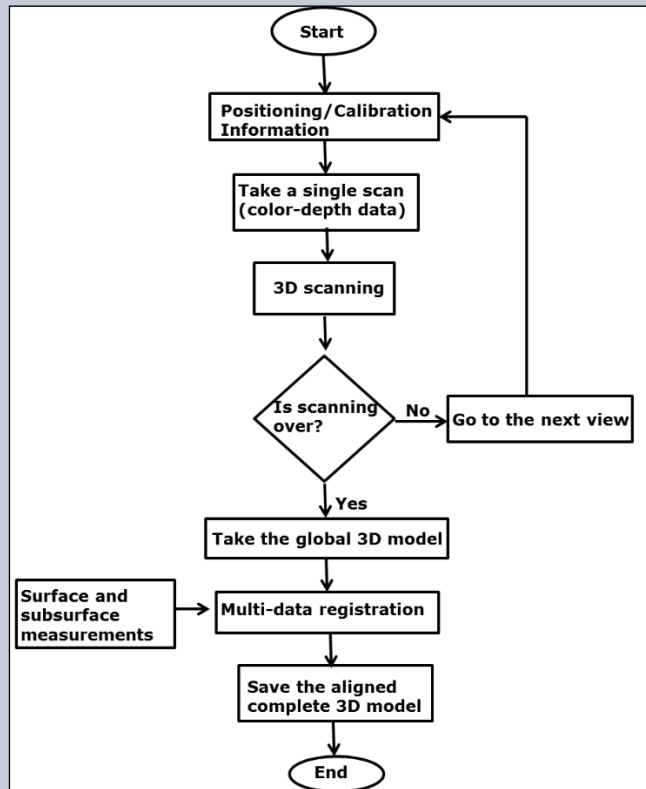


Figure 19: Algorithm for Global Scanning and Registration

Operating distance

All depth sensors have a working distance where the quality of depth information is adequate and, consequently, 3D reconstruction results in a reliable 3D model. Specifically, the effective range of the Intel RealSense F200 has a closer effective range (0.2-10 m), Structure sensor up to 15m and raster cameras from 1.5m to infinity.

Operating temperature

The operating temperature has to be from 10-25 C in order for the devices to function without problems.

Usability (Manual, Semi-Automatic, Automatic)

The user engagement to this sub-system is semi-automatic for the 3D reconstruction tool and automatic for the other components. The 3D reconstruction tool has pre-defined parameters, but the user may also change them, for example to select the type of another depth sensor (e.g., Intel Real Sense 435i, or older MS Kinect 2) or change some 3D reconstruction parameters (e.g., 3D reconstruction volume size).

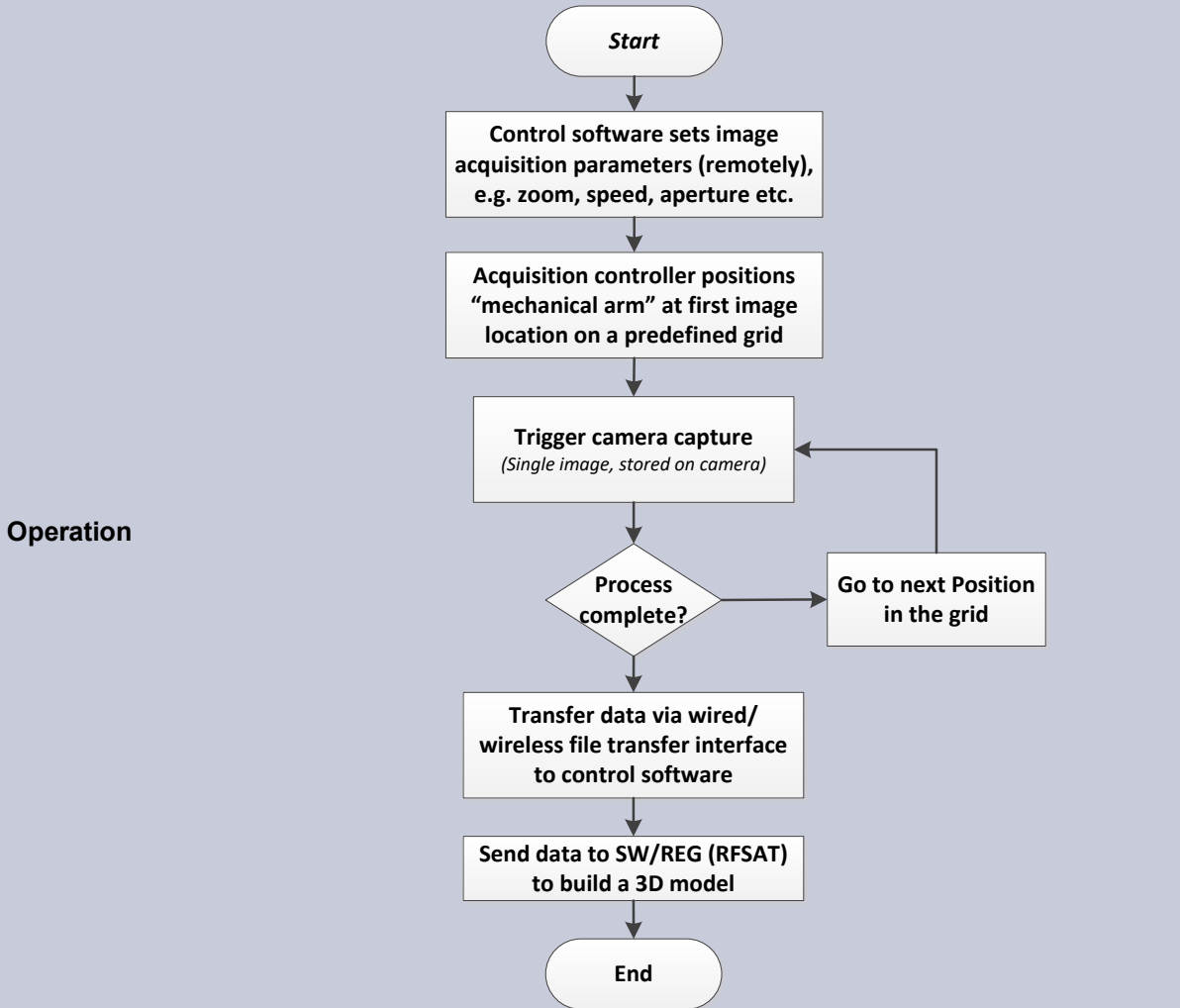
Calibration requirements

Calibration is required for the camera setup.

Special restrictions

Depth sensors are sensitive to intense light, while the 3D reconstruction may fail if the background is complex. Therefore, the environment, where the heritage assets are scanned, should be with controlled light conditions (in case of indoors) and without complex background. Outdoors, UV/light sensors are advisable, such that colour representation of model textures can be unified, especially in case of stitched scanning process.

3D Photogrammetric Scanning



Operation

Figure 20: Algorithm for 3D Photogrammetric Scanning

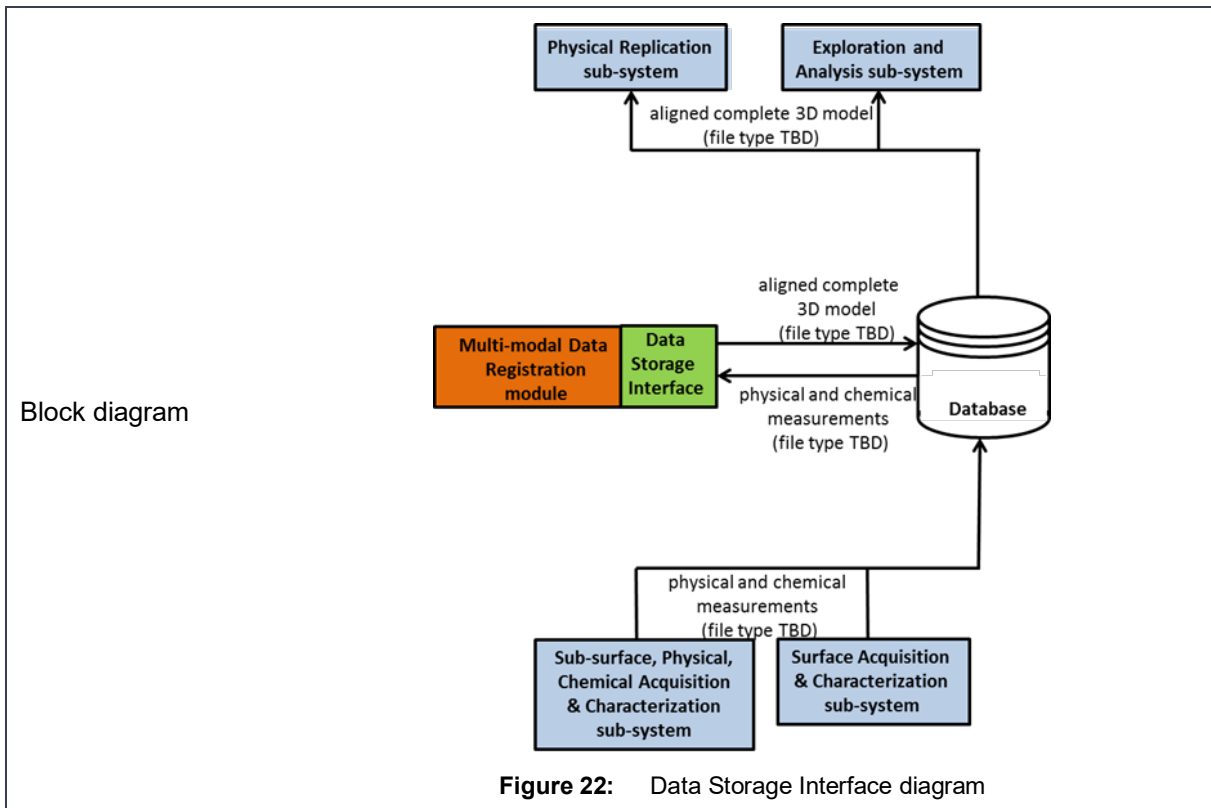
Usability (Manual, Semi-Automatic, Automatic)	Acquisition is intended to be fully automated. However, if needed, a user will have a capability to perform manual camera trigger via a remote.
Operating distance	Recommended distance to scanned objects is 0.4-0.5 meters, subject to using 56mm lenses. However, the distance can be alternated by changing zoom level or replacing camera lenses.
Operating temperature	The operating environment: 0-40 °C, 85% or less humidity.
Calibration requirements	The inherent property of the stereoscopic vision is that calibration can be performed within the 3D processing software by defining distances in three axes among reference points of the object. Hence no calibration is required during image acquisition, as long as camera settings are constant.

2.6.2.1.1. External Communication

External Interfaces	Positioning Interface
Description	The positioning Interface is responsible for the communication between the <i>Assisted Positioning</i> sub-system and the <i>Depth Sensor</i> and <i>3D Scanning</i> modules. Specifically, the <i>Assisted Positioning</i> sub-system provides the 3D position of the depth sensor and takes the updated 3D position as input from the “3D Scanning” module.
Block diagram	<pre> graph TD subgraph PI [Positioning Interface] DSM[Depth Sensor module] 3DSM[3D Scanning module] end PI -- "3D positions (double variables within a JSON file)" --> APS[Assisted Positioning sub-system] </pre>
Elements using the interface	<ul style="list-style-type: none"> • <i>Assisted Positioning</i> sub-system • “Depth Sensor” module • “3D Scanning” module
Message format (Communication protocols and/or file formats)	<ul style="list-style-type: none"> • <u>In memory</u>: 3D position is represented as 3 double variables. • <u>In disk</u>: They are stored within a JSON file. • When updating the 3D position of depth sensor, an appropriate acknowledgment message will be returned.
Function prototypes	<ul style="list-style-type: none"> • void get3DPosition(double &x, double &y, double &z): called by the “Depth Sensor” module to get the 3D position of the depth sensor provided by the <i>Assisted Positioning</i> sub-system • enum Flag{SUCCESS,FAIL} set3DPosition(double x, double y, double z): called by the “3D Scanning” module to update the 3D position of the depth sensor

Figure 21: Assisted Positioning diagram

External Interface	Data Storage Interface
Description	<p>The <i>Data Storage</i> Interface is responsible for the communication between the THIS database and the <i>Data Registration</i> module. The module takes surface and subsurface measurements provided by the Sub-surface, Physical, Chemical Acquisition & Characterization and the Surface Acquisition & Characterization sub-systems, while its output is used by the Physical Replication and the Exploration and Analysis sub-systems.</p> <p>NOTE: Chemical Acquisition and Characterisation module has been built in RFSAT earlier SCAN4RECO project by another partners and thus in ARCH it requires relevant material characterisation info to be provided by hosts of historical assets for their objects in THIS database. Based on this info further material ageing can be performed as described in section 5.4 of the D4.2.</p>



<p>Elements using the interface</p>	<ul style="list-style-type: none"> • Surface, Physical, Material Acquisition & Characterization sub-system • Surface Acquisition & Characterization sub-system • Physical Replication sub-system • Exploration and Analysis sub-system • Data Registration module, linking acquired data with physical objects
<p>Message format (Communication protocols and/or file formats)</p>	<p>Processed (filtered, compressed) data and features representing the physical and chemical measurements from THIS to describe material composition. A single data structure with the aligned complete 3D model (THIS)</p>
<p>Function prototypes</p>	<ul style="list-style-type: none"> • <code>getSurfaceProcessedData</code>: called by the <i>Data Registration</i> module to get the processed data corresponding to the physical and chemical surface measurements/data from THIS database • <code>getSurfaceFeatures</code>: called by the <i>Data Registration</i> module to get the features corresponding to the physical and material surface measurements/data from THIS database • <code>getSubsurfaceProcessedData</code>: called by the <i>Data Registration</i> module to get the processed data corresponding to the physical and chemical (material) measurements/data from ARCH database • <code>getSubsurfaceFeatures</code>: called by the <i>Data Registration</i> module to get the features corresponding to the physical and chemical (material) measurements/data from THIS database • <code>setAlignedComplete3DModel</code>: called by the <i>Data Registration</i> module to set the single data structure containing the aligned 3D model to the ARCH database at THIS <p>NOTE: in the current revision of THIS database, 3D models are stored in their original format as provided by hosts of the historical assets, which may require on the fly translation to FBX format before a structural analysis can be performed (originally developed for FBX models using Autodesk FBX SDK).</p>

2.6.2.1.2. Internal Communication Interfaces

Internal Interface	“Depth Sensor - 3D Scanning” Interface
Description	This internal interface is responsible for the communication between the “Depth Sensor” module and the “3D Scanning module”. The “Depth Sensor” module provides the consecutive scans captured by the depth sensor to the “3D scanning” module for performing 3D reconstruction.
Block diagram	<pre> graph LR A[Depth Sensor module] -- "sequence of consecutive scans (PNG or OBJ/3MF files)" --> B[3D Scanning module] </pre>
Elements using the interface	<ul style="list-style-type: none"> • “Depth Sensor” module • “3D Scanning” module
Message format (Communication protocols and/or file formats)	<ul style="list-style-type: none"> • <u>In memory</u>: A sequence of pcl::PointCloud objects. pcl::PointCloud is a class in PCL project for storing collections of 3D points. Each point is represented by the pcl::PointXYZRGBA struct with 3 double variables (x, y, z coordinates) and 4 unsigned char variables (r, g, b, a values). Alternatively, two sequences of unsigned char and double matrices containing the colour and depth information, respectively. • <u>In disk</u>: A sequence of OBJ or 3MF files containing the colour and depth information of consecutive scans. Alternatively, two sequences of PNG files containing the colour and depth information of consecutive scans, respectively.
Function prototypes	<ul style="list-style-type: none"> • void getNextScan(pcl::PointCloud<pcl::PointXYZRGBA> &scan): called by the “3D Scanning” module to get the next scan captured by the depth sensor. • void getNextScan(double[][] depth, unsigned char[][] color): called by the “3D Scanning” module to get the next scan captured by the depth sensor.

Internal Interface	“3D Scanning - Multi-modal Data Registration” Interface
Description	The “3D Scanning - Multi-modal Data Registration” Interface is responsible for passing the generated global 3D representation to the “Multi-modal Data Registration” module.
Block diagram	<pre> graph LR A[3D Scanning module] -- "global 3D model (OBJ or 3MF file)" --> B[Multi-modal Data Registration module] </pre>
Elements using the interface	<ul style="list-style-type: none"> • “3D Scanning” module • “Multi-modal Data Registration” module
Message format (Communication protocols and/or file formats)	<ul style="list-style-type: none"> • <u>In memory</u>: A pcl::PolygonMesh struct for representing the generated 3D model. pcl::PolygonMesh is a struct in PCL library and represents the 3D points and the faces of a 3D model. • <u>In disk</u>: An OBJ or 3MF file.

Function prototypes	<ul style="list-style-type: none"> void get3DRepresentation(pcl::PolygonMesh &mesh): called by the <i>Data Registration</i> module to get the global 3D model generated by the <i>3D Scanning</i> module
---------------------	---

Internal Interface	Visual Stereoscopic Scanning Interface
--------------------	--

Description	<p>This interface includes both the data transfer and control signalling. The first one is a dummy file transfer that may be executed over any IP protocol, e.g., FTP, HTTP and/or other. The latter one is the programming interface over IP that allows controlling the execution of jobs by either the image acquisition or execution of 3D modelling. The latter one also offers messaging allowing to monitor the progress and notification about completing the processing, allowing for transfer of the resulting models from RFSAT component back to the control system.</p> <p>The role of the <i>Query Process</i> (developed by RFSAT) deployed on the control system initiates the 3D model processing and monitor its progress, giving a notification to the software operating on the controller when it has completed such that the model can be downloaded from the remote processing system onto the controller.</p> <p>File transfers between the controller software and remote processing system by RFSAT is via FTP/FTPS protocol over IP. Alternatively, HTTP/HTTPS protocol can be utilized.</p> <p>The overall management will be up to the Control System, which will both control the image acquisition, as well as their subsequent processing to produce the 3D model.</p>
-------------	--

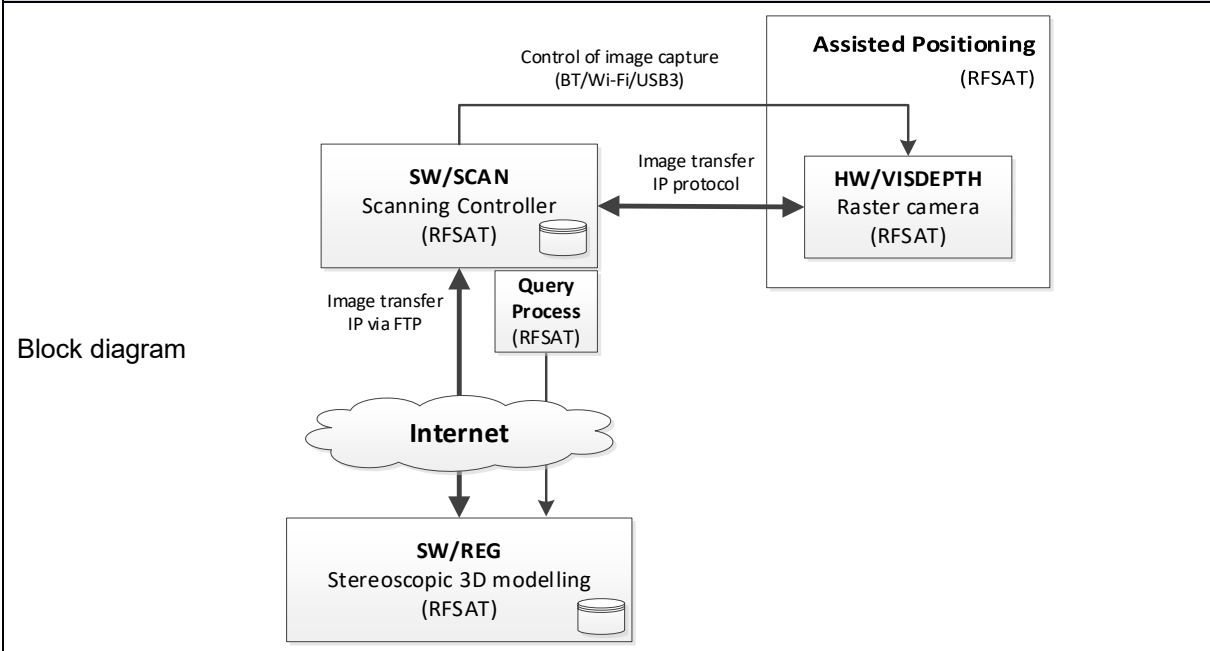


Figure 23 Data Storage Interface diagram

Elements using the interface	<ul style="list-style-type: none"> Raster camera SW/SCAN SW/REG
------------------------------	--

Message format	<u>Camera configuration</u> : Remote user Interface (HTTP) provided by CANON
----------------	--

	<p><u>Camera positioning</u>: Existing I/F for HW/POS built for UAS by RFSAT</p> <p><u>Image transfer I/F from camera</u>: FTP protocol via IP using USB3 or Wi-Fi</p> <p><u>Camera image trigger I/F</u>: remote software trigger (RFSAT)</p> <p><u>Data storage</u>: Persistent storage on the SD card embedded into the camera and temporary storage on the control workstation until the 3D model has been produced by SW/REG.</p>
Special restrictions / considerations	<p>The remote processing system of RFSAT shall keep a copy of images for all scan jobs, such that the controller can be relieved from keeping own copies. This way the 3D models pro-cessing can be re-done with different settings (e.g., to improve quality) without re-sending images again.</p>

2.7. Autonomous 3D aerial scanning

An important component for enabling automated 3D scanning in the system described above is the acquisition platform. In earlier projects like SCAN4RECO, an automatic arm moving the camera between image capture locations was used to ensure an optimum number of images taken at precisely known 3D locations such that to achieve required micrometre resolution of the resulting 3D model. A system like this was unfortunately bulky, non-portable and restricted to scanning of objects limited in size to not more than 3 meters. As a result, its applicability in its original form to the needs of ARCH pilot sites was very limited. In the ARCH project, the need is to perform large scale and wide area scanning of specific areas of interest rather than general scanning of the complete pilot area, especially that those pilot sites often have such overview 3D models of their respective areas already performed, even if not always recently.

Therefore the work in ARCH has pursued in the direction of complementing indoor fixed arm camera positioning system with use of cameras on-board of drones, in particular micro ones for their flexibility and low cost. Use of such drones as camera positioning system introduced also several complexities. For one, positioning of drones in outdoor spaces is less reliable due to inaccuracies brought in by errors in GNSS positioning from satellites, weather effects (especially winds and gusts pushing drones away from required position), variations in pitch and elevation when drone compensates for its drifts and other ones. Furthermore, RFSAT has investigated its earlier conceptual work in the FP7-AF3 project to autonomous operation of drones and in particular in using them in swarm formations for faster image acquisition, better area coverage and leveraging multiple drones for increasing the operational time of all drones in total as compared to a single one able to operate for not more than 20-30 minutes.

As such the system of controlling swarms of autonomously operating UAS / UAV become an integral part of the “*Positioning Interface*” mentioned in the beginning of section 2.6.2.1.1 with (optional) micro-sensors deployed on the same drones and feeding their data into the ““*3D Scanning - Multi-modal Data Registration*” Interface” described in the same section. The Figure 24 presents a concept architecture of the drone control system developed by RFSAT for automated scanning and analysis of heritage assets (objects and structures) for various types of deficiencies. It contains a Ground Station with a range of supported UAS/UGV/UUV drones that can be operated either manually (legal requirement) and automatically for capturing visual material (image and/or video) that can then be used to build 3D models of the objects and perform automated, neural-network assisted analysis for detection of various types of defects, from cracks to discolorations and physical damages.

The 3D modelling is mainly based on 3D photogrammetry and employs two different engines, depending on application, one being the PIX4D engine that operates on a dedicated RFSAT multi-GPU server, while the Autodesk engine offers the capability of using a cloud processing engine. An API for using both services has been developed by RFSAT for assisting integration into custom applications built with Microsoft Visual C++ 2019 IDE.

The analytics algorithm uses Machine Learning and Artificial Intelligence methods and thus requires prior teaching using example images of similar defects. The COVID outbreak has prevented RFSAT to acquiring actual data from ARCH pilot sites (such as rock foundation under Devin Castile in Bratislava, Huerta in Valencia, foundations of the Hamburg canals etc) and hence development of algorithms has been significantly handicapped with serious risk of not being able to produce operational system. To mitigate this risk to a reasonable level, the development has progressed with data limited to already existing 3D models of similar objects as those expected to be scanned and analysed from Open Source repositories of 3D models. In particular 3D models of mountain cliffs with various types of cracks have been used, example of which can be seen in Figure 24 for the Failles graben Gandailat Puy de Dôme France downloaded from Sketchfab⁴⁷.

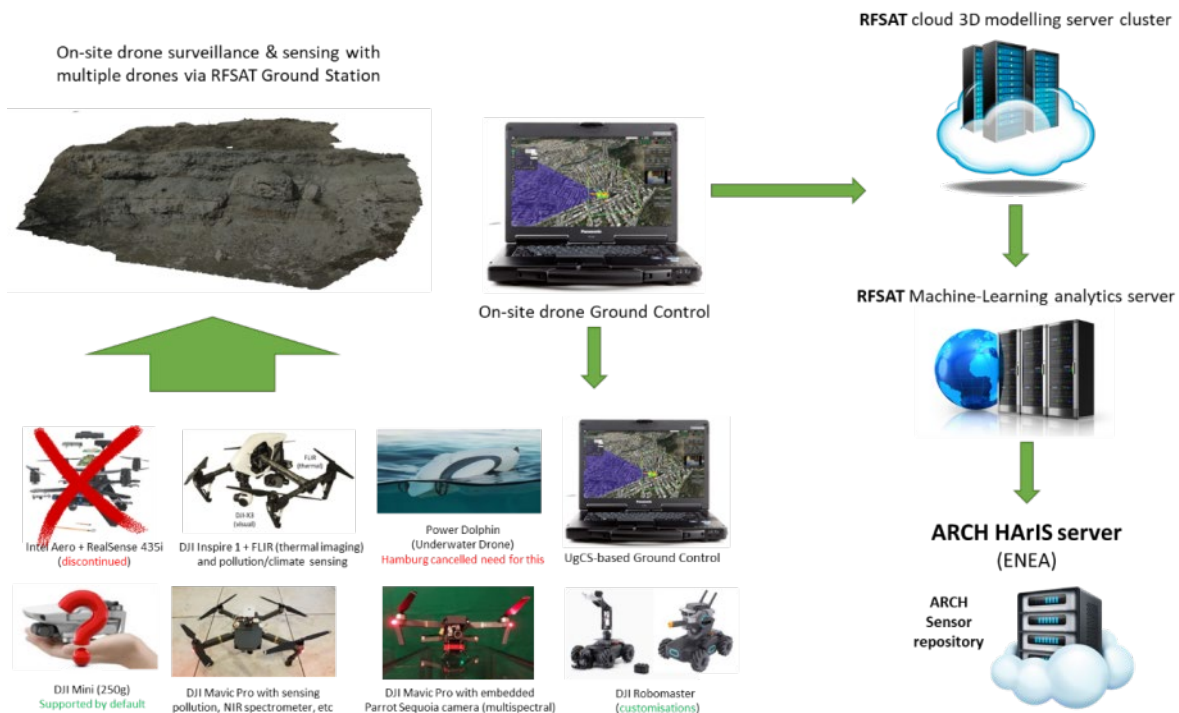


Figure 24 RFSAT automated 3D scanning and analysis of degradations to Heritage Assets

To produce the “input” images needed for the 3D modelling system and subsequent structural analysis of defects such as dangerous rock erosions, the existing 3D model was loaded into a gaming Unreal engine where it was “re-scanned” as if it was done using drone acquisition system. Such an approach has allowed us to simulate operation of a real system in synthetic environment. This had also an added benefit of reducing risks in crashing drones in case of errors in our ground flight control components. As it happened a live test of the system has

⁴⁷ <https://sketchfab.com/3d-models/failles-graben-gandailat-puy-de-dome-france-e7b59195dc6e41d8944eb9f97b88fbc3>

actually ended up with a drone crashing into the mountain rock (test performed in Crete, Greece). The images from simulation are fed to the RFSAT cloud modelling server as it would have been done in normal system operation, thus producing 3D models, suitable for both uploading them in their original form to THIS repository of INGV for use by end-users and to the RFSAT analytics server to search for high-risk degradations, results of which to be then transferred to the HARIS for possible further processing and visualisation by end users.

As shown in Figure 24, various types of drones can be used, a selection of which has been made after various co-creation meetings with pilot representatives. Such drones are primarily aerial ones (for all pilot sites purposes), semi-submerged UUVs (responding to Hamburg needs to scan underwater foundations of warehouses in its canal area), with an option to include also a ground drone (UGV) for possible future use in rural areas of Valencia.

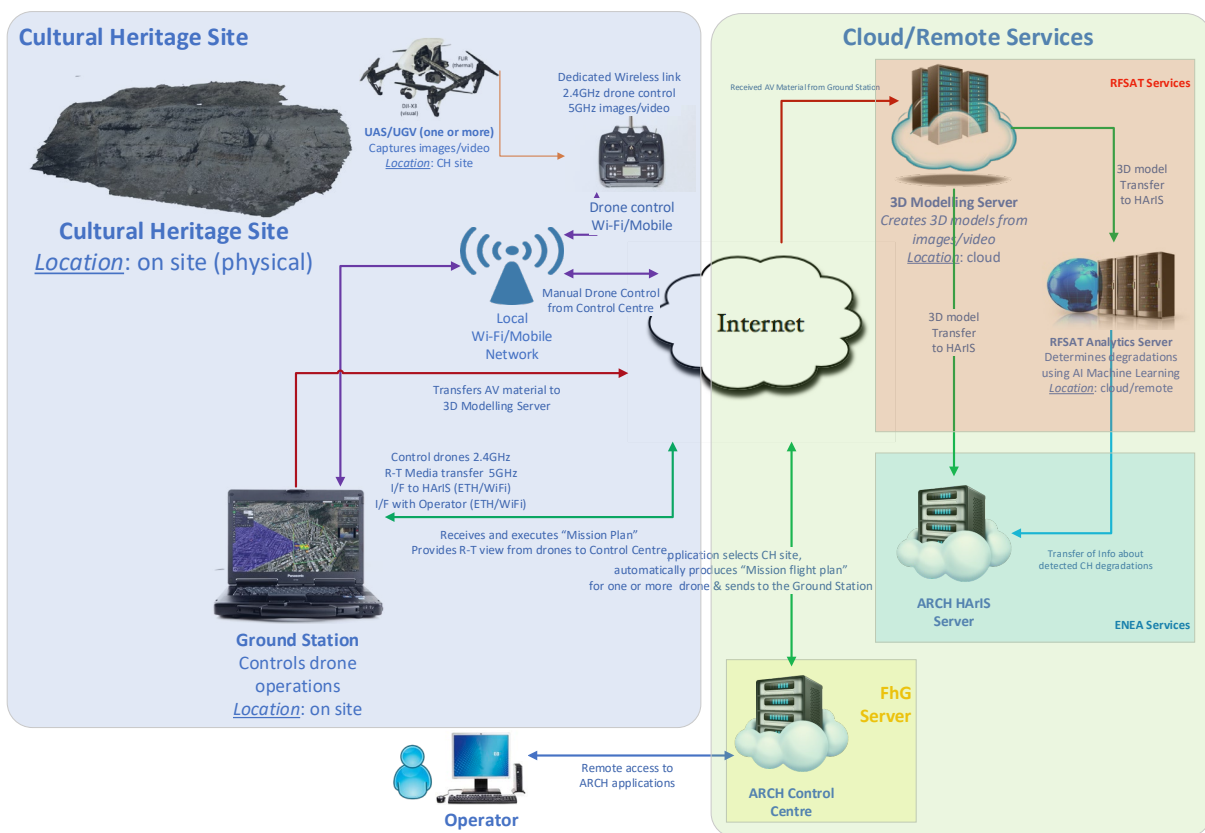


Figure 25 Physical architecture of RFSAT automated 3D scanning & analysis of degradations

A physical architecture of the system from Figure 24 is shown in Figure 25. It distinguishes among parts of the system that physically reside at different physical locations:

- Physical site of the Heritage Assets, where the following components are located:
 - **Ground Station**, installed on a Panasonic Toughbook with on Win10 aimed to:
 1. receive flight plans (file) from RFSAT app on the ARCH Control Centre
 2. launch & operates drones in automated mode to execute flight plan mission
 3. acquire visual material (images & video) of the CH site from various angles
 4. send visual material to RFSAT 3D Modelling Server (see below)

5. send directly (option) visual material to RFSAT Analytics Server (see below).
- **Drones** e.g. UAS (aerial), UGV (ground) and UUV (underwater) along with either their **Remote Controller** (preferable for extended control distance, communicating with drones using e.g. DJI Lightbridge 2⁴⁸ for up to 5km) and/or mobile devices with custom application and connected to drones via Wi-Fi (limits distance to less than 300meters in open space).
 - **Local wireless network access point** and/or cellular access network to ensure reliable network connectivity among parts of the system at CH site.
 - Remote and/or cloud-based services:
 - **RFSAT 3D Modelling Server:** operates in two (selectable) modes, as cloud services or on a multi-GPU parallel processing server installed at RFSAT offices. Two engines are available: PIX4D and Autodesk. An API written in MS-VCPP2019 has been developed to enable integration of 3D modelling into custom applications.
 - **Ground Control Centre (GCC):** provided by RFSAT to manage automated drone missions and 3D photogrammetric scanning of CH objects and areas. The RFSAT application will allow selection of the CH site and based on its structure to derive a flight plan for drones such that to acquire required audio-visual material, as required for performing 3D modelling and/or image-based analysis of degradations to CH structures. Semi-automatic approach will assist users in building a mission plan.
 - **RFSAT Analytics Server:** based on images acquired from drones of the CH site (optionally also the 3D models of the site from RFSAT 3D Modelling Server) will perform AI-based and Machine Learning driven analysis of the images and/or 3D model to determine type, location, and significance of degradations of CH object. This server operates on an embedded UP2 embedded computer⁴⁹ running Linux with Intel Movidius Vision Processing Unit (VPU)⁵⁰ employing neural network co-processor for faster data analysis.
 - End-user location:
 - **User Terminal:** used by end users to access ARCH applications from the GCC for any remote site. It can be either a workstation/laptop, tablet, or mobile phone

The Figure 26 presents a brief overview of the autonomous drone management system. It supports not only control of single, but also swarms of drones operating simultaneously. Note that all system components communicate using TCP/IP networking protocol. The components of the RFSAT system offer an API for integrating its functionalities into custom applications developed with MS Visual C++ 2019. Mobile applications (e.g. drone control) run on Android operated terminals and/or mobile phones.

⁴⁸ Lightbridge: <https://www.dji.com/gr/lightbridge-2>

⁴⁹ UP2 embedded computer: <https://up-shop.org/>

⁵⁰ Intel Movidius Vision Processing Unit (VPU): <https://www.intel.com/content/www/us/en/products/details/processors/movidius-vpu/movidius-myriad-x.html>



Figure 26: Autonomous drone operation from RFSAT

The main principle of operation is full compliance with EASA regulation governing the operation of civilian drones within EU Member States both for recreational and professional purposes. The implication is that despite capabilities to perform autonomously, the RFSAT system offers backup manual operation that can be switched to in case of need. This operates both in Line of Sight (LoS) operation as well as in Beyond Line of Sight (BLoS) missions. As shown in the figure, all drones are controlled from a Ground Station from a durable Panasonic CF-33 portable PC, which can be in principle located anywhere, either in the field (preferable option to ensure better video streaming especially for multiple UAVs) or at a remote location such as the host offices. Note that multiple Ground Stations can be used at different locations with capability of sharing their respective drones among them. The system supports live streaming of camera feeds from all of the drones operated from any of the Ground Stations.

The system operation starts with a definition of the scanning scenario, based on the size (3D dimension of the heritage asset to scan/survey), analysis of 3D obstacles, analysis of area flight restrictions, available permission to fly from local flight authorities etc. Once all conditions are satisfied, a mission plan is generated for either one or multiple UAVs, leaving it to the operator to do the manual check before launching the mission. Once it happens, individual flight plans are transmitted to each of the drone flight controllers, initiating their individual missions. Once all drones complete their missions, they automatically return to base (where they took off from). Once engines safely switch off, images and videos captured onto onboard memory is transferred to the Ground Station and then to the 3D processing server to produce 3D models of the surveyed area. At this point manual intervention is also possible to e.g. limit the processing area, modify quality options, types of file formats of models and point clouds, etc.

The system supports any type of a network, including mobile broadband for communication between Ground Station and the individual flight controllers for each of the individual drone. This directly permits them to operate at large distances in BLoS scenarios, such as when scanning large historical areas such as Huerta in Valencia or in complicated urban environments of Camerino, Bratislava or Hamburg. Since use of mobile broadband requires use of public operators, it is advisable that 4G-LTE or 5G networks are used for achieving best streaming performance and operational control, even though backup systems are offered for dealing with unexpected conditions like loss of connection to the Ground Station or the flight controller, impeding collision risk etc. In such cases various types of recovery actions kick in, from Return to Home (RTH), auto collision avoidance to manual override. A fast broadband connection is especially useful when taking advantage of the optional Virtual Reality headset for First Person View (FPV) experience when viewing video streamed from cameras of any of the drones. In the test setup either a mobile broadband Wi-Fi router from local operator or a global one (such as from Skyroam⁵¹ in case of demos at pilots sites) is used with dedicated Livestream Broadcaster⁵² device

The future list of options will include dynamic update of mission parameters mid-flight and improve collision avoidance among drones taking part in the same operation, which has been so far disabled due to losses of several vehicles due to accidental crashes, until simulations of such algorithms are completed successfully.

⁵¹ Skyroam Solid Wi-Fi hotspot: <https://de.simo.co/solis-wifi-hotspots-eu>

⁵² Livestream Broadcaster Pro: <https://livestream.com/broadcaster>

2.7.1. Development and Test Conditions

The current functional development supports the following operational platforms:

- Android application environment: Android Studio, DJI Mobile SDK, latest Android API
- Mobile OS Compatibility: Android 4.4 (KitKat) or later, both phones and tablet targets
- Server OS compatibility: MS Windows 10 (64-bit)
- Drone types supported: DJI Inspire v1 and v2, Mavic Pro, Matrice 200/300/600
- Test environment:
 - DJI Mavic Pro with Android Assistant as a simulation environment
 - UgCS Ground Station for simultaneous control of multiple aerial drones
- Mission Definition format support:
 - DJI format from DJI Ground Station for Windows
 - UgCS mission definition



Figure 27 Unreal synthetic test environment in flight mode over synthetic cliff and castle (DJI Inspire drone)

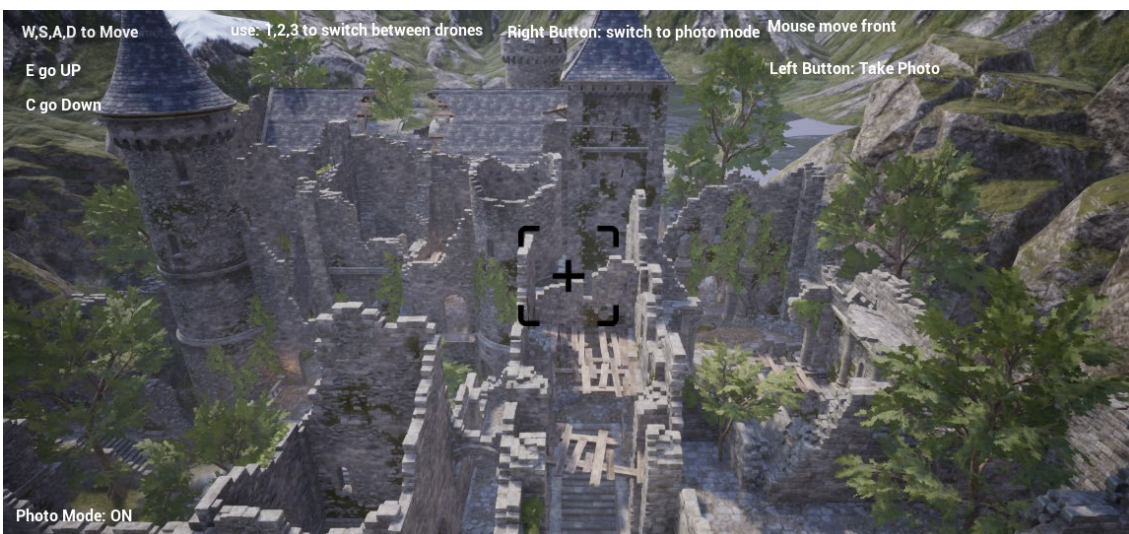


Figure 28 Unreal synthetic test environment in image capture mode for 3D photogrammetry testing

The system has been built with SDK support for integrating automated drone control with 3D photogrammetry under Microsoft Visual Studio 2019. It includes integration options via pre-compiled static and dynamic libraries (DLL) with full source code, if preferable.

In order to mitigate risks associated with lack of physical access to pilot sites during COVID imposed travel restriction period, RFSAT has built a synthetic Virtual Reality environment for simulating drone control and image capture without a need to operate actual drones.

For this purpose Unreal Engine version 26 was used to build, offering the following capabilities:

- Selectable (switchable) UAV/UAS types, currently supporting the following drones: DJI Inspire 1, DJI Phantom class and DJI Mavic class, all with embedded HD cameras
- Flight mode for testing drone controls (Figure 27)
- Image capture mods for acquiring images for 3D photogrammetry (Figure 28)
- Import of synthetic/real 3D environments in FBX format, e.g. models of real (pilot?) sites

2.7.2. Features supported

- Mobile Application (Android):
 - Loads and executes a flight mission (waypoints with custom operations: height, heading, speed, action etc.)
 - Flight mission can be modified, such as waypoints on the map and types of operation
 - Mission definition file downloaded from: local storage, WEB link or shared repository
 - Option to send status of mission execution to the server application
- Server WEB Application (MS Windows):
 - Loads missions for all drones from WEB repository or uploaded to Ground Control
 - Displays current location of all drones on Google Maps
 - Option to display the whole mission for the selected drone
 - The mission can be aborted/modified (new one uploaded) at any time
 - Routes and actions assigned to drones can be manually overridden at any time
 - Drones are in constant contact with Ground Station, otherwise Return To Home (RTH) is executed in compliance with FAA rules
 - Swarms of UAV aircrafts on multiple missions simultaneously (under development)



Figure 29 UgCS Ground Mission Control of multiple drones

2.7.3. Planned future developments

The current developments offer complete and functional system that allows automated 3D scanning of a required object or area by either one or more drones, operating either simultaneously or in a sequence, i.e. complementing one another in capturing the whole view

of the scanned object. However, in order to be fully autonomous, further developments and functional tests are still required for avoiding collisions between the drone and the scanned objects, including collision avoidance among drones operating at the same time. Therefore, when using the current version it is advisable to continuously monitor operation of drone such that any technical problems can be avoided. The swarm mission operation is currently semi-automatic and may occasionally require manual intervention. The system has been currently built to manually define the area of operation as part of the safety precaution. In the next version, it will be sufficient to choose an object for the system to derive the flight paths and employ safety margins. Lastly, to comply with European drone regulation from EADSA⁵³, the integration with online systems from national flight authorities shall be implemented to automatically register the flights and acquire necessary permissions for conducting drone flights as specific locations and times.

2.8. Multispectral surveillance technologies

Multispectral scanning from UAV/UAS devices has been developed in response to the needs of the Valencia pilot for monitoring the health conditions of Huerta agricultural areas, considered as the heritage of this region.

To perform such an analysis there was a need for aerial surveillance system capable of surveying large areas. Unmanned systems were the first and most obvious choice, necessitating a need for a micro lightweight sensor capable for detecting health conditions of crops. Satellite observations were another obvious option, but due to their low spatial resolution they can be only used for a global view of large areas, in the range of nations to regions, but quite unsuitable for in-situ checks of specific fields. Therefore, drones have been suggested as such a precise monitoring system.

The overview of the two land monitoring approaches is shown in Figure 30, from satellite observations by INGV in Figure 30a (showing Normalized Difference Vegetation Index $NDVI = \{NIR - Red\} / \{NIR + Red\}$ and/or other Indicators for vegetation health & biomass), and low altitude surveys using unmanned aerial systems by RFSAT, using DJI Mavic Pro equipped with Parrot Sequoia⁵⁴ multispectral imaging device installed on a drone using a purpose-built mount. Test maps shown below it indicate health conditions of a forest area alongside the 3D model of the area. Note that such drones can be operated autonomously using the system of RFSAT shown in section 5.

One of the most suitable multi-spectral cameras fitting the needs of the monitoring, while also small enough to fit on even micro aerial devices, was Parrot Sequoia. Such a multispectral sensor is a multi near-IR camera solution that can be mounted on a variety of micro drones with simple mounts such as one built by RFSAT for DJI Mavic Pro and shown in Figure 30. With its two sensors, multispectral one (16MP RGB visual, 1.2MP green 550 BP 40, 1.2MP red 660 BP 40, 1.2MP red edge 735 BP 10 and 1.2MP near-infrared 790 BP 40) and sunshine (UV) sensor, the Parrot Sequoia+ can analyse plants' vitality by capturing the amount of light

⁵³ EASA Civil Drone regulation: <https://www.easa.europa.eu/domains/civil-drones-rpas>

⁵⁴ Parrot Sequoia: <https://www.parrot.com/en/shop/accessories-spare-parts/other-drones/sequoia>

they absorb and reflect. A combination of 3D ground envelopes from photogrammetric scanner and 3D vegetation health models and multispectral images, offers valuable data for understanding what is best for vegetations in the large area fields. This is perfect for rapid and effortless monitoring of health condition for vegetations in the Huerta area in Valencia.

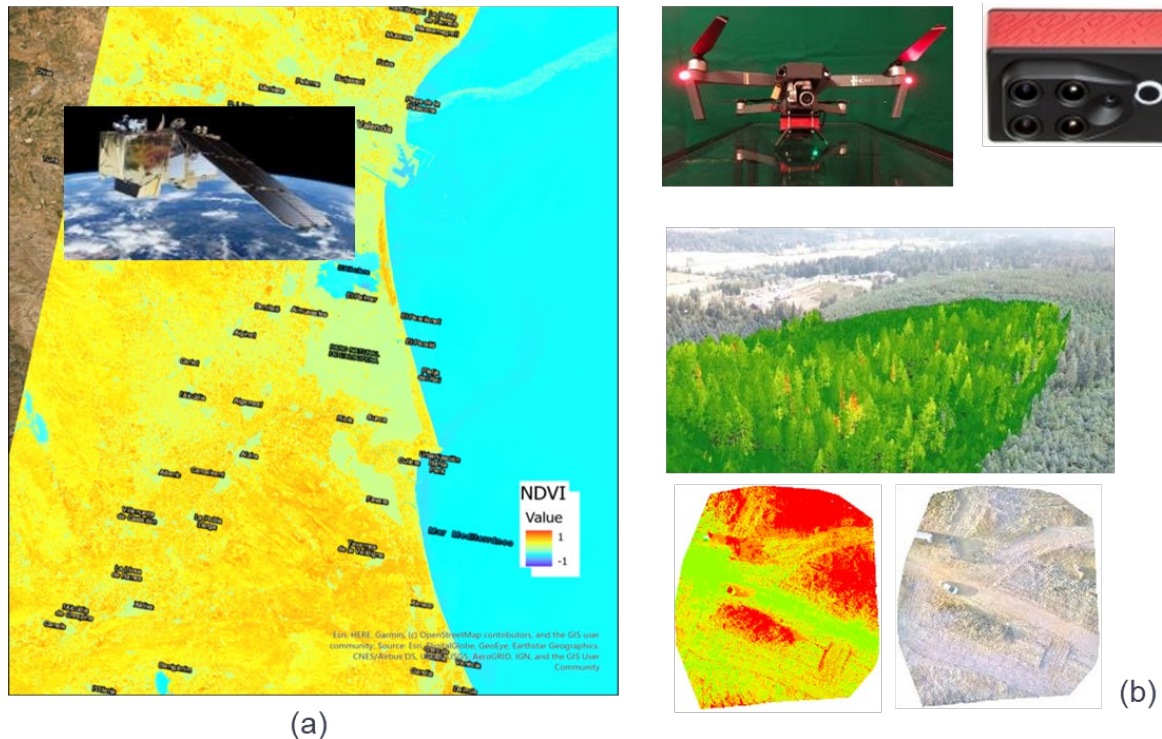


Figure 30: Satellite imaging by INGV (a) vs. UAV vegetation monitoring by RFSAT (b)

The RFSAT aerial surveillance system that was developed for 3D scanning and modelling in mind was readily adapted to accepting also multispectral images from the Parrot Sequoia. Thanks to the wireless interface embedded into the camera and its WEB based GUI, it can be both configured and managed in remote fashion, even during the flight. Similarly, images can be offloaded from the memory card embedded into the camera during the flight in lower resolution for quick check, while high resolution version can be downloaded on return to base.

Subsequently, multispectral processing of the data acquired from Sequoia can be performed automatically using an add-on to the same SDK developed by RFSAT for 3D modelling.

2.8.1. Experiments with land monitoring using UAVs

The proposed semi-automatic method using 3D photogrammetry algorithm described earlier in section 2.4 allows for low-effort estimation of the volume of historical objects present in the investigation area (also for preventive area scanning) from 3D models of the area built out of the geocoded images acquired e.g., from low-altitude UAVs or even fly-byes by mi-UAVs or even remote-control model planes or human controlled aircrafts, described in section 2.7.

The 3D modelling approach uses stereoscopic vision algorithms operating on multiple images of the same area (taken from different positions). The process of execution scanning mission and building the general 3D model of the area of interest has been described in section 2.4. In

this section we follow up by describing the method of terrain object classification within the observation area where 3D volume of e.g., forestation can be then determined in cubic meters.

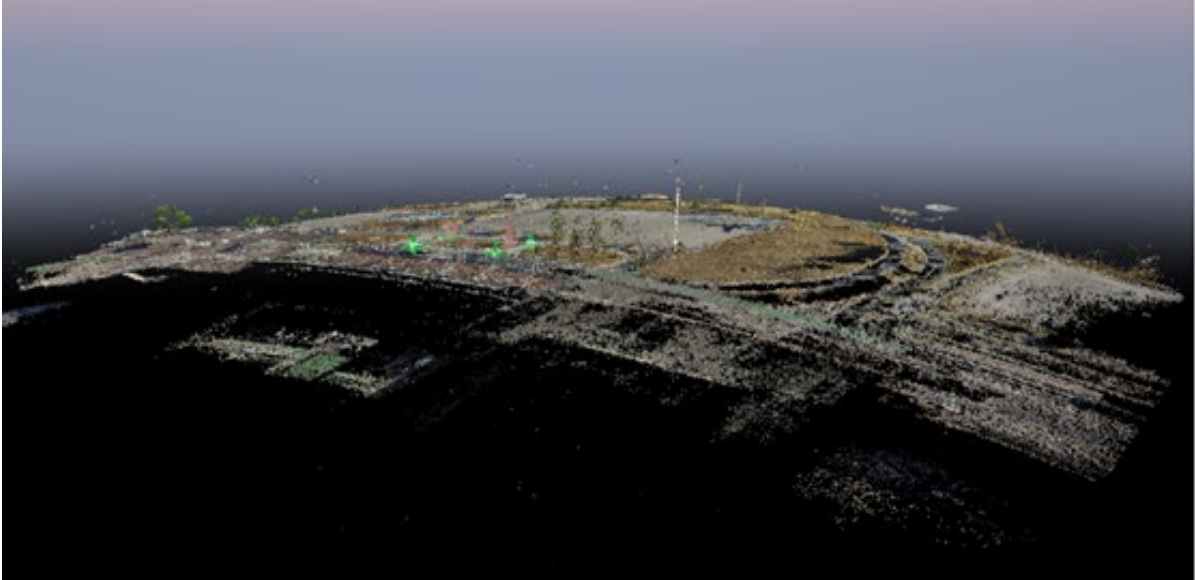


Figure 31: False ground level bending when UAV is moving during image capture

By combining this information with characteristics of the plants with environmental conditions, it is theoretically possible to determine the condition of the forestation and risks of e.g. from natural disasters like wildfires during draught periods, directly relevant to Huerta in Valencia [2], [5], [38]. The area first requires low level aerial scanning, preferably using regular grids, ensuring that images are taken vertically down at each capture point. In case images are taken from a moving aircraft and not directly down, there is a possibility that the resulting 3D model will exhibit false ground bending as shown in Figure 31, taken over the abandoned airport in Athens, where high altitude flights with UAS systems have been authorised to be conducted for research purposes to test technologies developed for ARCH.

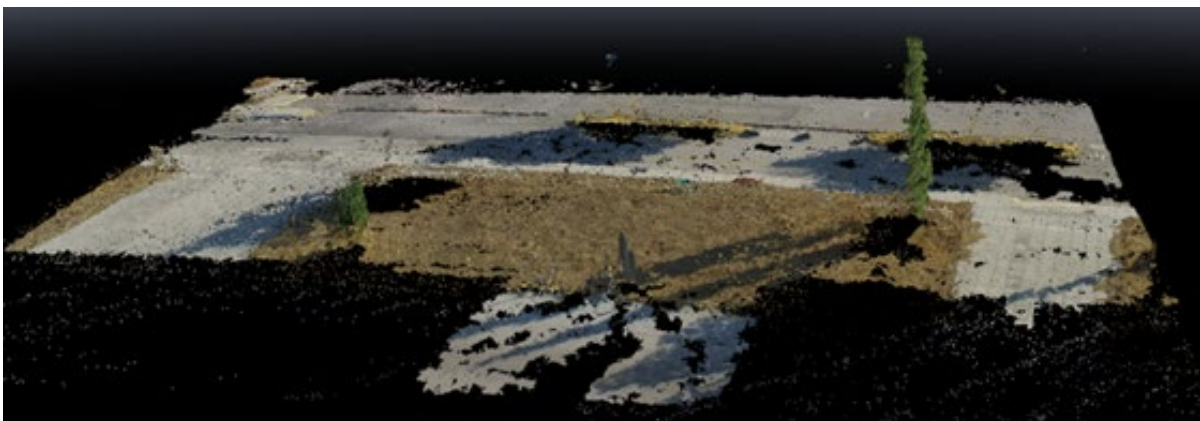


Figure 32: Zoom on the area of interest

Nevertheless, in case of a low speed and sufficiently high altitude with respect to the area under observation, this effect can be sufficiently negligible, as in Figure 32, where we zoomed onto the area where we intended to assess the amount of tree volume.

2.8.2. 3D Area Mapping

The next step is to build a 3D point cloud, from which a 3D mesh of the model can be built. Nevertheless, for the assessment of the volume of trees it may not be necessary to perform a time-consuming modelling, as calculations performed on initial point clouds offer sufficient approximation of the volume. This allows shortening processing time from several hours for an area scanned with e.g., 400 cameras (as for the airport area analysed in this example) to a few tens of minutes.

2.8.3. Crops Conditions Estimation

The 3D information about the area of interest can then be easily used to determine the volume in each and every part of the point cloud or a 3D model. This requires manual indication of the area of interest where the volume of objects like trees needs to be estimated. For simplicity, in the below analysis we assume a regular forestation (i.e., without objects like buildings), which may be sparse over the given area.

In the presented example we have chosen an area where there were only few trees, over an almost flat area covered by dry grass. The first step was to limit the area of interest. This has been done by drawing a polygon around the grass area, in our case a rectangle (Figure 33).

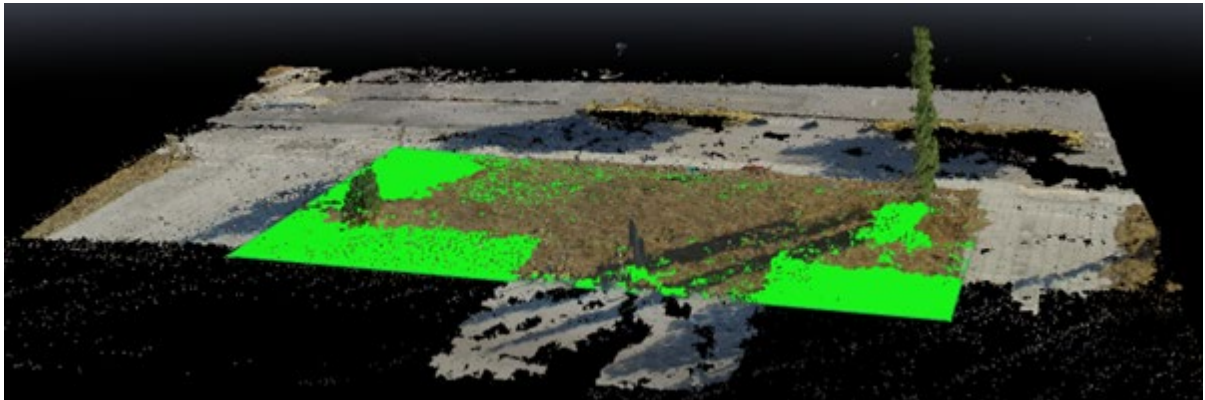


Figure 33: Limiting the area of interest with a polygon

The polygon is automatically attached to the ground, immediately showing the areas that are extruding above the ground level. This gives immediate information about the 2D ground area of interest, corresponding to various land usage areas by historical city assets in Hamburg and Bratislava, natural habitats as in Bratislava and Camerino, or historical agricultural areas such as the Huerta in Valencia. In crisis situations, this may become also an invaluable tool for quick assessment of damages to such area e.g., after earthquakes and thus applicable to Camerino, wildfires that endanger Huerta in Valencia, as well as landslides under the castle in Bratislava.

The volume can be already estimated at this point. However, it may not be very accurate in case that the polygon has not been well defined in 3D coordinates. Therefore, it is advisable to perform a quick calibration of the vertices with respect to actual photographs (Figure 34, bottom-right). The calibration process involves manually adjusting the position of the vertices of the bounding area on at least two photographs.

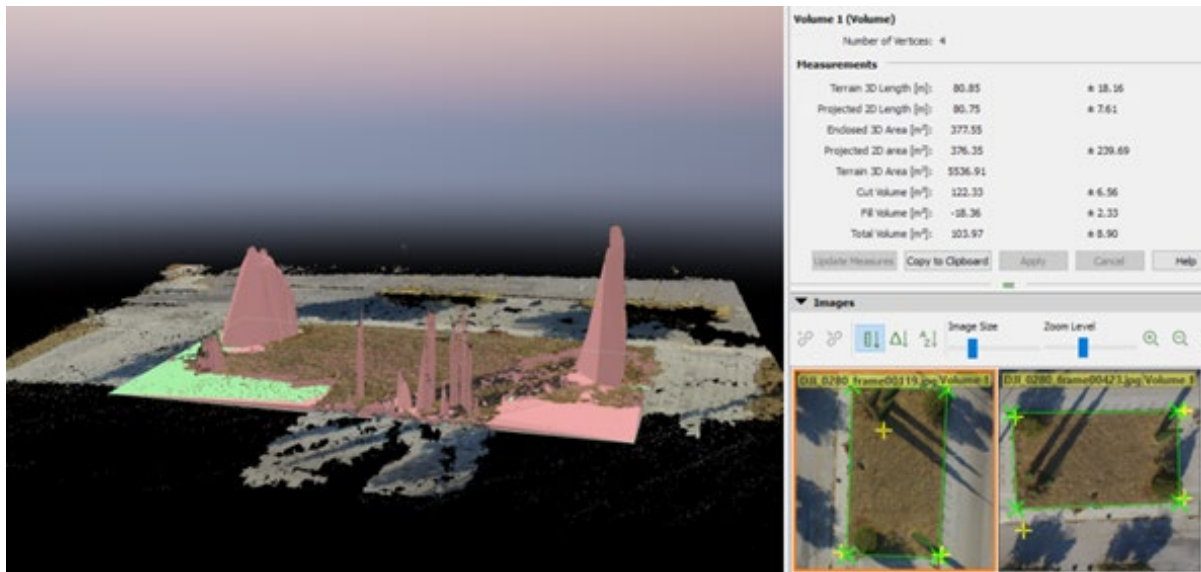


Figure 34: Volume in 3D (left), volume and area estimated (top-right), and calibration images (bottom-right).

A visual comparison of images in Figure 33 and Figure 34 may give an impression of a false positive extrusion in the farther left corner of the bounding area. However, when referred to actual images some trees can be noticed in this corner. The reason is that analysis has been performed on point clouds and not mesh, thus some information in the model is not easy to be visually noticed. In this example analysis the results were that in the horizontal area of $\sim 376\text{m}^2$, there are extruding objects (trees in our case) with volume between 95m^3 and 110m^3 . Considering than over 8 tall trees are in this area, those results are close to be the realistic numbers.

2.9. Conclusions

In this section a number of sensing technologies have been described that have been either fully developed for the needs of ARCH pilot sites or results of earlier projects adapted to the specifics of the pilot needs. The former ones involved large scale environmental, climate and atmospheric pollution data from systems like European (EEA), national and private Open Data Platforms (section 2.3) complemented with local in-situ measurements of very specific parameters requested by ARCH end users with custom sensors (2.1). The former ones have already been integrated and have been feeding the THIS platform with data for all pilot sites since over half a year.

The custom sensor development has been completed and undergoes currently discussions with interested pilot sites regarding the actual selection of the types of sensor nodes and the most important parameters to be captured. Ongoing discussions with end users in Hamburg and Valencia have been also focussing on the economic aspects of such deployments taking into consideration a cost compromise between using calibrated versus non-calibrated sensing elements. Additional discussions with Barcelona pilot has been also focussing on the use of micro sensors for indoor monitoring of climatic conditions at historical sites. Regarding data storage, current approach is for using THIS repository for storing all data captured by all ARCH sensing systems, though questions regarding long-term (in terms of futured decades)

availability of such data to pilot sites has been raised and will require further consultation within WP2 about future sustainability and exploitation of ARCH technologies.

Regarding 3D modelling of pilot sites and heritage assets, there has been a lot of data already captured by pilot sites. However, considering that current 3D models do not provide a complete set of data required for protection of specific sites (e.g. warehouses in canals of Hamburg, rock foundation under Devin Castle in Barcelona or Arabic irrigation system in Valencia), the 3D photogrammetric scanning system presented in sections 2.6 and complemented with an integrated automated aerial drones described in section 2.7 will offer an ability to perform effortless, one-off and/or frequent comparative 3D scans, with very high accuracy [4]. Such a system, due to COVID outbreak caused restrictions could not have acquired relevant scans of the pilot sites for fully evaluating its functional reliability, instead synthetic data had been used. In terms of integration into the ARCH system, the automated 3D scanning will be offered as a self-contained system that will help end users to make custom scans of selected heritage assets and historical areas (semi)automatically with integrated option to directly upload resulting 3D models to THIS, for subsequent use by HARIS for e.g. structural defect analysis.

3. Monitoring of heritage assets

The conservation of architectural heritage is a major problem as historic buildings are particularly prone to damage caused by climate change and natural events, such as earthquakes, floods, and subsidence. This is a consequence of their intrinsic fragility that is commonly traced back to structural aspects (empirical conception to vertical loads and rarely to face horizontal loads and other unexpected actions) and natural degradation of materials, often exacerbated by environmental pollution and more aggressive climate conditions, as well as by inadequate management.

Generally, historical buildings are characterized by complex and irregular geometries, with interventions and alterations stratified over time, often made with poor materials more prone to environmental degradation phenomena and adverse interactions with the original construction materials. For these reasons, the assessment of the structural behaviour of historical buildings and the interpretation of their crack patterns is one of the most complex tasks in structural engineering.

In this situation, experimental analysis is an essential tool for structural engineers to investigate the state of conservation of cultural heritage, understand the evolution of damage or the possibility that damage might develop, make the evaluation of possible intervention of restoration. Such an experimental analysis requires the acquisition of various structural response quantities over time, from monitoring during assigned time windows and up to permanent monitoring. Acquired data is then processed and adopted to implement and calibrate simulation models (digital twins) able to predict the evolution of the investigated cultural heritage construction and provide warnings if safety levels drops below acceptable thresholds. This schematized procedure is commonly referred to as Structural Health Monitoring (SHM). SHM represents the set of processes that aim to evaluate the alteration of the structural behaviour of the system, observing the response parameters over time through periodic measurements, and statistically evaluates their sensitivity to damage, to provide the state of the health of the considered construction [44].

SHM is, hence, a non-destructive technique for evaluating the characteristics of structural behaviour and therefore it can be used for the historical and artistic heritage according to the principle of “minimum intervention” [45]. In accordance with the ICOMOS/ISCARSAH, the decision-making process relating to conservation activities is based on four phases: anamnesis, diagnosis, therapy and control. The SHM provides support in all four phases, especially for the “Anamnesis and Control” part.

In general, SHM through its measurements provides the information that allows reducing the uncertainties related to the actual conditions in terms of structural behaviour, improving the estimate of its safety [46].

In the operational conditions, SHM observes the normal functionality of the system and it can be used to improve ordinary maintenance as well as extraordinary interventions in case of major degradation. In fact, by acquiring quantitative information on the system behaviour, SHM provides real-time information on the structural conditions, especially in the case of anomalous values of the monitored parameters.

During unexpected events, SHM allows the acquisition of information regarding the state of structures and its more fragile elements such as frescoes, stuccoes etc. It also allows direct information of the building response during such events and permits to organise an efficient management of the emergency, e.g. evacuation, securing of movable assets.

Finally, in the post-event event, it can support the organization of phases to recovery and intervention, increasing knowledge of the condition of the structure after the event, optimizing the recovery plans and verifying the performance and effectiveness of the interventions implemented in the past.

SHM is subdivided in two main phases:

- 1) data acquisition using sensors connected or incorporated into the structure
- 2) processing and interpretation of the acquired data.

This allows evaluating the level of degradation, the severity of the damage suffered during extreme events and the current state of conservation [47], [48], [49].

Advances in sensors and the exchange of information via the internet made SHM promising for better management of cultural heritage. Although the specifications and layout of each SHM system could vary substantially from case to case, Figure 35 shows a typical flowchart and the ideal scheme that apply to any SHM [50].

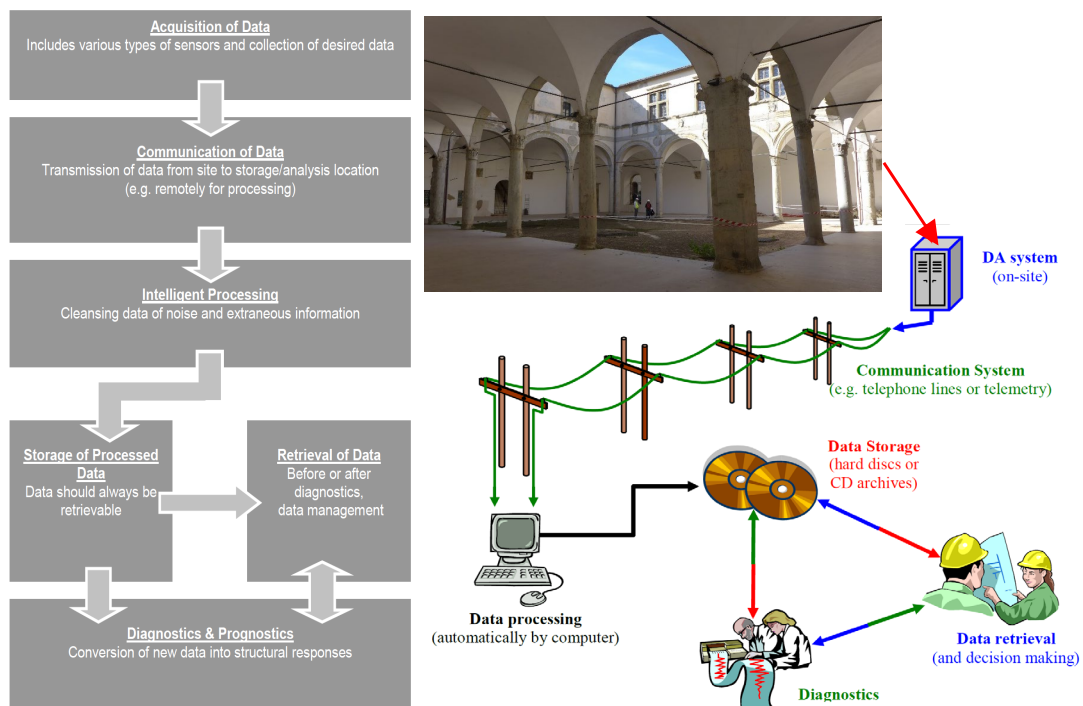


Figure 35 Flowchart and ideal scheme of an SHM system [50]

Once the parameters and quantities to be measured have been identified (e.g. displacements, rotations, accelerations, temperatures, etc.), the first step for an effective SHM system is represented by the selection or development of appropriate and reliable sensors. Absolute and relative displacements and rotations can be monitored (for example opening cracks, overturning of walls), through the use of displacement transducers and inclinometers. To

separate the seasonal variations in measurements, environmental sensors to capture relative humidity and temperature are also necessary.

Discrete electronic crack sensors placed at locations where cracking is visible, or in certain cases invisible, in structural connections along with walls and floors can detect even the smallest movement. Other sensors that often find applications in SHM are tilt sensors, small devices attached to the walls/floors of a building externally and/or internally to monitor the tilt (rotation) of the walls, beams, deck of a structure.

However, vibration-based monitoring techniques are the preferred choice of structural engineers as a very effective way to detect any change in the mechanical properties of a structure through variations in its dynamic properties such as natural frequencies and modal forms of vibrations [51], [52], [53]. The dynamic properties of the building can be evaluated using controlled or environmental excitations and the most used sensors are accelerometers. In recent years, contactless systems such as image processing (digital image correlation of video recordings) have been adopted to evaluate the vibration properties [54]. While vibration-based monitoring approaches are suitable for monitoring the structural behaviour of the monument on a global level, their efficiency in locally monitoring slight changes in structural dynamic properties is still an unexplored path. Since damage usually occurs locally, strain measurement-based monitoring methods can be used as an optimal tool for locally monitoring key elements of the structure. Fibre optic sensors [55] and strain gauges [56] are among the most widespread and used sensors for strain monitoring.

After the collection of sensor measurements, SHM deals with their processing using analysis algorithms to deduce the physical conditions of the structure. Machine Learning techniques are widely used in SHM thanks to their evolutionary “self-learning” capabilities. In the evaluation of the characteristics and recognition of evolutionary models, machine learning methods are applied to analyse the distributions of the extracted characteristics with the aim of assessing the health status of the structure. These algorithms normally belong to the outlier detection category, which considers training data exclusively from normal facility conditions (unsupervised learning). It is worth mentioning the work done by [57] in monitoring structures using machine learning techniques such as neural networks, genetic algorithms and support vector machines. Diez et al. [58] proposed a Clustering-based data-driven Machine Learning approach for damage assessment. [59] proposed an assessment of structural damage based on the posterior probability of the Support Vector Machine (PPSVM) and the theoretical evidence Dempster-Shafer (DS). Santos et al. [60] presented a new early-damage strategy based on data detection that combines a static SHM with Machine Learning methods. Other much more sophisticated methods of damage assessment are available in the literature as reported in [61], [62], [63].

Finally, in addition to the structural system, it is also important to monitor the environmental parameters inside buildings intended for museums and art sites, to prevent the main phenomena of degradation, such as detachment, efflorescence and subflorescence, depigmentation, dilatation and narrowing, cracks and chemical-biological processes [64].

3.1. Seismic structural monitoring

Architectural heritage is constituted by a wide number of historical masonry structures such as churches, towers, buildings, and fortresses, characterized by both structural and typological vulnerabilities, which are often responsible for their poor seismic performance [65],[66]. These intrinsic characteristics, combined with the high cultural value of historical constructions often lead to a significant seismic risk. Among historical masonry constructions, palaces and churches have commonly a special role in the national architectural heritage of many European Countries as they are widespread in urban, rural, and mountainous areas, and have generally significant importance for local communities, and very often present high artistic value.

The evaluation of a historic masonry structure is a difficult task because of many uncertainties associated with the knowledge about its current conditions (original structure and structural changes due to enlargement and retrofit works, different construction systems and materials, structural damages and material degradation, soil and foundation modifications) and the complexity of modelling techniques as well as analysis methods. In this sense, after a comprehensive historic analysis and a complete geometrical and structural survey, sophisticated experimental techniques are necessary to identify the actual behaviour of a structure, especially the mechanical properties of the structural materials and the global dynamic behaviour [67].

Traditional techniques and innovative methods are available for material survey. Among them non-destructive techniques are generally preferred when dealing with historic and valuable structures. An extensive test campaign on material may permit to identify large parts of parameters for the definition of a structural numeral model (digital twins based on the finite element method, commonly used for numerically solving differential equations arising in engineering and mathematical modelling [68]). The global dynamic behaviour of a structure can be experimentally determined by means of several kinds of tests such as forced, impulse, release, or ambient vibration tests, by using modal identification methods [69], [70]. In the last decades, ambient vibration tests, with the relevant output-only modal identification methods, have become the preferred test typology for evaluating the modal parameters of full-scale structures. Such an approach is especially appealing for historic structures since no artificial excitation is required and the test is carried out in operational conditions without interrupting the use of the structure or providing hazardous excitations that might cause damage [71]. The experimental modal parameters can then be used to update refined numerical models able to describe the real behaviour of structures, which can be required for structural verifications and for designing repair and retrofit works.

3.1.1. The Ducal Palace in Camerino

This case study was selected as representative of the many historic palaces widespread in European cities. Although the unique characteristics that each heritage building inevitable inherits from its past, the methodology for structural monitoring presented in this section is general and applicable to any other heritage building, regardless its dimensions and geometric complexity. The Ducal Palace (shown in Figure 36) is one of the main Renaissance monuments of Camerino, hosted the headquarters of the University of Camerino before the 2016 Central Italy seismic events. The nucleus has ancient origins, remodelled at the end of the XIV century and completed in the second half of the XV century under Giulio Cesare da

Varano. Over the centuries, the layout of the Palace saw many changes thanks to acquisitions that led to the incorporation of the other surrounding buildings. Each of these brought a continuous structural reorganization and maintenance works, resulting in a very complex and strongly stratified palace. Continuous interactions between the building and the city led to architecture and urban spaces that were mutually conditioned. For this reason, the Ducal Palace is defined as “part of the city”.

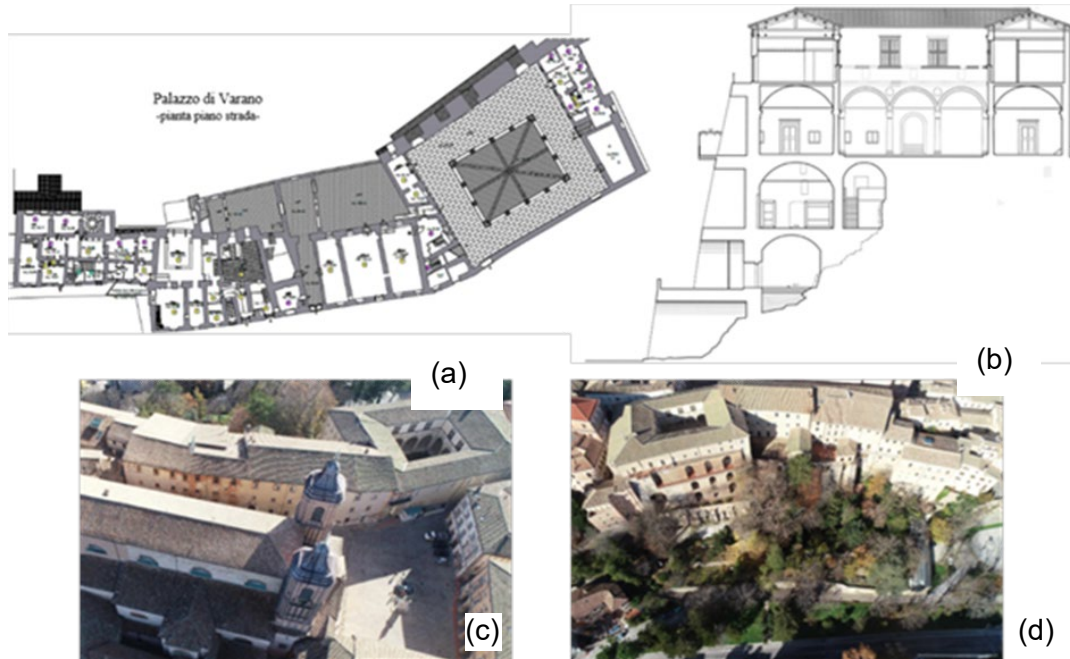


Figure 36: Images of the Ducal Palace in Camerino (Italy) taken by UNICAM during the survey of the building a) layout at the street level; b) vertical section; c) aerial view from the North-West side d) aerial view from the South-East side.

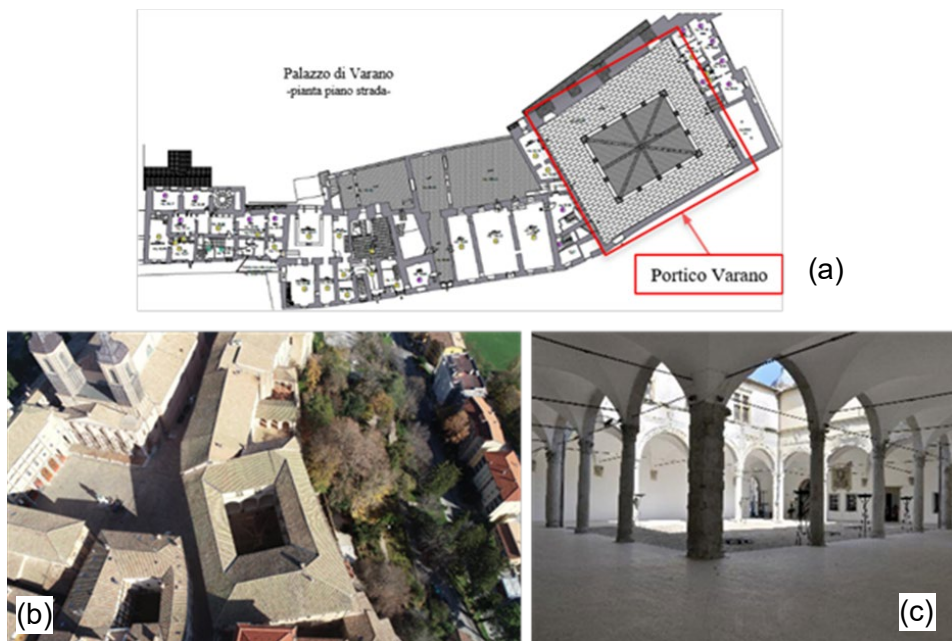


Figure 37: Portico Varano”: a) identification in the layout as the street level; b) aerial view; c) view of the inner courtyard from the North corner of the quadriporticus.

The quadriporticus courtyard (Figure 37), also called Portico Varano or Sottocorte, probably designed by the great military architect Baccio Pontelli, is the centre around which there are various rooms that were transformed over the centuries. After the latest seismic sequence that hit central Italy in 2016 year, many structural vulnerabilities were exposed, with damage observed both in the elevation structures and in the floors (Figure 38).



Figure 38: Examples of the damages in “Portico Varano” after the 2016 Central Italy earthquakes.

The Ducal Palace is a very complex case study and realistically accurate structural models were not available in the first stage of the field activities foreseen in the ARCH project. For this reason, preliminary structural monitoring tests were made in June 2020 to provide an active characterization of the dynamic behaviour of the quadriporticus under ambient-induced vibrations.

The instrumentation adopted during this preliminary experimental campaign consisted of 12 uniaxial high sensitivity piezoelectric accelerometers (PCB model 393B31 with 10V/g sensitivity and $\pm 0.5g$ measuring range) connected through high-quality shielded coaxial cables to the acquisition system (National Instruments cDAQ-9178 installed with NI 9234 analogue-to-digital converters) controlled through a Dell Precision laptop running National Instruments Signal Express software. The accelerometers were placed on the first floor as depicted in Figure 39 by a “L” metal bracket section attached on the floor with an adhesive thin layer. This configuration is able to provide a comprehensive description of its horizontal motion, given that such floor cannot be realistically modelled as a rigid diaphragm due to its geometry and

materials. The adopted configuration was made possible because the interesting portions of the first floor were safely accessible. Other configurations keeping some of the accelerometers as fixed (reference sensors) and the other as roving sensors, were not explored given the major difficulties in safe access to other areas of the same floor and the impossibility of accessing the roof level just above the first floor.

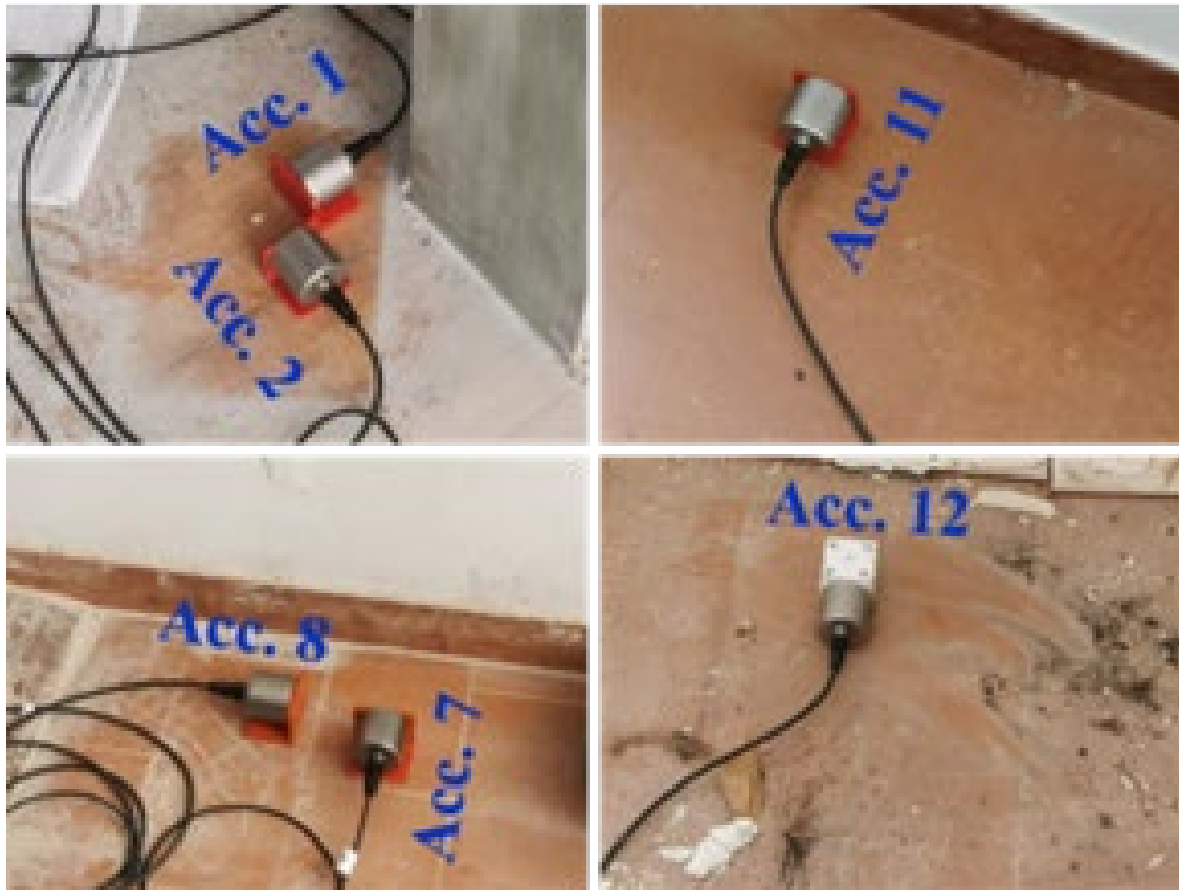


Figure 39: Configuration of the installed 12 accelerometers in preliminary monitoring.

Data acquisition was performed at 2048 Hz for about 30 minutes. This duration corresponds to more than 4000 times the fundamental period of the building.

Afterwards, the signals were pre-processed to remove the linear trend by subtracting the logged signal with a zero-degree polynomial, filtering with a low-pass filter with a cut-off frequency of 49 Hz, and a resampling at a frequency of 102.4 Hz to reduce the amount of data and to make analyses faster. Subsequently, the identification of the modal parameters (frequencies and damping ratios) was carried out by the Covariance data driven - Stochastic Subspace Identification (SSI/Cov) ([72],[73]).

The results are summarized in Figure 40; the identification of the stable modes, indicated on the graph by a solid black circle, was carried out considering a difference less than 1% in frequency and a MAC greater than 95% on mode shape. The first mode is essentially a translational mode along the X-direction and has an estimated frequency 3.36 Hz (period 0.298 s) and damping ratio 1.86%. The second mode is essentially a translational mode along the Y-direction and has an estimated frequency 4.52 Hz (period 0.221 s) and damping ratio 3.71%.

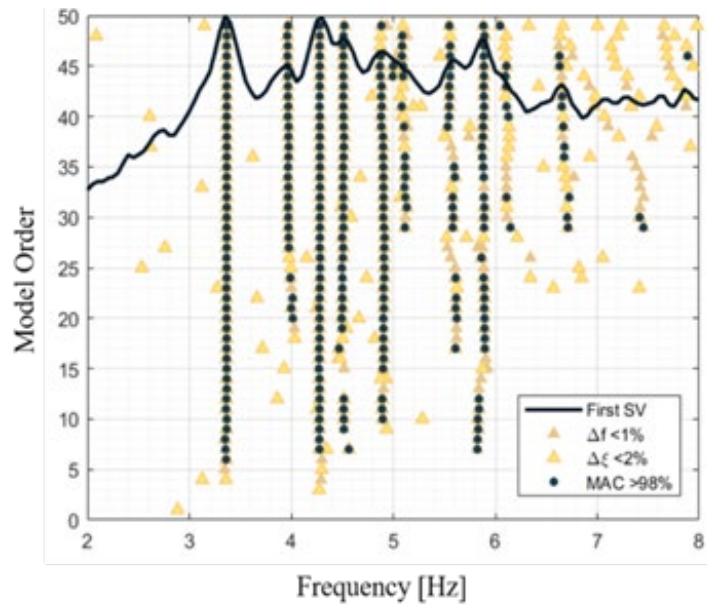


Figure 40: Stabilization diagram as results of preliminary monitoring (June 2020).

The results of the preliminary structural monitoring made in June 2020 provided the support for the definition of a simpler configuration using a limited number of accelerometers. The selected configuration for long-term monitoring uses four accelerometers located as depicted in Figure 41a. The adopted accelerometers are uniaxial high sensitivity piezoelectric accelerometers (PCB model 393B31).

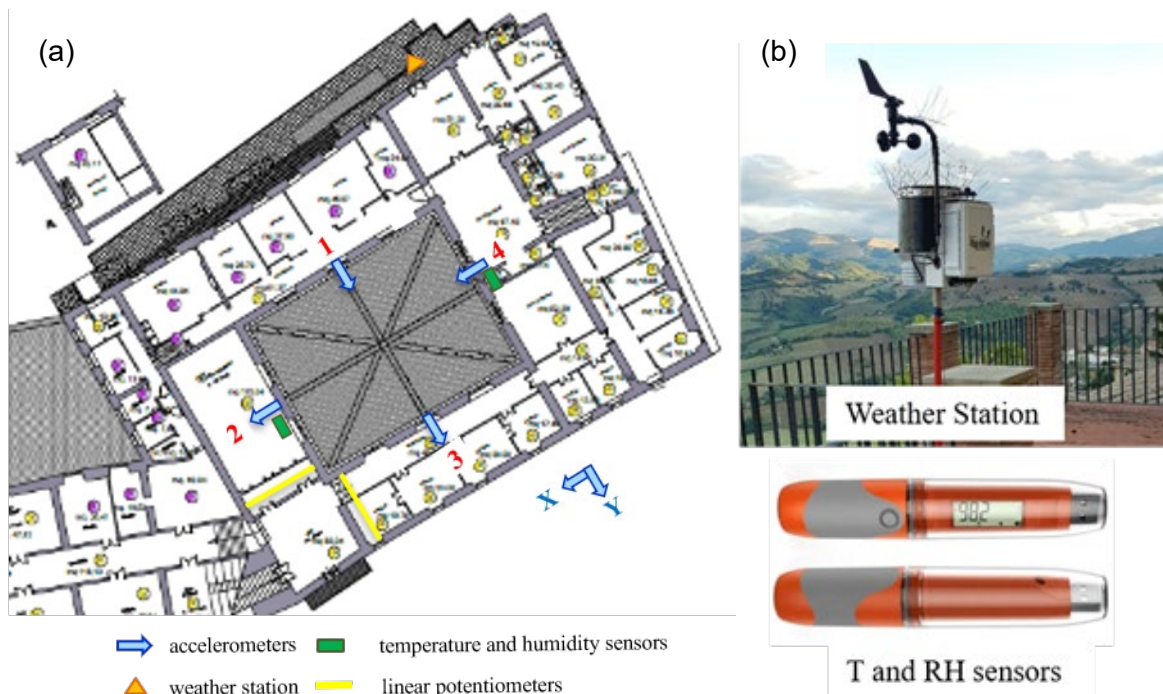


Figure 41 Configuration of the sensors position in the monitoring system (a), and environmental sensors (b).

Environmental parameters are monitored using an independent system comprising two wireless sensors for internal temperature and relative humidity as well as a weather station (temperature, relative humidity, wind speed and direction) located just outside the Ducal Pal-

ace (Figure 41b). In addition, a triplet of linear potentiometers (Gefran model PZ67-A) was installed across the cracks in the cross vaults in order to measure their movements (Figure 42a). The configuration of the displacement transducers is composed by three linear potentiometers placed across the vaults connected by two galvanised metal sheets (2 mm thickness) to follow the curvature of the vaulting. Each pair of linear potentiometers forms an angle of 60 degrees. Such configuration permits to evaluate every motion of the cracks, such as side scrolling or stretching movements leading to an opening of the crack itself (Figure 42b).

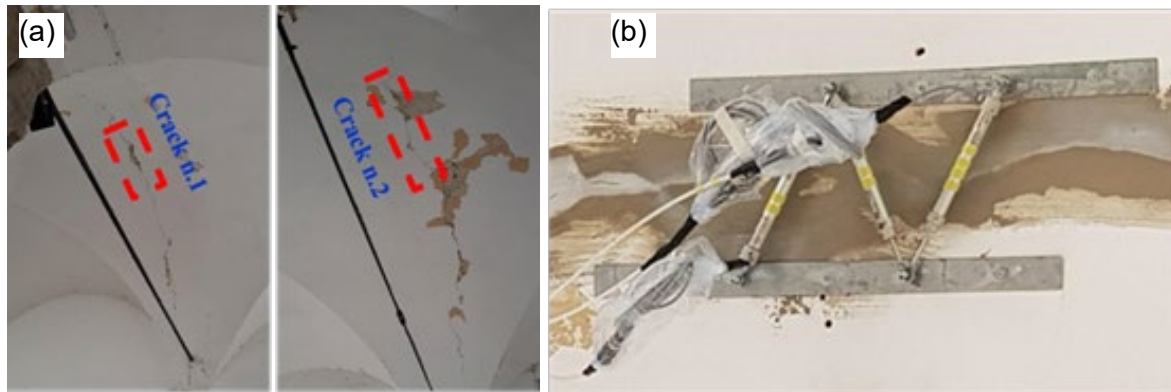


Figure 42: Recognition of the monitored cracks (a) and monitoring system of the cracks (b).

Both accelerometers and linear potentiometers were connected through high-quality shielded cables to the acquisition system (National Instruments cRIO 9045 installed with NI 9234 analogue-to-digital converters for acquiring accelerometers and NI 9209 for acquiring potentiometers). The acquisition procedure was developed in the cRIO 9045 using the programming environment National Instruments LabView [74] to control the entire process, i.e., 30-minute time logging every 2 hours, local data storage, data transfer on cloud storage accessible for remote verifications. This acquisition procedure is characterized by a continuous data acquisition of the data and a timing control that activate the logging data; within the logging cycle there is another timing control that stops the logging procedure when the assigned time elapsed. To optimize the accelerometers and linear potentiometers acquisition, the physical channels definitions were divided into two parallel cycles with specific sample clock to synchronize the analogue to digital converters modules (Figure 43).

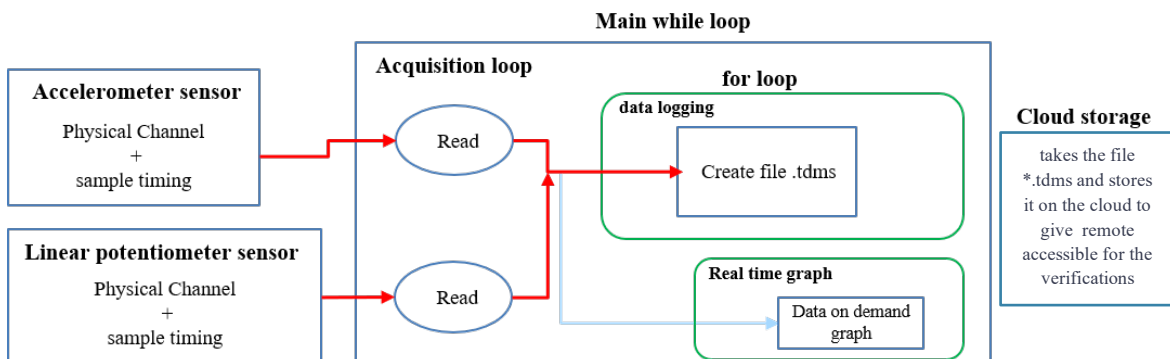


Figure 43: Schema of the acquisition procedure

3.1.2. The Santa Maria in Via Church in Camerino

This case study was selected as representative of the many historic churches widespread in Europe. As already commented for palaces, although the unique characteristics that each heritage building inevitable inherits from its past, the methodology for structural monitoring presented in this section is general and applicable to any other church, regardless its dimensions and geometric complexity.

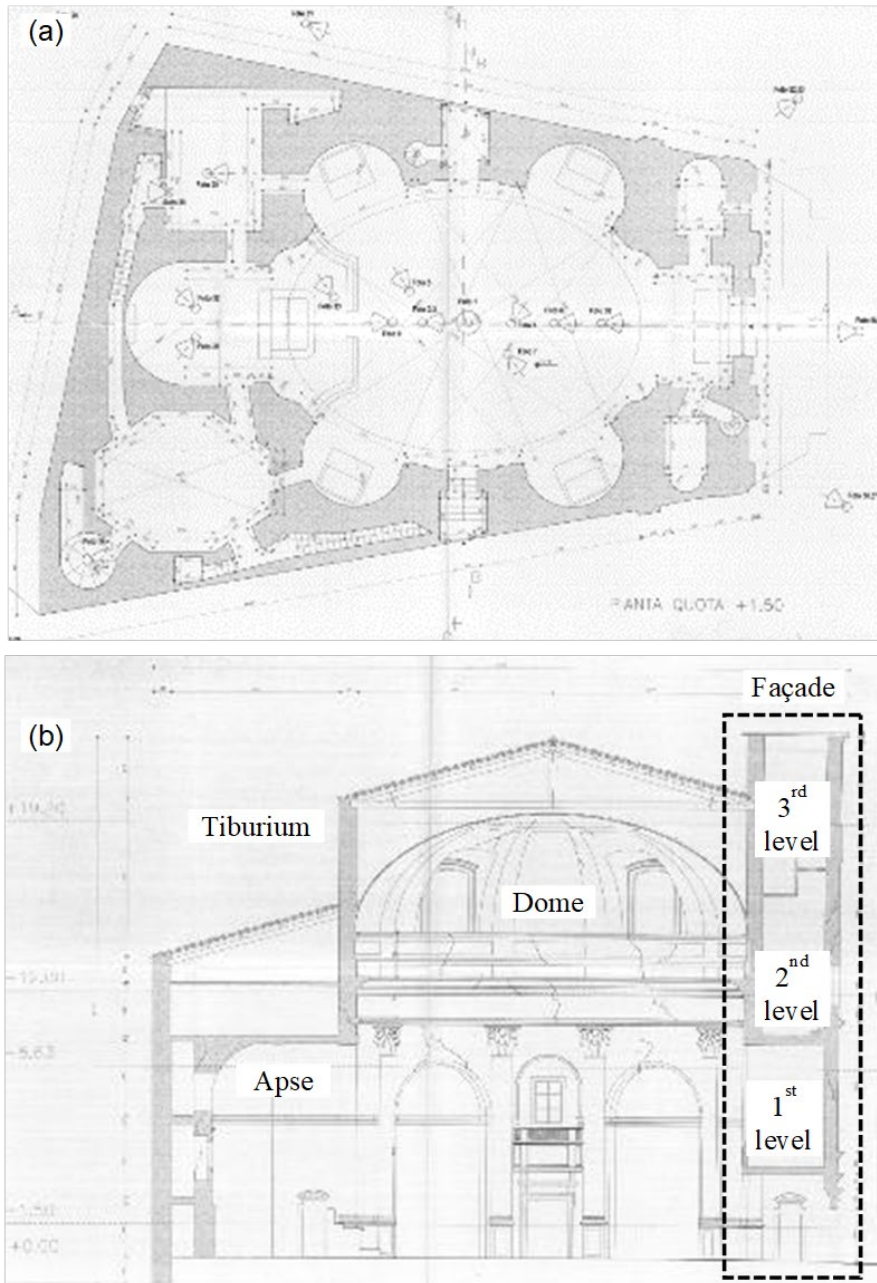


Figure 44: Santa Maria in Via church: Plan scheme (a) and longitudinal cross-section (b).

The church of Santa Maria in Via is located in the historical centre of Camerino (Figure 44a). The construction of the church dates back to the XIII century; historical documents demonstrate that the original church was smaller and very different with respect to the current construction. In the XVII century, between 1639 and 1642, the church got the actual baroque

appearance after heavy rehashes which consisted in merging and suitably modifying neighbouring buildings and in the erection of the towering anterior body that today still gives the monumental appearance to the façade of the church. In 1799 a strong earthquake affected the town, destroying many buildings including the cathedral; Santa Maria in Via church underwent impressive damage that consisted mainly in the failure of the elliptical masonry dome that was replaced with a fake dome richly decorated with gypsum stucco and frescoes. The church, in its current configuration, underwent other strong earthquakes in 1873 and 1997 that also severely damaged it.

The church has a trapezoidal plan that incorporates a central elliptical hall, the octagonal sacristy, and other rooms. The hall major axis passes through the entrance and the opposite main altar located in a deep presbytery; on the minor axis, above two side entrances, there are two small chancels. Four radial chapels, characterized by hemicycle niches, open on the central hall. The plan of the church appears to be massive and strong. Parts around the central elliptical hall are characterized by three levels and constitute a confinement for the elliptical hall, which rises about 8 m higher with an octagonal tiburium, which approximates the elliptical shape of the hall. Four large windows are realised on the tiburium walls above the lateral chapels. At the outside, the tiburium is stiffened by buttresses in correspondence of corners. Another peculiar element of the church is the octagonal bell tower which rises at a corner of the plan above the last level served by a spiral staircase.



Figure 45: Earthquake damage: aerial view (a), changes to an upper part of the façade (b), internal view (c).

The last element composing the church is the already mentioned anterior body of the façade. This part is placed against the building (Figure 44b) interacting, at the lower part, with the main body of the church and, at the upper part, with the tiburium for a maximum height of about 23 m. The plan of the façade body is trapezoidal with an average length of the bases of about 16 m (façade width) and depth of about 6 m. Inside, the body has three floors, the first at a level of 4.5 m from the ground floor, the second at the level of the first eaves and the third at the level of the clock that characterises the façade elevation. The plan is divided into three rooms, separated by two masonry orthogonal spine walls with communication openings. The upper block of the façade body is characterized by the presence of a system of steel ties in the two orthogonal horizontal directions, anchored to the masonry walls. To access the chancel and the upper floor, a spiral staircase is incorporated into the façade wall, on the left side, producing a significant discontinuity within the wall body of the façade.

After the latest seismic sequence that hit central Italy in 2016, many structural vulnerabilities were exposed and underwent a progressive damage, starting from the first shock on August 24th that produced shear cracking patterns at the lower part of the façade body. Events on October 26th worsened the situation of the façade body produced an impressive collapse of the bell tower and damaged the top level of the tiburium at the roof connection. An event on 18th January 2017, which was associated with heavy snowfall, finally produced the collapse of the tiburium rear part, a portion of the roof, and of the fake dome. Figure 45 depicts the main collapses of the church.

An external retaining steel structure was designed to prevent the anterior body collapse (Figure 46a). Other important securing systems are the provisional roof built to protect the internal part of the church against weather and the latticed structure built on both sides of the tiburium walls to prevent their out of plane collapse (Figure 46b). This latter system is also connected to the main system.

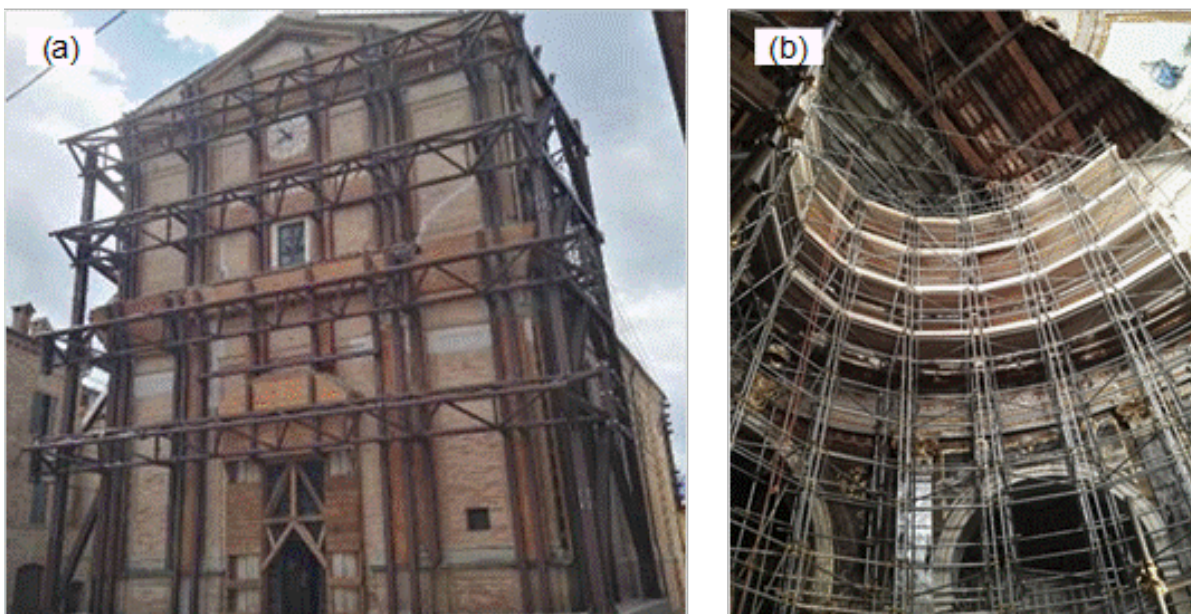


Figure 46 Securing Systems: External retaining steel structure (a) and internal scaffolds (b).

3.1.3. Monitoring system and preliminary dynamic characterization

Santa Maria in Via Church is a very complex case study and realistically accurate structural models were not available in the first stage of the field activities foreseen in the ARCH project. For this reason, preliminary structural monitoring tests were made in November 2020 to provide a dynamic characterization of the church behaviour under ambient-induced vibrations.

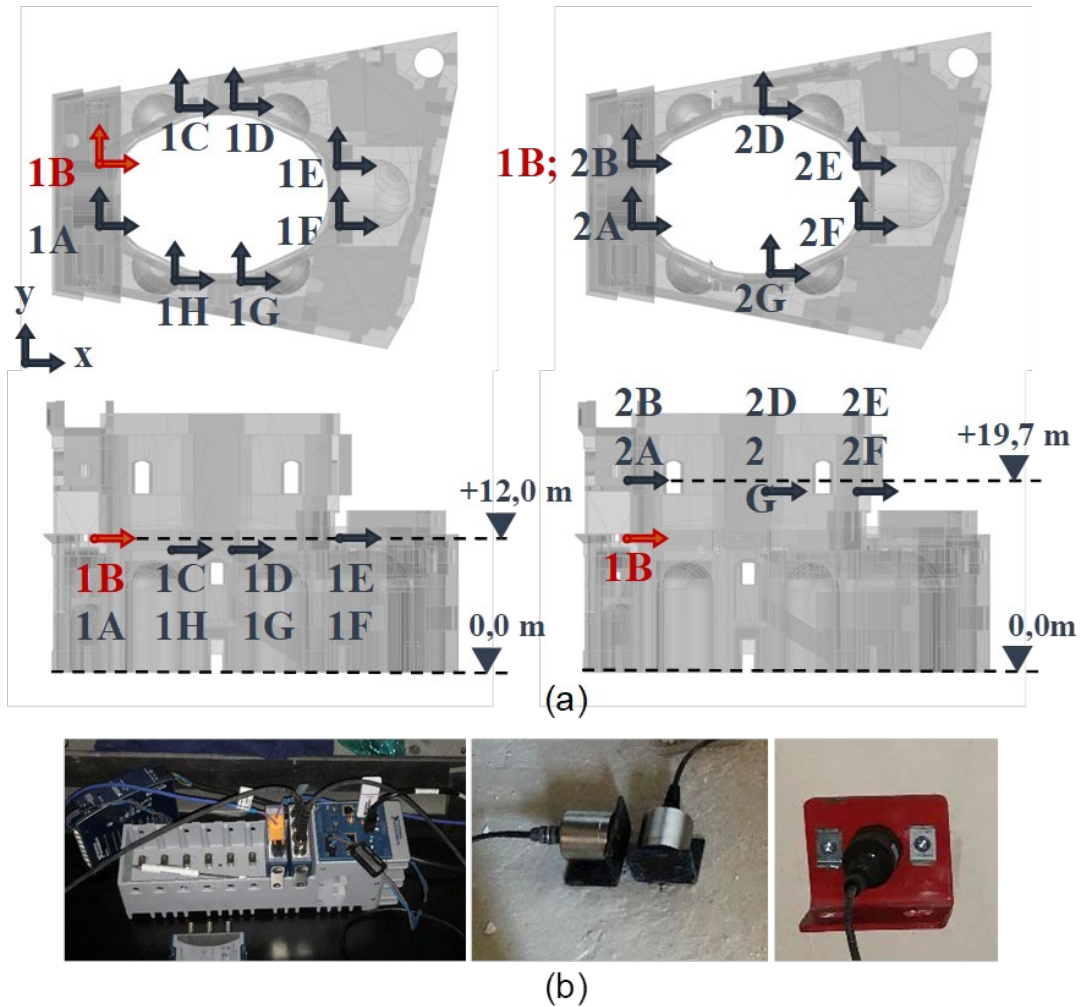


Figure 47: Accelerometer layout (a) and instruments installation (b)

To provide a dynamic characterization of the church, ambient vibration tests were carried out through 16 accelerometers considering two sensor configurations shown in Figure 47a and Figure 47b. In particular, uniaxial piezoelectric accelerometers (PCB model 393B31 with 10V/g sensitivity and $\pm 0.5g$ measuring range, PCB model 393A03 with 1V/g sensitivity and $\pm 5.0g$ measuring range), connected through high-quality shielded coaxial cables to the acquisition system (one National Instruments cRIO-9045 and three National Instruments CDAQ 9185 installed with NI 9234 analogue-to-digital converters) were used. A distributed sensor network was set up by placing the cRIO for the measuring station close to the reference point 1B (Figure 47a) and the three mobile cDAQs near the remaining measuring points. Synchronization was achieved through TSN technology providing distributed time synchronization and deterministic communication using standard ethernet networks.

Regarding the tiburio side, the installation of the accelerometers was carried out by an “L” section metal bracket place on the masonry wall through an adhesive thin layer. Instead, on the façade side, the installation of the accelerometers was carried out by an “L” section metal bracket fixed by n.2 wall plugs of 8 mm in diameter as these remains on the facade for permanent dynamic monitoring purposes shown in Figure 47c.

Data acquisition was performed at 2048 sample/s for about 30 minutes. This duration corresponds to more than 4000 times the fundamental period of the building, as suggest in the topic literature. The identification of modal parameters was carried out using the Principal Component - Subspace Stochastic Identification (SSI-PC) technique. Since the acquisitions relevant to the two configurations are asynchronous, to obtain a correct mode shape, it was necessary to proceed with a data merging operation; in this case the results obtained with the PoSER (Post Separate Estimation Re-scaling) technique are shown.

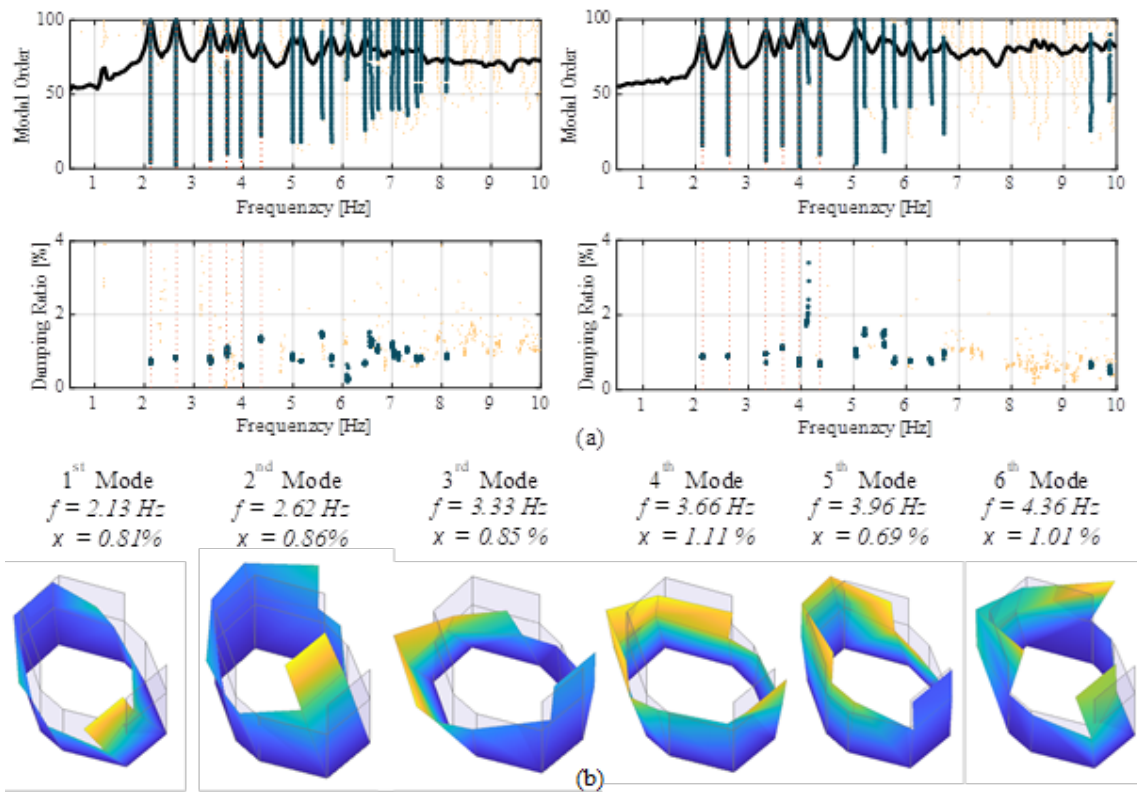


Figure 48: Results of the dynamic identification: Stabilization diagrams and Frequency-Damping ratio plot (a), identified modal parameters (b).

The Figure 48(a) shows the stabilization diagram obtained from the tests in configuration 1 and configuration 2, respectively. The stable modes in terms of frequency (difference less than 1%) and mode shape (MAC greater than 95%) are identified by a solid black circle. In the same figure, the frequency-damping diagrams are also shown, where the values of the damping ratios relative to the stable solutions can be appreciated.

The Figure 48(b) shows the selected modal parameters, i.e., frequencies, damping ratios and mode shapes. Globally, 6 modes of vibration have been identified. It is interesting to note that, despite the complex crack pattern, the dynamics of the structure, presents the first two

translational and well decoupled modes and a third torsional mode, which could be expected for the undamaged system. This is proved with values of the autoMAC matrix in Figure 49.

2.13	100	0.0	2.7	4.8	0.0	4.3
2.62	0.0	100	0.0	11.4	0.7	8.6
3.33	2.7	0.0	100	28.9	2.0	0.5
3.66	4.8	11.4	28.9	100	1.1	1.1
3.96	0.0	0.7	2.0	1.1	100	0.6
4.36	4.3	8.6	0.5	1.1	0.6	100
f [Hz]	2.13	2.62	3.33	3.66	3.96	4.36

Figure 49: AutoMAC matrix obtained from the identified mode shape.

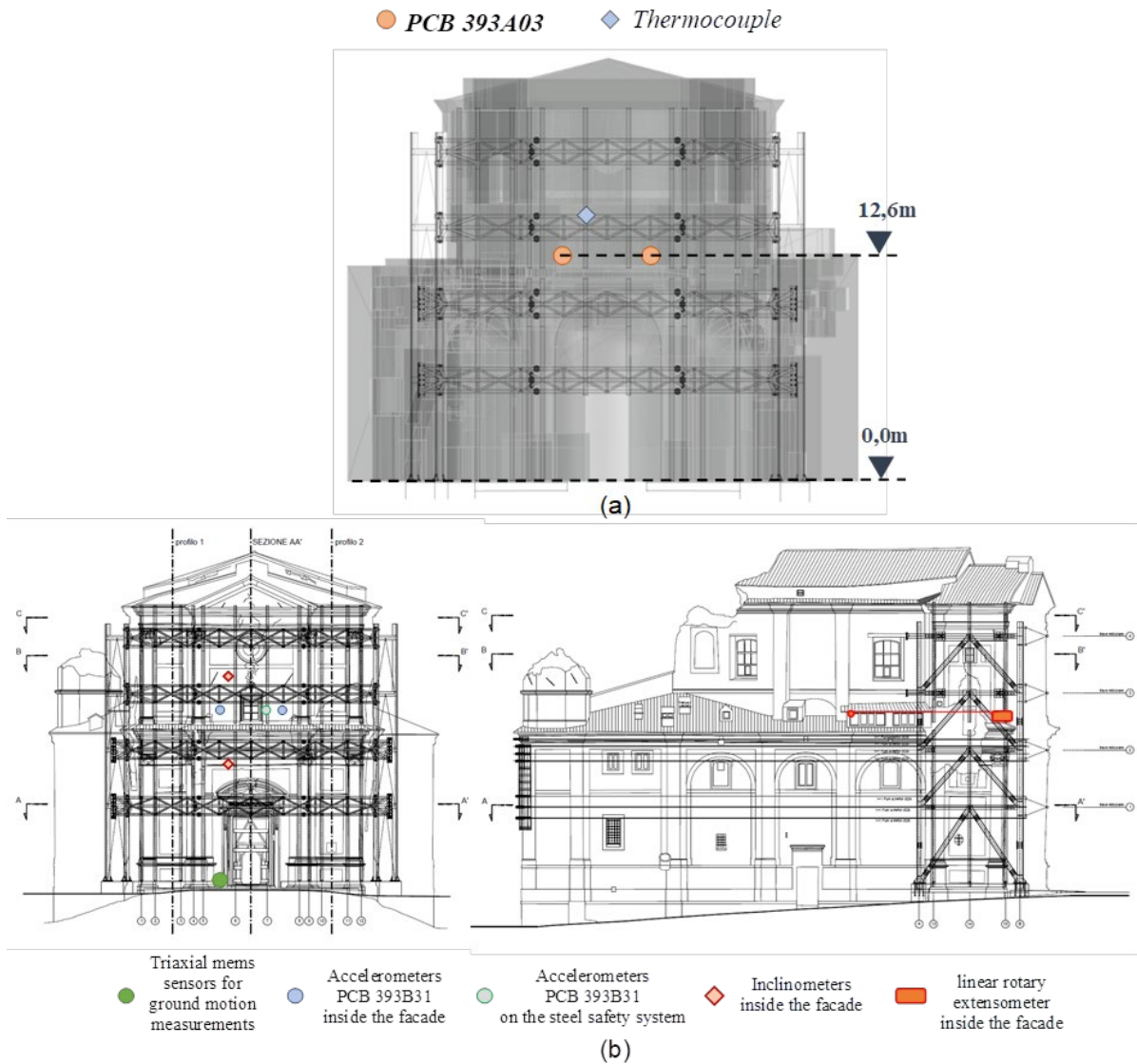


Figure 50: Layout of the installed sensors of the monitoring system(a); integration of sensors(b).

The main purpose of the Structural Health Monitoring (SHM) of the church is to control the evolution of the façade overturning mechanism activated by the 2016 seismic events. In this sense, a permanent continuous static and dynamic monitoring system remotely controlled, is designed. Currently, the monitoring system is still under development and will be completed in the next two months, but it already includes some permanently installed sensors and the system for the remote control is activated.

Based on the result obtained in the preliminary dynamic identification, two piezoelectric accelerometers PCB 393A03 were installed perpendicular to the façade, at 12.6 m from the ground (Figure 50a). The accelerometers were chosen with a larger measuring range (± 5 g) to assure recording without clipping also in case of seismic activities. Regarding the measure of environmental condition, two T thermocouples with a plate terminal were installed on the steel securing system and inside the church.

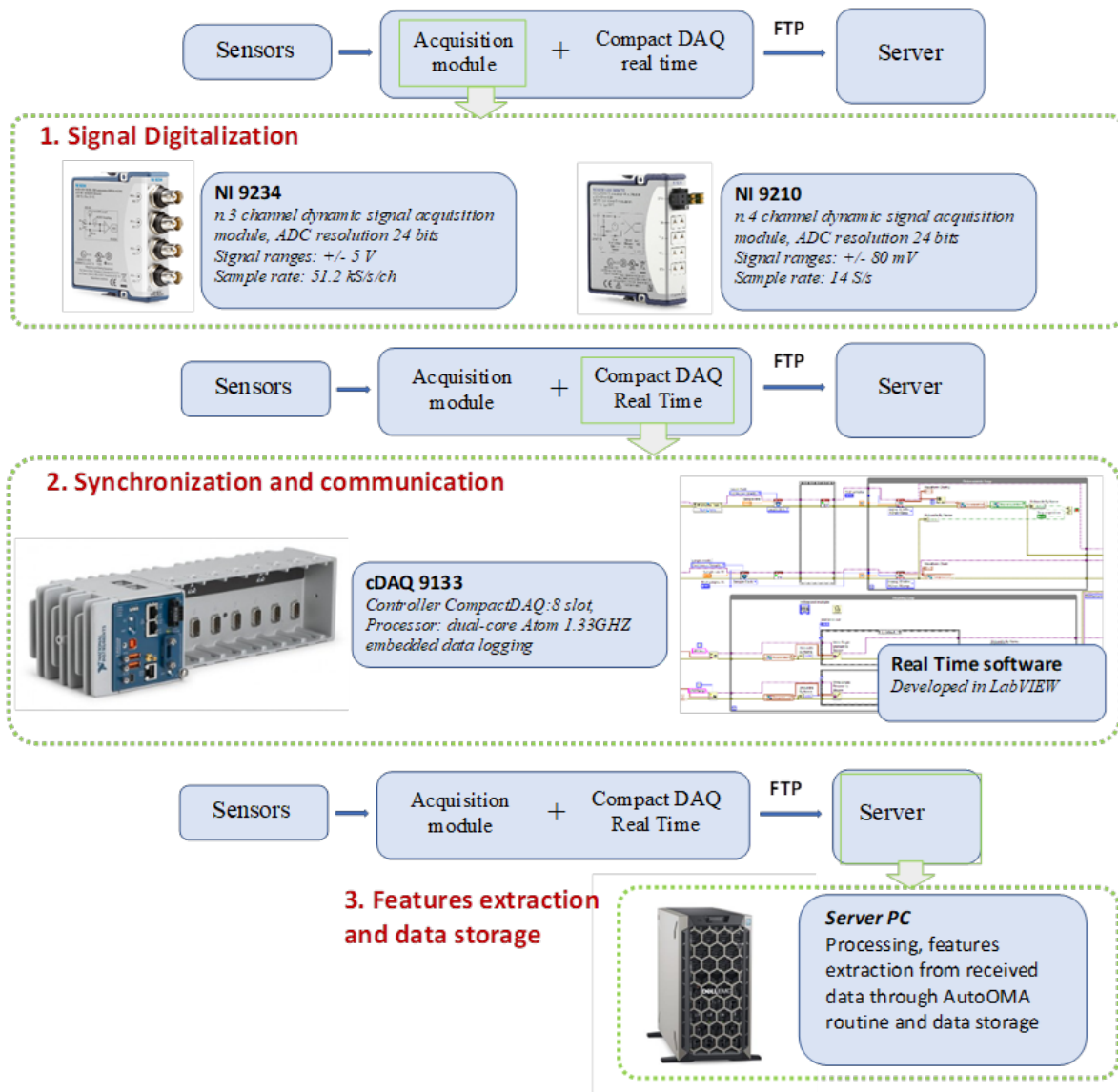


Figure 51: Schema of the monitoring system

As previously mentioned, the installation of the monitoring system is still ongoing and will be integrated with the following instrumentation (Figure 50b):

- n.1 PCB 393A03 accelerometer with the measurement direction parallel to the façade, to detect and track the 1st mode,
- n.1 PCB 393A03 accelerometer with the measurement direction perpendicular to the façade and installed on the safety steel system to capture the interaction between the façade and the steel trusses of the safety system,
- n.2 linear rotary extensometers and n.2 inclinometers to statically monitor the evolution of the façade overturning mechanism,
- n.1 triaxial MEMS accelerometer on the base of the church to acquire the input motion in case of earthquake,
- n.1 humidity and temperature sensor inside of the church.

The piezoelectric accelerometers of the currently installed monitoring system are connected to a NI 9234 module while the thermocouples are connected to a NI 9210 module. Data acquisition, storage and data transfer are controlled by a real-time cDAQ NI 9133 connected to the network via a router and remotely controlled.

The acquisition software deployed on the cDAQ, which was developed in Labview [74] environment, acquires data continuously, in real time, and sends it via ftp protocol to a remote server. This approach, thanks to the continuous streaming of data and the determinism guaranteed by the acquisition system, makes it possible to investigate possible dependencies on environmental conditions in a short time, but also to record the response to seismic events without the risk of losing data samples. A schematization of the monitoring system is shown in Figure 51.

The data are stored in 20-minute-long files, and the modal parameters are automatically identified and selected with a homemade Matlab Tool [75]. The automatic identification algorithm involves a first step in which the stabilization diagram is obtained by applying the SSI-PC algorithm ([72],[73]), after which the modal parameters are automatically selected by means of an Agglomerative Hierarchical Clustering (AHC) based algorithm.

3.2. Analysis of the data collected via monitoring

A preliminary analysis of the data collected by structural and environmental sensors installed on the selected buildings is reported in this section, in order to evaluate the variation of the eigenfrequencies also considering any potential effects due to the temperature.

3.2.1. The Ducal Palace

The analysis of the first results presented in this document is based only on the first month (October 2020) of acquisition. Two translation modes identified in the preliminary monitoring are considered. In the Figure 52 is reported trend of daily variation of frequency, evaluated adopting the SSI-COV methodology ([72],[73]). In the figure, the missing points are those when the instrument noise was comparable with the background environmental accelerations that would have made the results of post-processing rather unreliable. In fact, it should be remarked that the historical centre of Camerino has restricted access following the major damages after

the 2016 Central Italy earthquakes; this condition makes the area characterized by very low level of environmental noise during the day (a condition possibly exacerbated by the current pandemic restrictions) and even more during the night. At this regard, Figure 53 compares the power spectral density of the same accelerometer in the evening and daytime.

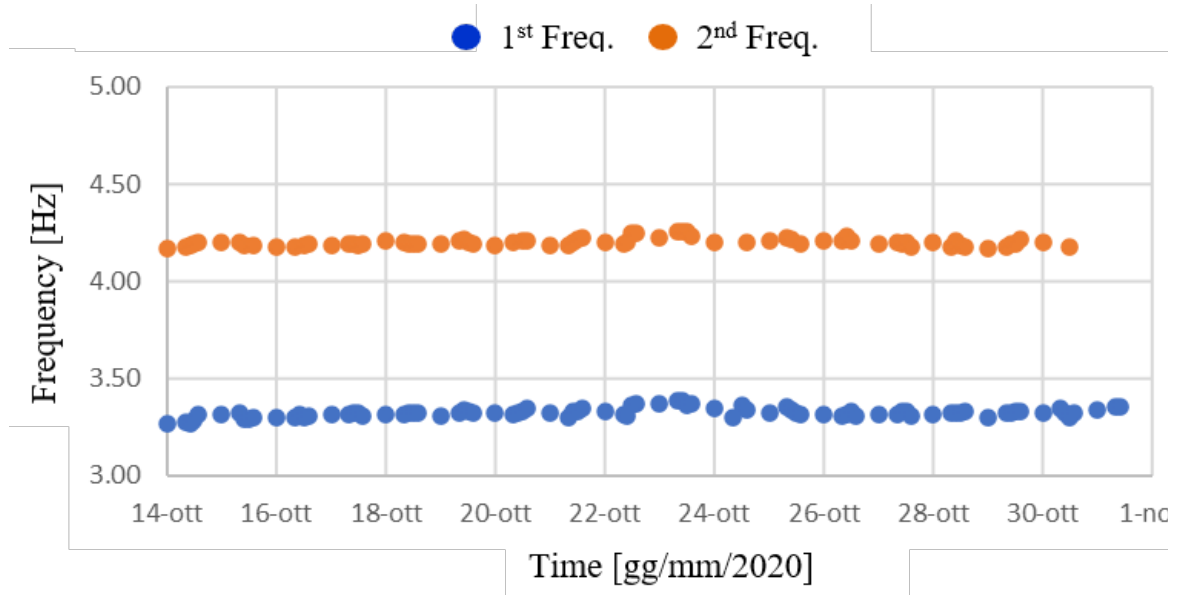


Figure 52: Monitored eigenfrequencies in the first month – October 2020.

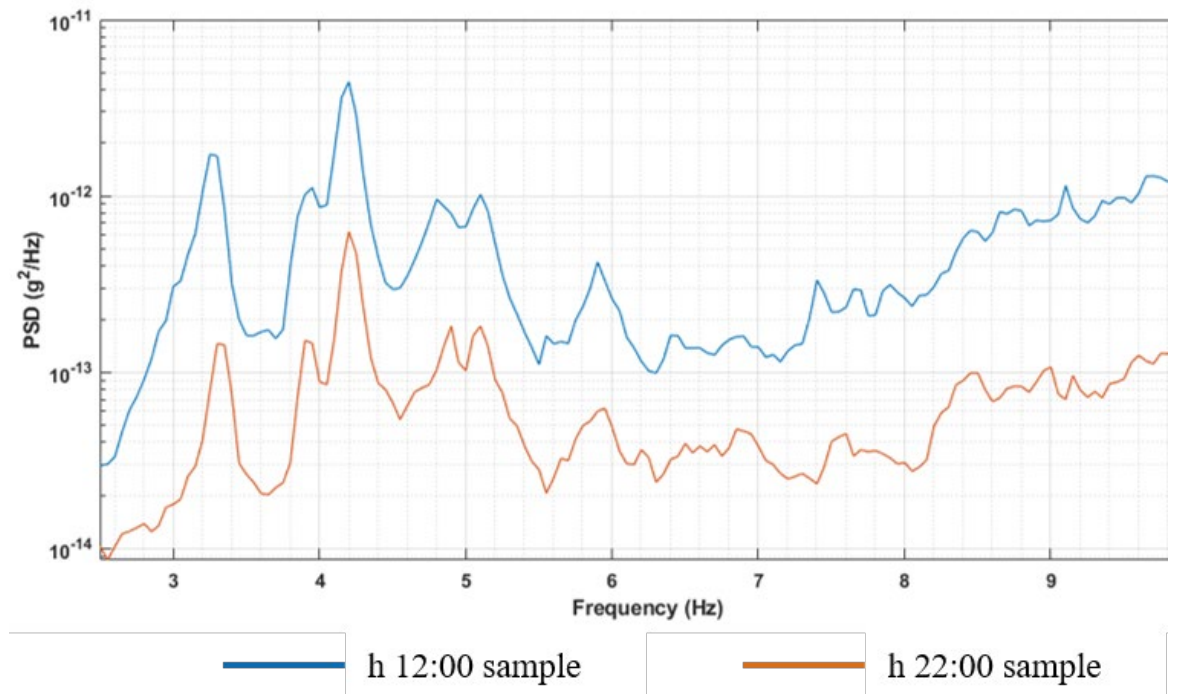


Figure 53: Power Spectral Densities compare at different time.

3.2.2. The Santa Maria in Via Church

The analysis of the first results presented in this document is based only on the first month (16 November-10 December 2020) of acquisition. The attention is focused on the six first frequency of modes (Figure 54a) identified in the preliminary monitoring with the SSI-COV

methodology. It should be remarked that in the first configuration adopted for monitoring, the first mode is never captured from sensors as it is a transverse mode with respect to the measuring direction of the installed accelerometers. Figure 54b shows the temperature values of the steel securing system and the temperature inside the church. A clear dependence of frequencies on temperature cannot be easily appreciated, probably due to the limited set of data, which refer to only one month of monitoring. Thus, a deeper investigation based on a larger amount of data must be performed to get a possible correlation.

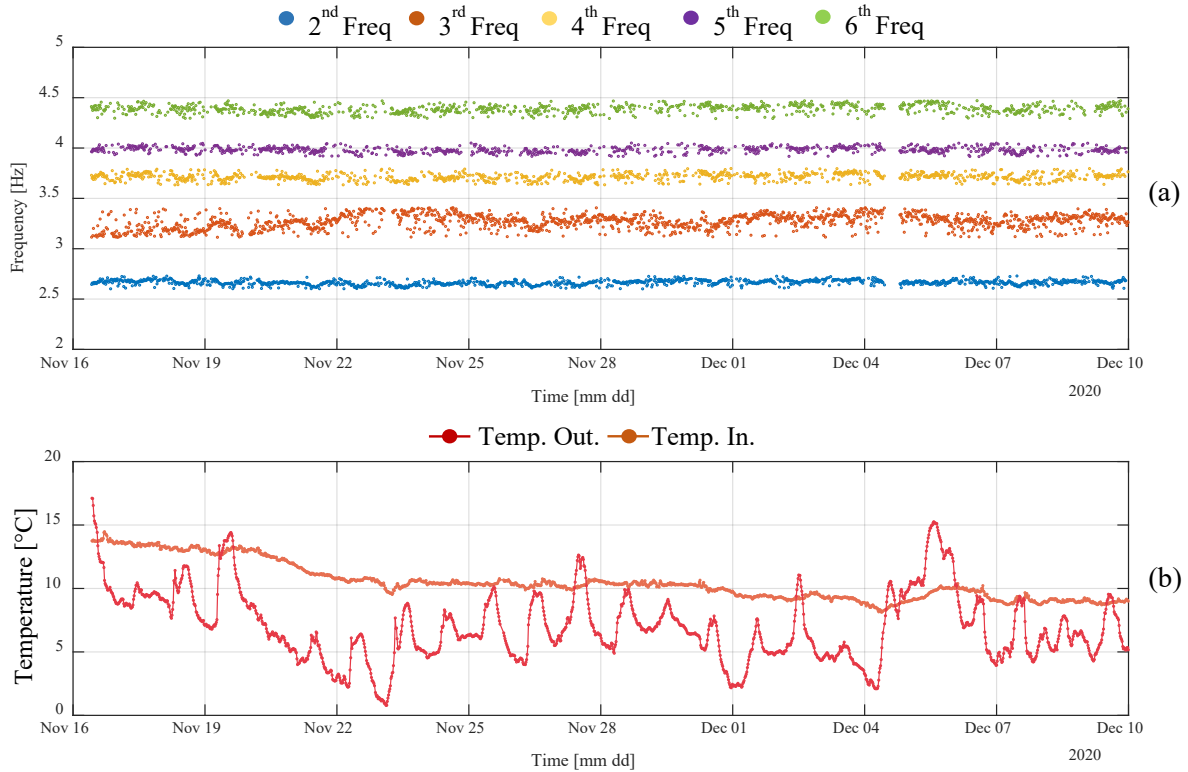


Figure 54: Results from the first month of the dynamic monitoring: (a) Monitored eigenfrequencies (b) temperature values.

4. The Real-Time Urban Seismic Network

This section describes the design of the MEMS seismic stations of the Real-Time Urban Seismic Network and its deployment in the historic centre of Camerino. The network is aimed to provide information about ground motion at the occurrence of an earthquake, also taking into account the site effects on the shaking level. The engineering parameters (e.g. peak ground acceleration, spectral accelerations, duration) will be calculated in near real-time and used to improve the local shaking scenario, that will be elaborated in the framework of the WP5. The processing of the recordings will provide measured parameters, without having to rely on approximations about the elements influencing the local amplification of the ground motion. Moreover, in the coming years the network will allow to collect data to study early warning methodologies, which however require due reliability and caution before being implemented.

The main advantages of this network are its sustainability and feasibility. In fact, the cost of a single station is about one thousand euros, also considering the transmission equipment, therefore at least 20 times lower than that of the stations generally used for seismic monitoring. However, MEMS accelerometers guarantee good signal recording performance, especially in the frequency range useful for earthquake engineering and in an urban environment where noise is significantly high. In addition, high-quality instrumentation often needs very strict installation site requirements to function properly, which can hardly be insured in a built-up area where anthropic noise would still dirty the recorded signal, or worse it would send in saturation the system. MEMS accelerometers, on the other hand, can be installed without spending too much for their orientation and levelling. Therefore, local geology and topography can be taken into account in the selection of the recording sites, at the same time counting on greater flexibility in the choice of installation method. Moreover, these advantages (low-cost, lower-sensitivity, etc.) allow to use them for a diffuse urban monitoring.

From a long-term point of view, the costs of maintaining are limited only to the data transmission. Currently, for each single station, data SIM cards are used with a subscription costing a few euros per year using an LTE router. In addition, potential costs for extraordinary maintenance - if a fault occurs in a network node - depend on the device to be replaced, however in the worst case it is few tens of euros. As for the interventions on the network, a first level for minimal maintenance will be possible by municipal technicians, supported remotely by the INGV staff, and a second level which directly involves the presence of an INGV specialized technician operating in the area.

The network prototype is part of the multi-scale seismic monitoring [7]. In particular, the network permits to integrate the information from the national monitoring services with those obtained on urban scale, in order to support a better knowledge on the local effects for the decision makers, as well as the stakeholders involved in the civil protection activities. In addition, the prototype is strongly exportable; in fact, similar networks could be deployed in other HAs subjected to high seismic hazard. However, the consistency, in terms of the number of nodes, cannot be defined a priori, as it mainly depends on the geological and morphological characteristics of the area, as well as on its extension.

The sections are organized as follows:

- Section 4.1 shows hardware components, including their main technical characteristics;
- Section 4.2 briefly describes software to acquire, compress and transmit the accelerometer data using the provided SEED link protocol
- Section 4.3 focuses on LTE and SIM transmission equipment, including IT security
- Section 4.4 shows three types of scenarios foreseen for installations
- Section 4.5 illustrates a deployed network and applications running on the acquisition server to manage recordings and state of the sensors

Note that configurations for each of the stations are provided in Annex 8.1.

4.1. The seismic station

The MEMS seismic station prototype is shown in Figure 55. The station was built according to the project scheme in Figure 56. This includes a power source (electrical network, battery or other source) for the electronic components, a UPS designed to stabilize the supply voltage and ensure operation of the station even in case of suspension of the power source, a synchronization system of the acquired signals with time accuracy of less than 1 ms, a high-performance motion sensor, able to perceive the shaking generated by a strong earthquake, an acquisition and compression system finally, a data transmission system in real time based on the miniSEED protocol (Ring-Server). The elements that make up the seismic station, for simplicity, indicated below as POWER, UPS, GPS, SENSOR, NETWORK and SBC, can be replaced with components or devices that perform the same functions, but which may have different technical characteristics and better performance. This represents a strong point of the monitoring system because of the possibility to adapt the seismic station to different needs and installation conditions. The functionalities and technical characteristics of the stations implemented for the monitoring in the historic centre of Camerino are outlined below with a detailed description of all components.

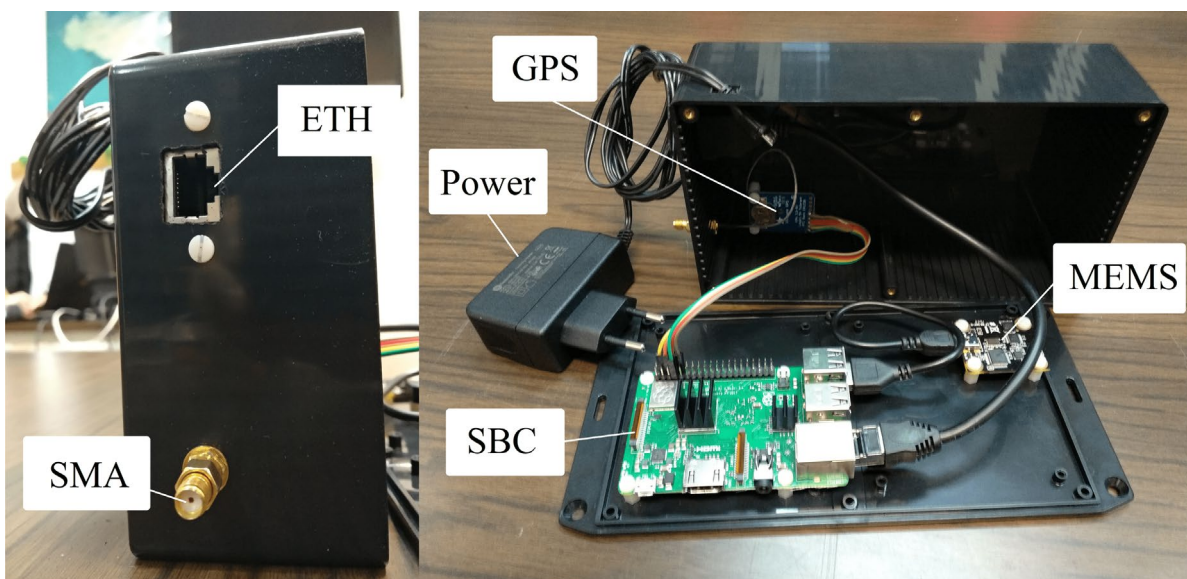


Figure 55: Example of an operational MEMS station in an urban seismic network (after [8]).

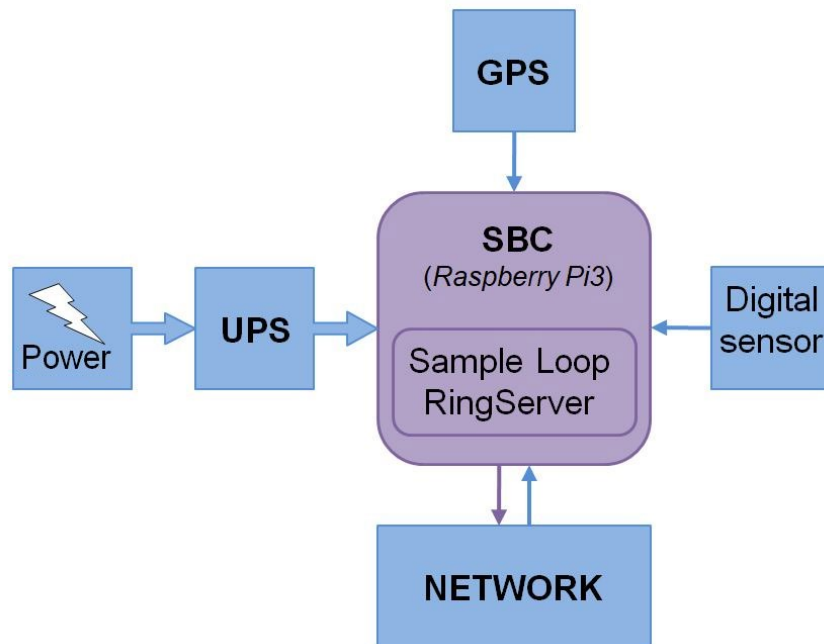


Figure 56: Working scheme of the MEMS seismic station (after [9])

4.1.1. POWER

The power, or primary power source, has two types of sub-systems that can be interchanged depending on the type of locally available power supply (electric network or batteries / photovoltaic). If the station will be powered by an electricity grid, an AC-DC converter will be used, if powered by a battery or photovoltaic system, a DC-DC converter will be used. In both cases the most important technical characteristics to be observed are the input voltage range and the output voltage / amperage.

4.1.2. UPS

The Uninterruptible Power Supply (UPS) consists of a large capacity battery (buffer battery) with an adjoining charge controller, a bypass system, and a DC-DC converter to adapt the voltage output to the load. This device allows the system to obtain hours or days of autonomy in the absence of primary power. In particular, the system conserves energy inside a large capacity battery, which is charged through the charge regulator taking energy from the primary power source, when this is available. During the charging phase the bypass system intervenes by directly connecting the primary power source to the DC-DC converter input. If the primary power supply fails, the bypass system provides a very short time to connect the buffer battery to the DC-DC converter input, guaranteeing a stable voltage at the UPS output, even during the phase of transition. In addition, the DC-DC converter allows the electronic part to be protected following voltage and current surges from the primary power source. The most important technical characteristics to be observed are the input voltage / amperage range, the output voltage / amperage, and the buffer battery capacity in Ah.

4.1.3. GPS

The use of a Global Positioning System (GPS) apparatus is necessary to carry out high precision (maximum synchronization error equal to a few tens of nanoseconds) synchronization of the seismic signal with the UTC time (reference time for the scientific community) or the time of the zero meridian (of Greenwich), and carry out the georeferencing of the seismic station with sufficient precision (confidence interval of the localization of the order of a couple of meters). Precision time synchronization is essential to make the acquired data valid for scientific use and to be able to carry out useful processing also for example for the location of earthquakes. The most important technical characteristics to be observed are the data update time and the uncertainty of the PPS signal (pulsation per second).

4.1.4. SENSOR

The digital sensor is the "detector" of the ground movement. It must be selected based on the specific needs of the project, taking into consideration the numerous specifications such as: frequency band, sensitivity, full scale, dynamics, linearity range, sampling frequency at output, number of bits, instrumental self-noise, etc. The choice of the sensor is decisive and must be made with great care, verifying in every case the specifications declared by the manufacturer. Moreover, among all the elements listed here, it is the one that can actuate over a higher price range, depending on its performance (cf. [10],[11]).

4.1.5. NETWORK

The network is composed of all those devices that allow interfacing with a data network. There are different technologies to connect: Wi-Fi, Ethernet, Bluetooth, GSM or Satellite. The criterion of choice for the device to be used depends strongly on the data traffic, on the reliability of the technology to be used and on the annual cost to keep the network active and functional.

4.1.6. SBC

The Single Board Computer (SBC) is the heart of the system: a miniaturized computer made entirely on a single board, with an operating system on board and equipped with all the peripherals needed to carry out the processes of forfeiture, compression, and data transmission. The main technical characteristics to be observed are related to the operating system and the applications should run on the system, in particular the type and performance of the processor, its clock, the size of the RAM and ROM.

4.2. Software upgrade

4.2.1. Native software structure

The software components of the station can be schematically divided as follows: the programs supplied by third parties for the functioning of the components and for the implementation of

the Seedlink protocol⁵⁵. software developed for the acquisition and writing of the seismic signal, as well as software for the synchronization of the card with the GPS device. For the use of the MEMS Phidget1043 accelerometer and the GPS device it is necessary to install the relative "libphidget22" libraries for the Linux operating system provided by the manufacturer⁵⁶.

The Seedlink protocol is an international standard for the robust transmission of data on internet networks using the TCP/IP protocol. It also allows the management of an output data buffer to manage any momentary connection losses and avoid signal loss in such cases. It is normally managed by a Seed link server, which has the task of providing seismic data as a web service. In the MEMS station, the sever program used is the "ringserver" software⁵⁷ and the Seedlink web service is available on the standard 18000 port. The Python⁵⁸ programming language was used for the development of the components necessary for the acquisition and packaging of the seismic signal. The main program for the operation manages the two basic operations for data transmission: signal reception from the sensor and association to a precise time interval, as well as the actual writing of the packages according to the "miniseed" standard⁵⁹. The two main processes operate in parallel: data reading and file writing. In fact, the main program takes care of the reading directly, and it launches, at start-up, a secondary process called "writeSamples" that has the task of receiving data and save the miniseed when the number of samples is available to close the file. The number of samples depends on the duration of the package and is provided to both processes through a configuration file called "set.conf". The data exchange between the two processes takes place via a shared data structure, specifically a FIFO (First-In-First-Out) queue in which data is returned in the same order in which it was written. The reference time of each packet is the system time, with the precision of milliseconds, in which the packet was received. The system time is constantly updated through a separate software called "gpsDate.py". This interfaces with the GPS device present in the station and every N number of seconds (where N is a parameter set before the start of the process) requires the GPS time and updates the system time. The last application developed in python was "deleteOldFiles.py", which simply takes care of emptying the folder of miniseed files created by the "writeSamples" process. The folder must be periodically emptied to avoid overfilling the system SD memory and deteriorating performance, considering that such an SD memory is used for recording of data by the client device for several days. In the current version of the software, the process keeps only the files related to the last 24 hours of signal in the folder. The "ringserver" software also has an internal data transmission buffer (1 GB by default, but extendable by changing the appropriate parameters) that it uses to guarantee the delayed sending of the signal when the connection is temporarily unavailable. For a step-by-step procedure, from the complete configuration, to the implemented Python codes, up to the start of acquisition of the MEMS station.

⁵⁵ <https://ds.iris.edu/ds/nodes/dmc/services/seedlink/>

⁵⁶ <https://www.phidgets.com/downloads/phidget22/libraries/linux/libp-Phidget22-tar.gz>

⁵⁷ <https://seiscode.iris.washington.edu/projects/ringserver>

⁵⁸ <https://www.python.org/>

⁵⁹ <http://ds.iris.edu/ds/nodes/dmc/data/formats/miniseed/>

4.2.2. Latest software updates

The previous section describes the native software structure of the accelerometric station. However, in the last months of the project several updates have been made to improve the performance of the acquisition system [12].

After different registration tests, it was possible to verify that the Python library of the sensor loses samples every now and then, the GPS synchronization does not occur if the system does not have a recent date, the ringserver writes the archive to SD creating serious problems if you forget to maintain the local database, the SD suffers several “erase and write” cycles with high possibility of peripheral failures and it would be advisable to record the data locally on an external drive. Furthermore, it would be advisable to be able to enter the Euler angles and to be able to rotate the traces according to the fixed reference, as the scenario could often arise of not being able to correctly orient the sensor according to the Up-Down, North-South, and East-West convention.

To overcome the problem of samples loss due to Python libraries, it was necessary to rewrite in C++⁶⁰ the process that reads the values received by the sensor and assigns the time reference. It also takes care of creating packages in mSEED format. The rewriting of this application took 6 months because the C++ code, even if more efficient, has a low-level management of variables and hardware. Furthermore, it was necessary to spend some time to acquire all the necessary C++ packages and make them work on the purchased platform. In particular, we refer to the “thead”, “libmseed” [13], “pipe”, and “phidgets_22” libraries.

Failure to update the time from GPS, if the system does not have a recent date, was resolved by changing the synchronization method. An application has been installed that directly manages GPS information including the Packets per Second (PPS). The “gpsmon” application [14] makes information available on the “localhost” address and various ports. In this way, it will be possible to set the “localhost” as the time synchronization server on the “NTP” application, giving it precedence over any other method. It is also a more reliable system than the previous one since there is a robust control of the information coming from the GPS, avoiding incorrect synchronizations. Since the GPS locks on at least 4 satellites, the system time will begin to correct itself, obtaining an uncertainty of the system time of about 10us in a few minutes. Given the sampling frequencies of interest, the uncertainty of 10us was considered acceptable and saving computing power.

The problems related to the ringserver archive and the SD erasing and writing cycles have a single solution. In particular, for the ringserver we proceeded by studying in depth all its functions to set it adequately for its purpose, that is to transmit the data in mSEED format and keep a few hours of data in memory without writing to SD. The solution found for the ringserver [15] suggested how to solve the SD problem, that is, only write anything to SD when strictly necessary. After installing all the application packages and compiling the various programs, writing to disk has been disabled except for the “journal” process (process that takes care of not corrupting the operating system in the event of sudden power failures). Special RAM partitions have been used for the temporary files of various applications (also for ringserver).

⁶⁰ <https://www.cplusplus.com/>

The need to have a local archive was solved by adding a USB pen drive on the Session Border Controller (SBC), mounting the USB device directly on the system file as if it were a hard drive. The archive is created by the "slarchive" application. "lsarchive" queries the "ringserver", the "ringserver" replies with the mSEED packets which are subsequently recorded in a single trace file by "lsarchive". Since there is no control over the USB disk by "slarchive" it was necessary to develop a script that would delete the data that are n days old (n is the number of days you want to keep in the archive before the entire pen drive fills up and corrupts). The script that takes care of deleting the old data in the archive is executed every day at midnight by the "crontab" service. The result is that in the local archive there will be the last n days of data compared to the current date.

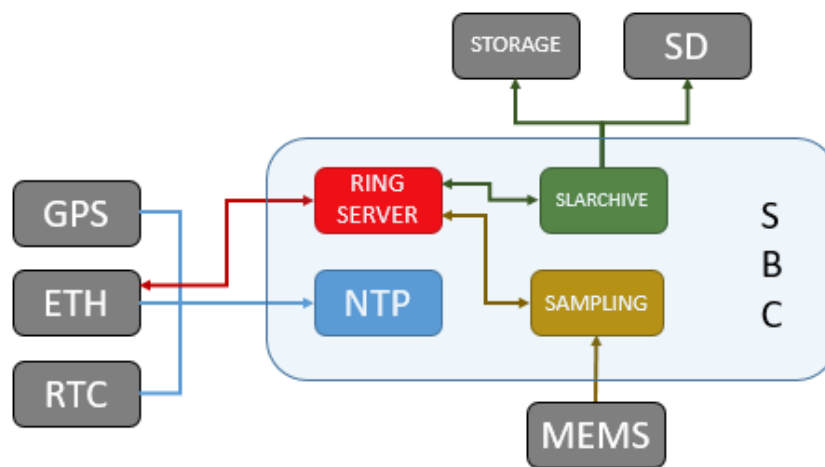


Figure 57: New Structure Scheme for an earthquake monitoring station based on MEMS.

A part of the code that rotates the accelerations measured on the Up-Down, North-South and East-West reference axes has been implemented. Using a "setting.conf" file, it is possible to introduce measured Euler angles. When the station is restarted, the software returns correctly oriented signals. The Figure 57 shows the evolution of the software part in a schematic way.

4.3. LTE and SIM transmission equipment

Long-Term Evolution (LTE) devices chosen for ARCH are the same as those used and extensively tested in INGV national seismic network stations. In particular, we are talking about the ADVANTECH devices, model RL77, the LTE routers that have robust characteristics. They have two slots for SD to have network redundancy, two ethernet ports that allow in the future to be able to expand the network with other devices if necessary. They also have a robust protection system with various passwords and an IP filter built in. The possibility of being able to protect our devices with an IP filter allows us to have excellent IT security, since only the devices that have the set IPs can interact with the system. At the moment the IPs of the INGV headquarters of Rome, Palermo and Rende have been set. The IPs of Rende for data acquisition, the IP of Palermo for redundancy of data acquisition, management, maintenance of the network and equipment. The Subscriber Identification Module (SIM) cards used for data transmission have the particularity of being Machine to Machine (M2M) cards and the NAT (network address translation) service active. The latter services are essential to be able to reach devices on the RL77. The SIM cards have a capacity of 30 GB data traffic per month.

4.4. Installation scenarios

4.4.1. Indoor installations with local connectivity and permanent electricity network

This type of installation is foreseen for those rooms where there is always guaranteed electrical network and connectivity, in particular these conditions are often respected by server rooms or in buildings with UPS electrical network. In this case, it is often not possible to place the sensor on the ground by drilling holes, so the sensor will be installed inside a case together with all the electronics. In this way it is possible to carry out the installation by fixing it to the wall with plugs (see Figure 58). During the installation phase it will be necessary to detect the Euler angles (roll, pitch, yaw) to rotate the tracks using the rotation matrix. These angles must then be entered in the "setting.conf" file when setting up the network and restart the machine. From the restart, the code operations take into account the new parameters, returning the signals along the Up-Down, North-South and East-West reference axes to the output.



Figure 58: Example indoor installation using local network and mains power supply

4.4.2. Outdoor installations in a cabin on the road

We thank the municipality Camerino and the Camerino collaborators for preparing the external sites on the road. Thanks to their work, we were able to carry out installations on the plinth. In particular, as shown in Figure 60, concrete bases were built on which lockers suitable to house electrical equipment and cabling were fixed.

In this typology the sensor is fixed on the plinth by means of a plug. The sensitive devices have been installed and fixed on a wooden base to simplify the installation operations. The battery of the UPS system is simply placed on the plinth. Since the cabinet used is made of mom plastic material, it is necessary to bring the antennas outside.

The power supply of these sites was provided by the municipality of Camerino, the cabinets are connected to the municipal electricity network with the appropriate safety measures (differential thermal magnetic switch), the power supply is supplied continuously. For greater safety, a small buffer battery has been provided which guarantees 3 hours of energy autonomy, and also protects the downstream electronic device in the event of voltage fluctuations.

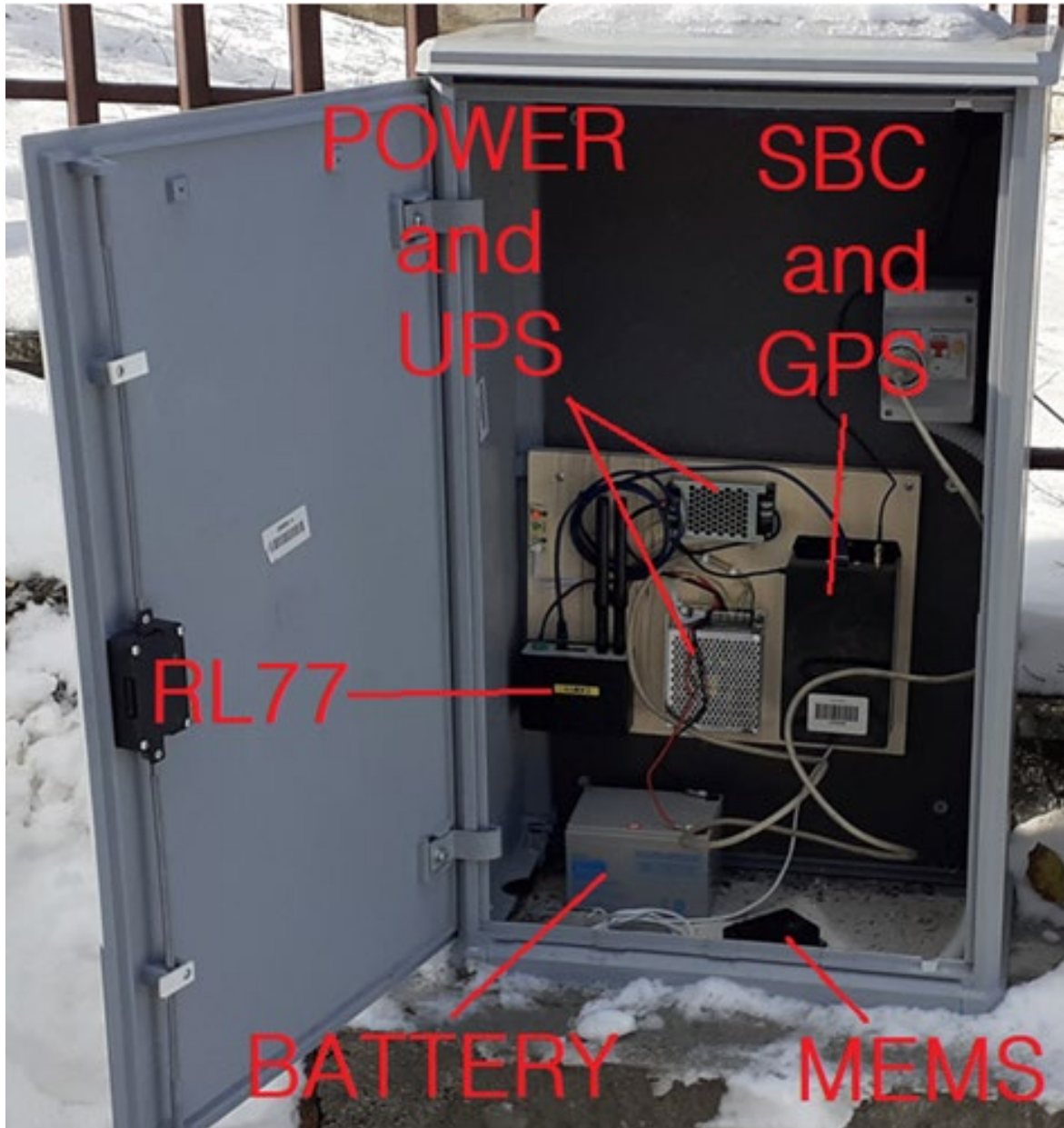


Figure 59: Example Outdoor installations in the cabin on the road.

4.4.3. Indoor installations without local connection and unstable power grid

In this type of installation scenario, the sensor can be installed on the floor and oriented correctly in respect to the convention. The sensor is equipped with 2 meters of cable to be able to fix it to the ground. The SBC and the GPS are inside an IP 54 watertight box, together with the power supply – UPS (and Battery) including the RL77 transmission equipment (As shown in Figure 59). The only limitations of the installation are the length of the power and sensor cables to be able to go outside the GPS and LTE antenna. As the GPS antenna cannot be placed outside, the service needs to rely solely on the NTP service, thus requiring a mobile communication outside of the case to receive reliably the LTE signal.

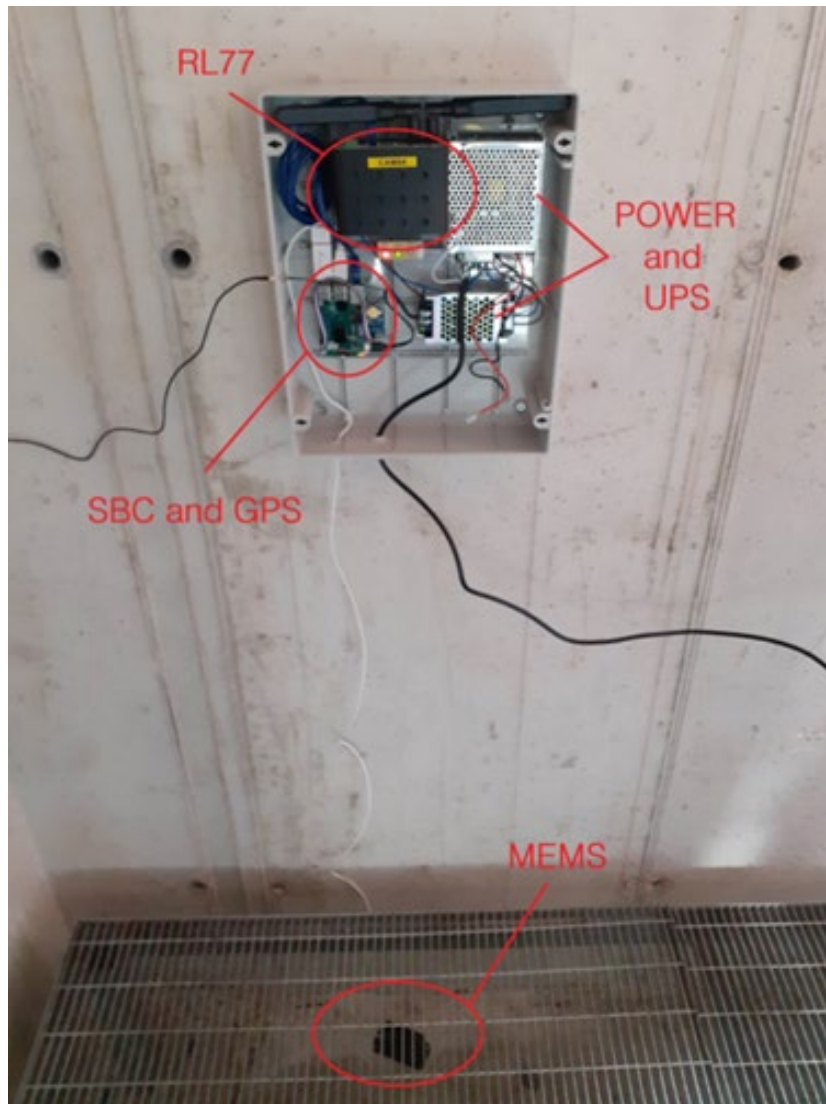


Figure 60: Example indoor installations without local connection and unstable power grid.

4.5. Network and data acquisition

Every monitoring station is linked to a main hub by means of an internet connection to form a monitoring network. The network topology chosen for the Structural Health Monitoring (SHM) and Open Edge (OE) applications is a star network where each host is connected to a central hub with a point-to-point connection (Figure 61). This topology has been chosen because it complies with the main needs of our system: flexibility and reliability. From the hub n linear connections can depart, therefore further devices (i.e., monitoring stations) can be added or removed without disturbing the network. Moreover, two or more endpoints can be merged in a sub-network and, similarly, two or more networks can be merged into a unique network simply connecting their hubs. Every node (i.e., monitoring station) can be accessed remotely to fix possible malfunctions or to update the software. The set-up and the arrangement of the monitoring stations at the sites, and within the edifices, have been accurately planned. All the details about the device, the hardware and software components, and about the code and the can be retrieved in the technical report by [16].

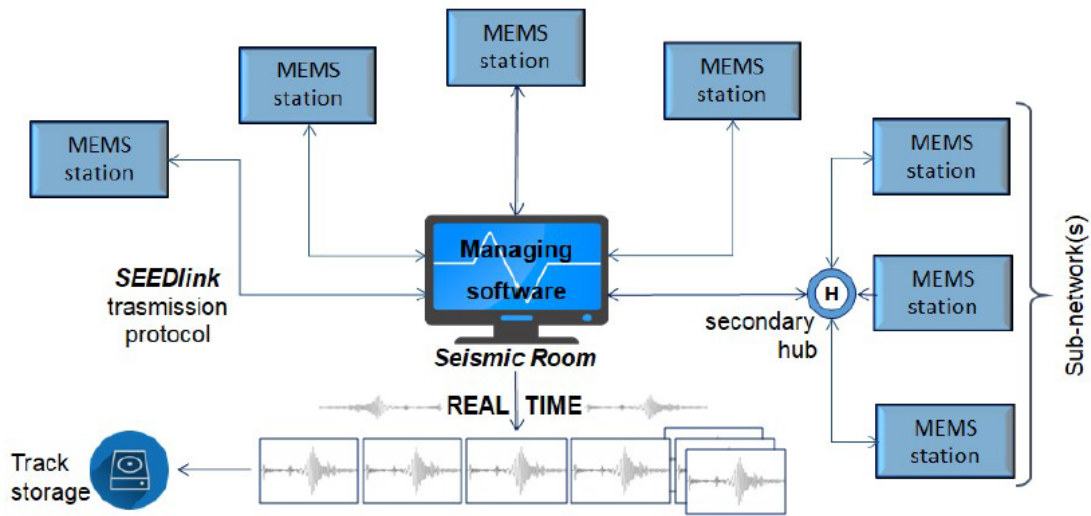


Figure 61: Scheme of the monitoring network (after [17])

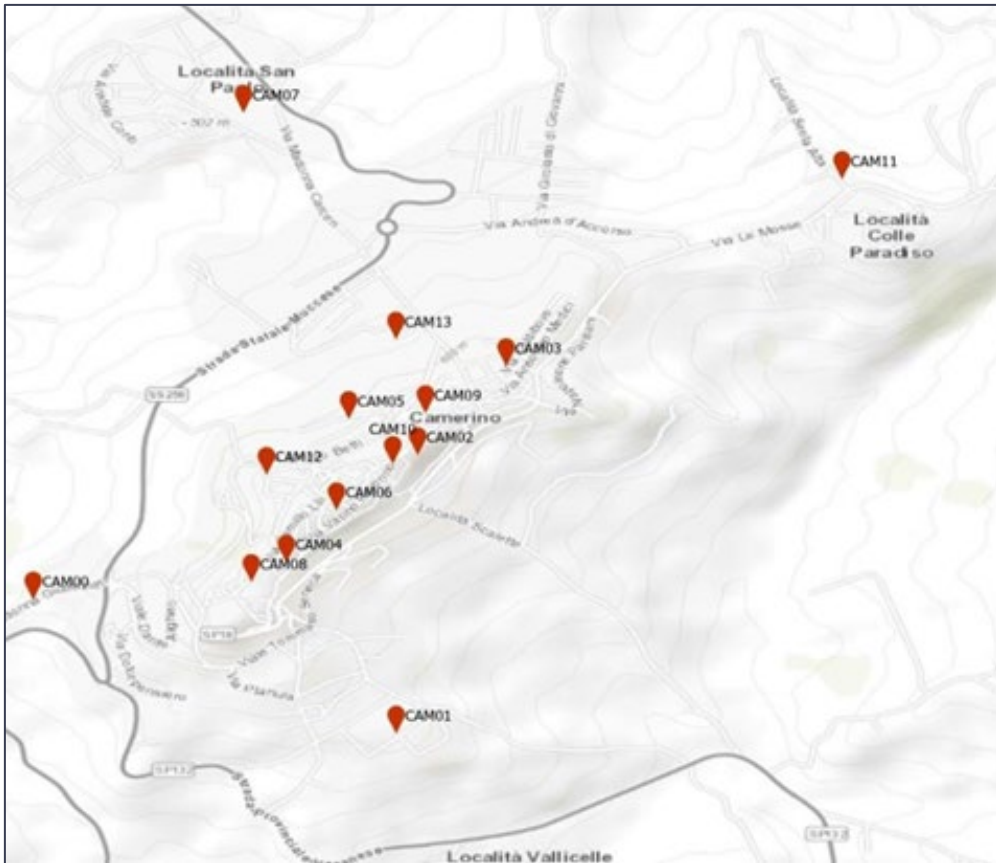


Figure 62 Map of nodes of monitoring network.

The Figure 62 shows the plain of installation, on the map the name and position of network nodes are specified. Each node of network has an installation sheet which can be consulted in the appendices of the document. Implementation details of each node are specified in installation sheets, from them it will be possible to trace the place and rooms of installation, type of data transmission, type of time synchrony, type of power supply and other details such as the Euler angles detected to rotate the traces on the reference axes.

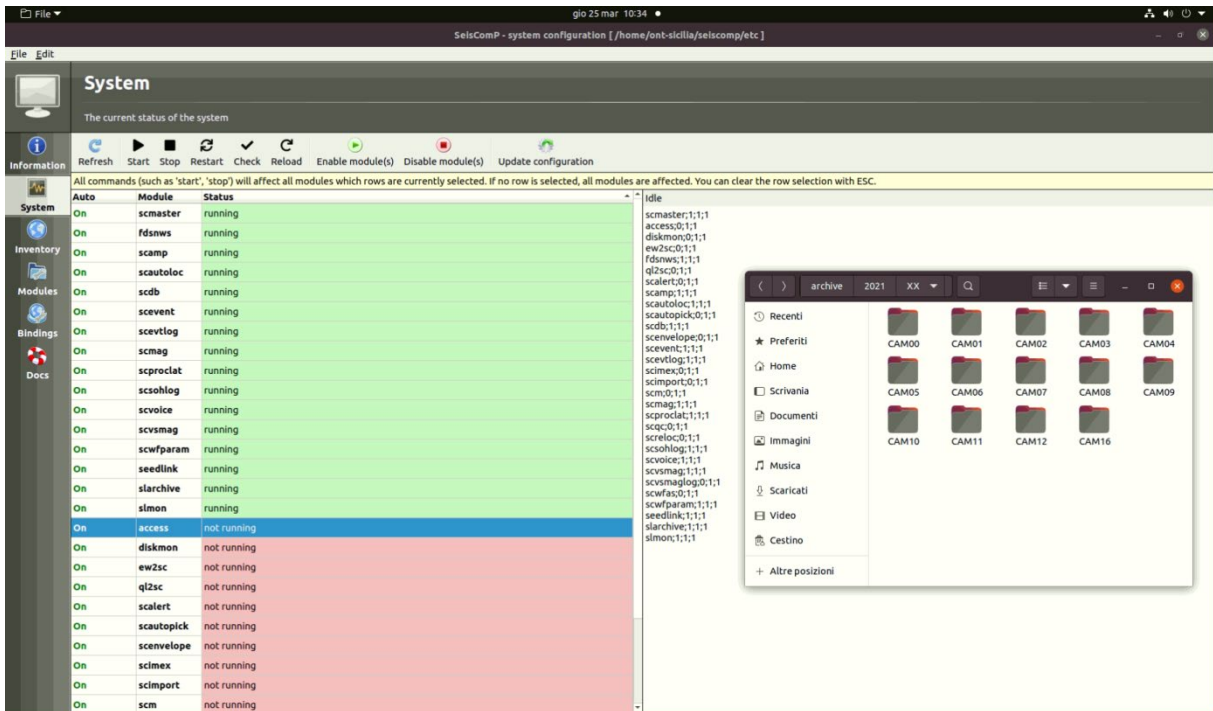


Figure 63: SeisComP4 software for recording seismic track (on format mSEED) coming from nodes of network.

The Figure 63, Figure 64, and Figure 65 show applications used on the server for data acquisition, viewer and control state of the network. In detail, Figure 63 shows the SeisComP4 [18] dashboard, that is the software dedicated in this application to the management of the seismic data. It queries the stations and creates package by package a daily trace file.

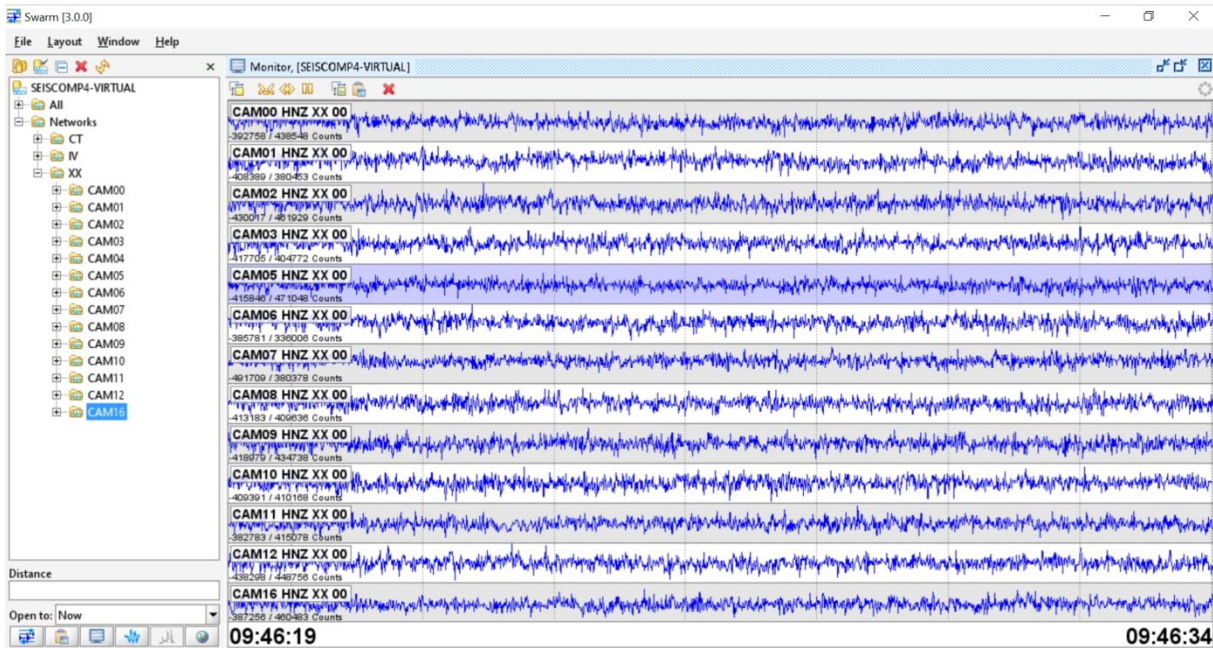


Figure 64: Swarm software view of seismic track (mSEED format) from SeisComP4 or nodes of network

The packages are sent with a frequency of about 1Hz. If the network fails for a few minutes, SeisComP4 will contact the node again to re-establish the connection. Once the connection between server and node has been stabilized, the node takes care of the waiting times to send

the missing data to the server. This buffer is limited to only 24 hours, for the reasons described in the previous section. In the event that you do not reconnect in time due to connectivity problems, a track remains saved locally on the pen-drive archive and can be recovered remotely via SSH File Transfer Protocol (SFTP) and Secure Copy Protocol (SCP) software.

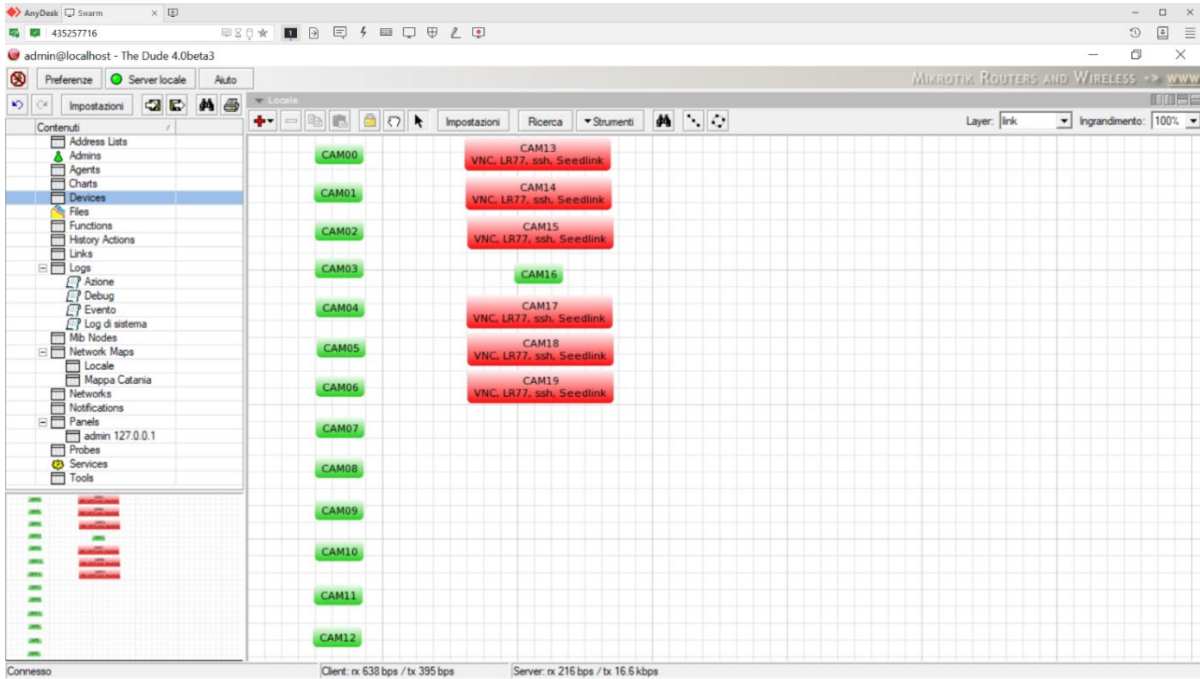


Figure 65: The DUDE software interpretation the state of network nodes. If a service is down target change colour and form which add information relative of service that not work.

The Figure 64 shows the visualization of the recordings through Swarm⁶¹, once data is archived on the repository by SeisComP4. The traces can be viewed in real-time, as is shown in the figure, by selecting the network in the archive organization.

The seismic recordings are continuously written in files stored in server folders, which are named as:

[year][network.code][station.code][channel.name.D]

(eg. 2021\XX\CAM00\HNE.D\)

The daily files are named as:

[network code].[station code].00.[channel code].D.[year].[Julian day]

(eg. XX.CAM00.00.HNE.D.2021.095)

⁶¹ <https://doi.org/10.5066/P93A9MWK>

An account of the current state of the network can be obtained with DUDE⁶² (cf. Figure 65), a software that takes care of interrogating different services periodically to monitor the status of the connectivity of the node. This software allows you to perform connection statistics, in order to change the type of transmission or improve the one already implemented, if necessary with physical interventions on site (e.g. change LTE antennas or move antennas outside LTE).

⁶² <https://www.darknet.org.uk/2015/05/the-dude-automatic-network-discovery-layout-tool/>

5. Earth Observation Data

In this section, the collection and processing of Earth Observation (EO) data by INGV is described with reference to:

- satellite middle-resolution images - radar, optical, and thermal - to characterize land use as well as land cover and to produce specific information on the ARCH pilot cities;
- high-resolution LiDAR data from aerial sensors to produce digital elevation models

Furthermore, very-high-resolution satellite images for the ARCH pilot city areas are acquired and will be processed in the following months of the project (see Table 6 for more details).

Table 6: Schedule of processing High-Resolution satellite data for each of the ARCH pilot sites.

City	Acquisition date	Spatial Resolution	Spectral range
Bratislava	To be acquired for the ARCH project	Worldview-3 ⁶³ 0.31m - Panchromatic (provided at 0.40cm by law) 1.24m - VNIR 2.70m - SWIR	Panchromatic+VNIR+SWIR
Camerino	25/06/2017		Panchromatic+VNIR
Hamburg	07/08/2020		Panchromatic+VNIR+SWIR
	24/06/2020		VNIR
Valencia (city)	30/01/2019		Panchromatic+VNIR
	05/04/2018		Panchromatic+VNIR
Valencia (Albufera)	05/04/2018		Panchromatic+VNIR
	28/10/2020		Panchromatic+VNIR

Moreover, satellite EO has been recognised in ARCH as a source of valuable data about climate, land use and atmospheric conditions, both current and historic. Despite lower resolution of available data, i.e. at grids in the range of 0.125-0.4 degrees, such data still offers high level overviews of global conditions over pilot cities. As such, data from ARCH pilot cities has been collected from the following services and is available via ARCH information systems:

- Copernicus Atmospheric Monitoring Service (CAMS)⁶⁴
- Atmosphere Data Store (ADS)⁶⁵ aimed to replace CAMS service
- Copernicus Climate Change Service (C3S)⁶⁶
- ECMWF Meteorological Archival and Retrieval System service⁶⁷
- Copernicus Land Monitoring Service⁶⁸

⁶³ Worldview-3 DigitalGlobe: <http://worldview3.digitalglobe.com/>

⁶⁴ Copernicus CAMS service: <https://atmosphere.copernicus.eu/>

⁶⁵ Atmosphere Data Store (ADS): <https://ads.atmosphere.copernicus.eu>

⁶⁶ Copernicus C3S Service and API: <https://climate.copernicus.eu/>

⁶⁷ Copernicus MARS repository: <https://confluence.ecmwf.int/display/UDOC/MARS+user+documentation>

⁶⁸ Copernicus CLMS: <https://land.copernicus.eu/>

Copernicus services have been implemented in collaboration among RFSAT, INGV, and Tecalia. A collection of service integration agents has been developed to obtain relevant data from Copernicus Climate Change Service (C3S) and Copernicus Atmospheric Monitoring Service (CAMS) as they become available. Additionally, integration of historic data for both air quality and weather data from Copernicus MARS service is also foreseen. All raw data as well as overlay maps are passed to the THIS server using dedicated WEB services built by INGV.

5.1. Ground motion by interferometry

Within the domain of ground deformation measurements, we adopted a multi-temporal Interferometric SAR (InSAR) technique, namely the Permanent Scatterers[®] (PS) technique [19], that allows to generate mean ground velocity and the related time series of deformation, starting from the collection of a large stack of SAR images. In particular, the PS technique implemented in Sarscape[®] software⁶⁹ has been used to elaborate data collected by the ESA SAR mission Sentinel-1, over the city of Hamburg.

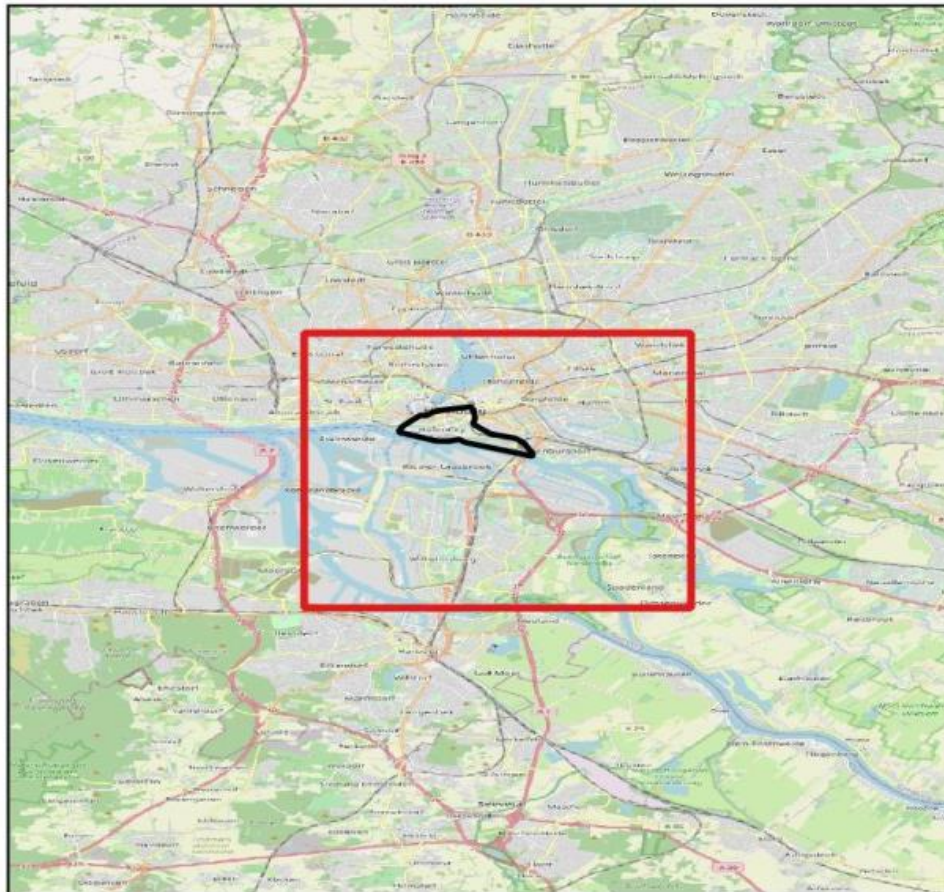


Figure 66 Location map: red rectangle refers to the area used to process SAR data; black polygon refers to Speicherstadt district.

⁶⁹ www.sarmap.ch/wp/index.php/software/sarscape/

The analysis aims to provide the basic information for the planned subsidence risk analysis in WP5. Therefore, a subset area has been selected to focus the analysis in the zone of the city most prone to subsidence. Afterwards, the InSAR analysis has been performed, over a small region of about 10km x 10 km, centred on the main interesting district of Speicherstadt (Figure 66).

For the data processing, we selected and downloaded 93 images from ascending path and 107 from the descending one from the Alaska Satellite Facility repository⁷⁰. The temporal window of the S1 observations range from 30/04/2015 to 10/01/2020, and from 1/06/2016 to 24/01/2020, for the ascending and descending set, respectively.

The maps show a general stable behaviour with some small parts that report slow subsidence between -5 and -10 mm per year, along the SAR Line of Sight (yellow-orange points in the maps of Figure 67).

Only two points in the ascending dataset, inside the HafenCity district which contains the world heritage site, have mean ground velocity of about -18 mm/yr. However, new buildings are in this zone, therefore probably this higher values could be related to construction works. The Figure 68 reports the time series of deformation of such points.

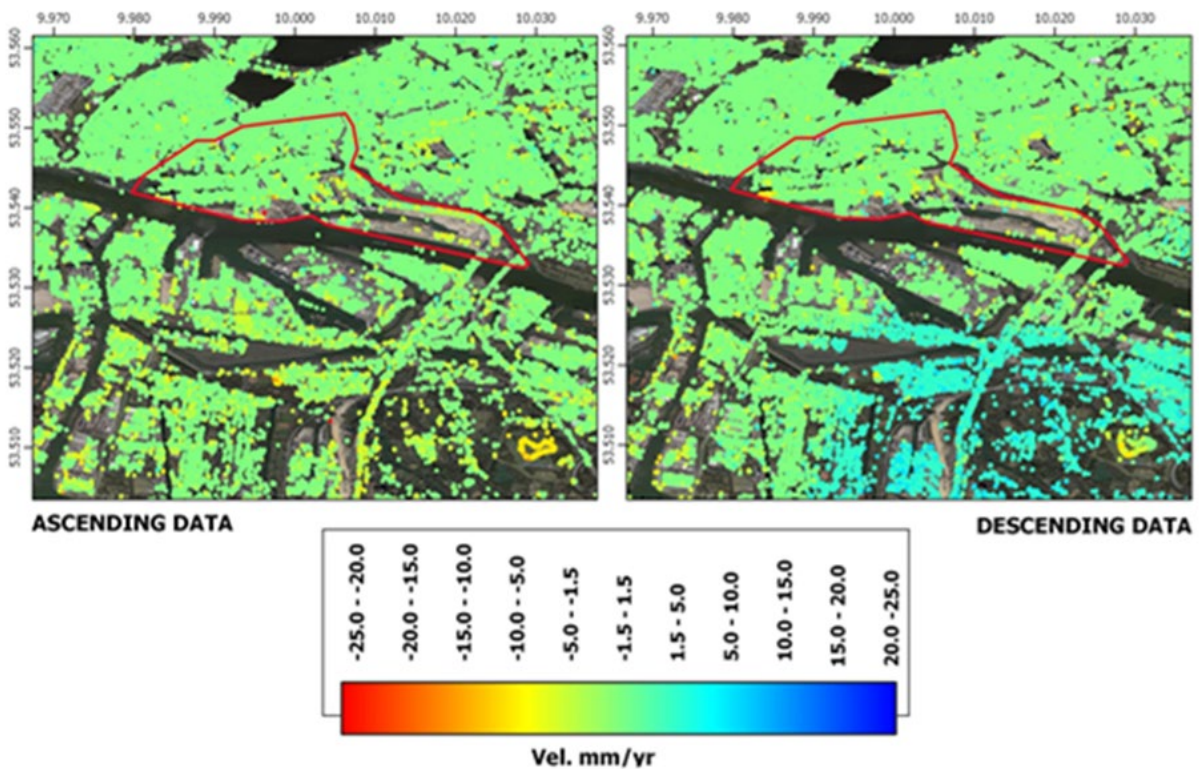


Figure 67: PS ground velocity map from ascending data (left) and the descending data (right).

⁷⁰ <https://search.asf.alaska.edu/>

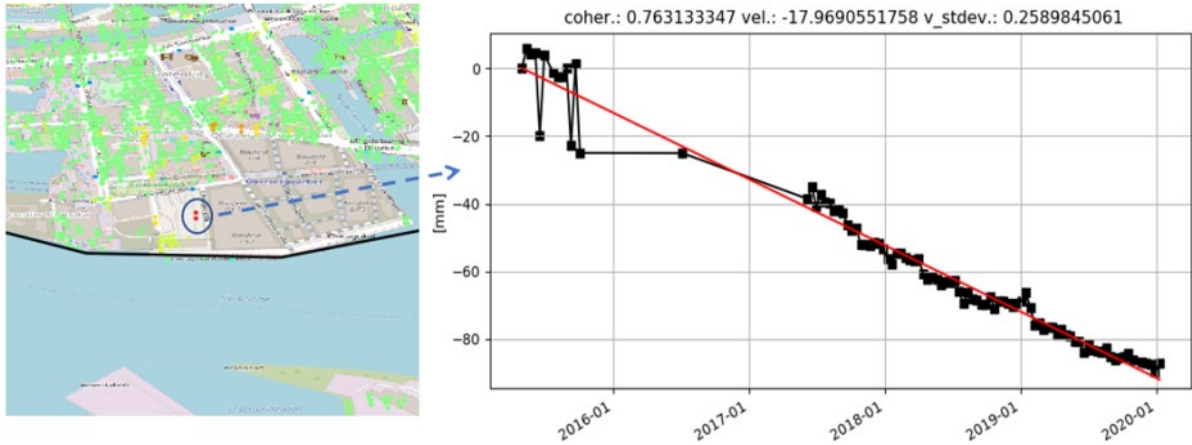


Figure 68: Example of deformation time series related to one of the most subsiding points within the analysed area. The measure is along the LoS of S1. Red line is the linear trend of the deformation.

It is worth noting that the same peak of velocity is not present in the descending map. Therefore, a more accurate analysis (e.g. by means of in situ data) is needed to confirm and validate this value. Another issue to be considered is the data gap between the end of 2015 and June 2017, that can affect the resulting velocity maps.

To better assess the ground velocity maps, we plan to update the PS processing by adding SAR images to extend the temporal windows, at least to the end of 2021. Moreover, the data gap should be removed, therefore, the images before June 2017 have to be discarded from the ascending stack of SAR images.

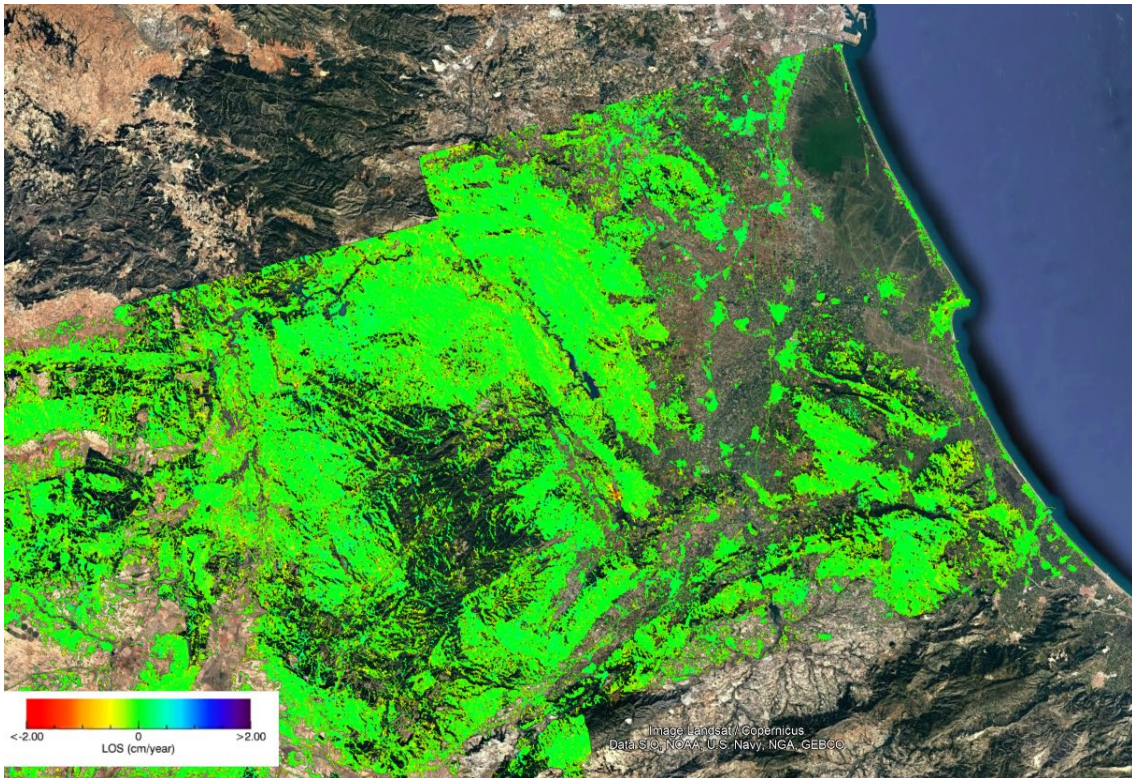


Figure 69: Ground velocity map including the area of the Albufera

The InSAR technique has been also used for the site of Valencia. In fact, following the co-creation process with the city, we decided to apply the InSAR technique to the Albufera Natural Park by using the GEP (Geohazard Exploitation Platform) service provided by ESA. In this case, the capability of Sentinel-1 imageries and P-SBAS technique [20] has been applied to retrieve information on possible deformation processes (Figure 69) in the natural area.

5.2. Thermal maps and Heat Islands

Thermal maps were developed using satellite data for the urban areas of Valencia and Bratislava, following the co-creation process with the cities, in order to provide information for the thermal risk analysis planned in WP5.

Current satellite missions, providing imagery in the Thermal InfraRed (TIR) spectral region at 60-100 meters of spatial resolution, give the possibility to estimate the land surface temperature (LST) and highlight the main surface thermal anomalies, i.e. areas where the surface temperature has a value significantly different from the background. Thermal anomalies are potentially related to underground energy sources or to land use and coverage variations, e.g. urban areas, where the urban heat island (UHI) phenomena can be observed. UHI is considered as one of the most important problems of overheating in urban areas and result, amongst others, in increases of urban smog, increased need of air-conditioning in hot climate regions (with a consequence increasing of energy consumption), and impacts on human health.

TIR Earth Observation satellite sensors measure top-of-atmosphere (TOA) radiance, which consists of the upwelling radiance emitted by the ground, the upwelling radiance emitted by the atmosphere, and the part of the downwelling irradiance emitted by the atmosphere and reflected by the ground which reaches the TOA. Accurate LST retrievals are challenging due to different effects, which include atmospheric interactions, transmittance and mainly absorption by gases, water vapour and clouds and surface emissivity.

As of today, ASTER (Advanced Spaceborne Thermal Emission and Reflection Radiometer, [21][22]) on Terra and TIRS (Thermal InfraRed Sensor) on Landsat 8 ([23][24]) offer such a capability with 90-100 m of spatial resolution (swath width of 60 Km and 185 Km respectively, within the 8-12 μm atmospheric window) and low revisit time (16 days). ECOSTRESS (ECOsystem Spaceborne Thermal Radiometer Experiment on International Space Station, [25]) is the new experimental stage space mission of NASA-JPL, launched on July 2018, with a multispectral thermal infrared radiometer to measure radiance in five spectral channels ranging from 8 to 12 μm and an additional band at 1.6 μm for geolocation and cloud detection (six bands in total).

Night-time image analysis is essential for most applications because the thermal contrast due to solar heating is absent, then the thermal anomalies can be discriminated more easily due to the absence of topographic effects and the reflectance component of the surface (common in daytime images). Another advantage of night-time images is that surface radiant temperature is more constant than during daytime. For these reasons, ASTER and Landsat 8 TIRS night-time image series have been considered in this project.

5.2.1. Methodology

Different algorithms to retrieve surface temperature from mostly TIR data have been proposed in the last years ([26]-[31]). Accurate LST retrievals require a good characterization of the surface emissivity, so algorithms and methods for Land Surface Emissivity (LSE) retrieval should be also included in any discussion on optimal LST algorithms. The literature includes an exhaustive review of LST and LSE methods as well as an optimal selection of LST algorithms to be applied to the main TIR sensors with minimum bands configuration ([26]-[31]). Main LST algorithms can be classified according to the number of TIR bands used:

- Single-channel algorithms (SCA), using only one TIR band;
- Two-channel (split-window) algorithms, using two TIR bands;
- Temperature and Emissivity Separation (TES) algorithms, using three (or more) TIR bands.

For this project, the Temperature and Emissivity Separation (TES [31], for ASTER data) and single-channel algorithm (for Landsat 8, inverting Radiative Transfer Equation - RTE of eq. 1) have been considered. In particular, even if Landsat 8 has two thermal bands, considering the United States Geological Survey (USGS)⁷¹ announced caution in the use of Band11 of Landsat 8 due to the calibration uncertainties [32], a single-channel algorithm on Band10 was applied.

$$L_{\lambda\theta}^{sat} = \varepsilon_{\lambda\theta} \tau_{\lambda\theta} B_{\lambda}(T_s) + L_{\lambda\theta}^{\uparrow} + [1 - \varepsilon_{\lambda\theta}] \tau_{\lambda\theta} L_{\lambda}^{\downarrow} \quad (1)$$

In Figure 70 the mean temperatures computed on 10 LST images acquired on Valencia and 9 LST images on Bratislava are shown. For Valencia 10 ASTER data cloud-masked and night-time estimated LST have been collected. For Bratislava, 9 ASTER data have been collected. In Table 6 the acquired data are reported for both sites.

Table 7 LST processed for Valencia and Bratislava test sites using ASTER data

Valencia	Bratislava
5 December 2005	17 May 2011
19 September 2015	19 July 2014
18 January 2016	23 August 2015
3 July 2016	30 May 2016
28 July 2016	22 November 2016
24 November 2016	29 November 2016
16 March 2017	15 October 2017
26 October 2017	8 March 2018
30 January 2018	11 November 2018
23 November 2018	-

Unfortunately, no night-time Landsat 8 data are available from 2013, but following the specific procedure⁷², a special request to USGS for night-time Landsat 8 acquisition has been submitted and in the next months the available data will be processed.

⁷¹ USGS: <https://www.usgs.gov/>

⁷² <https://www.usgs.gov/core-science-systems/nli/landsat/landsat-acquisitions>

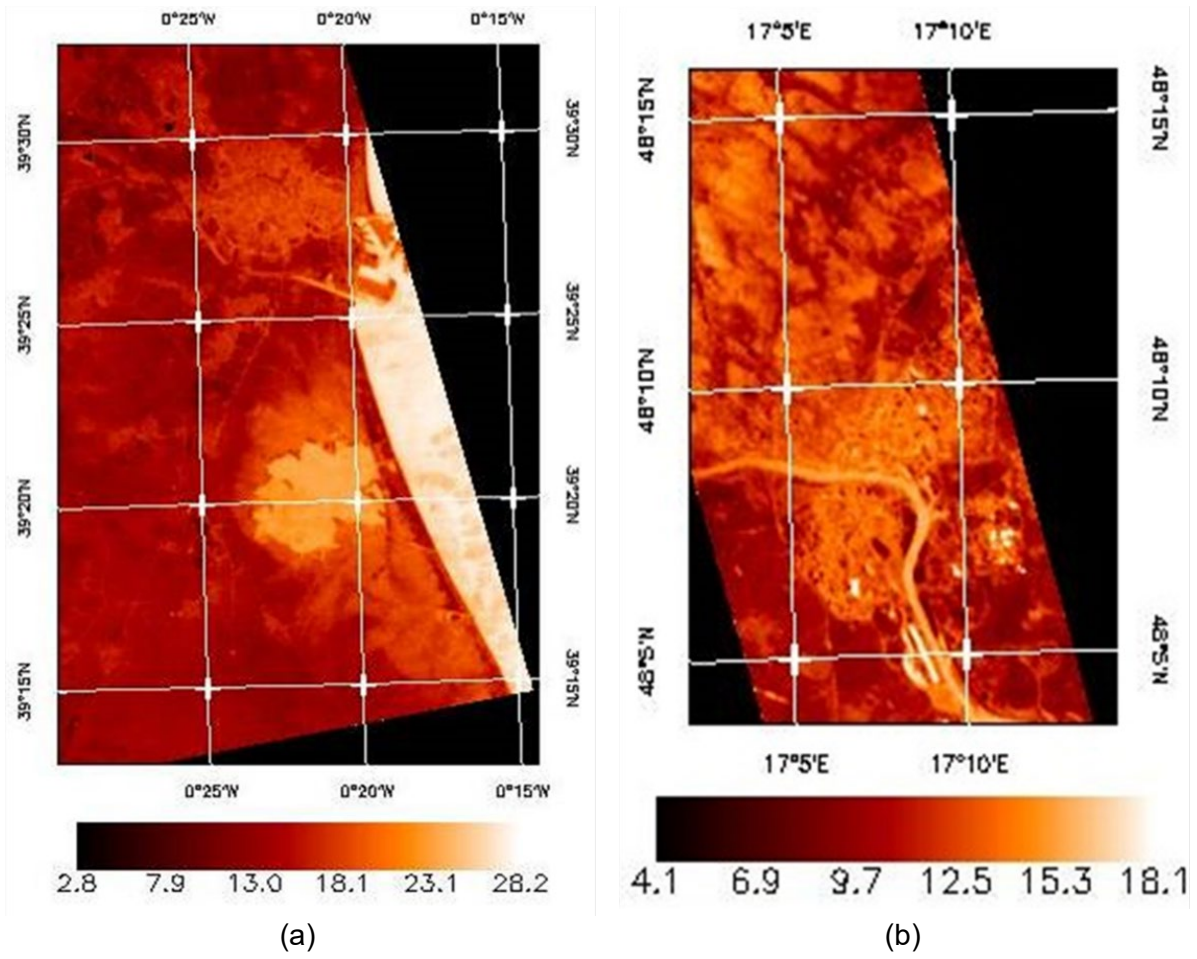


Figure 70 Mean temperature map of Valencia (a) and Bratislava (b)

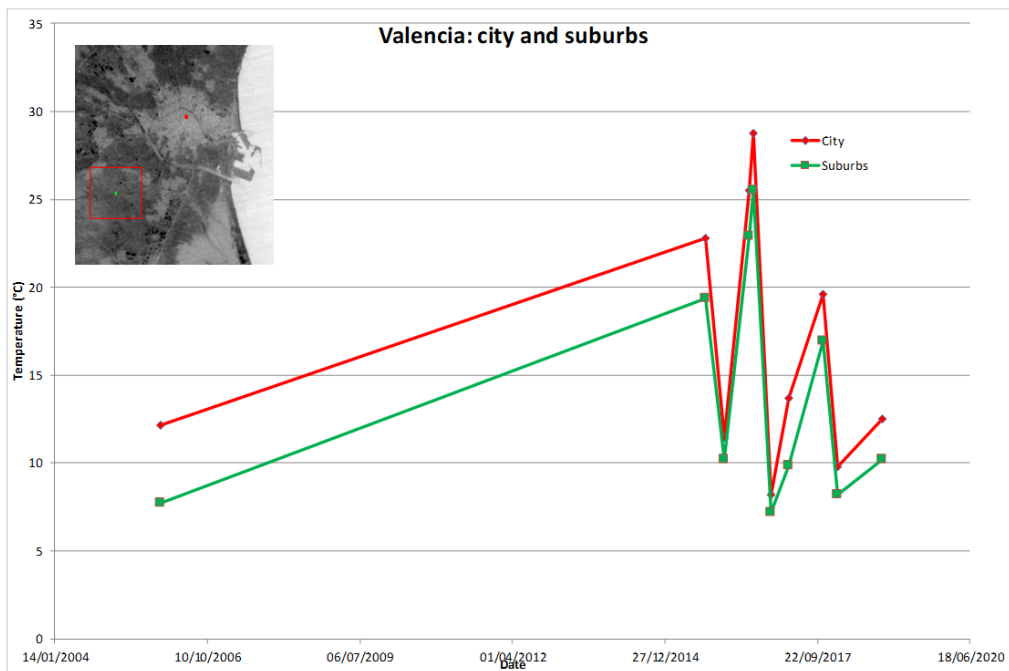


Figure 71: LST Time series on Valencia test site

Two representative points, city and suburbs, are reported. The “city” points have been selected in the cities. The suburbs point have been selected outside the cities. Figure 71 and Figure 72 show the location of these representative points and the related trend for the whole LST dataset for Valencia and Bratislava, respectively.

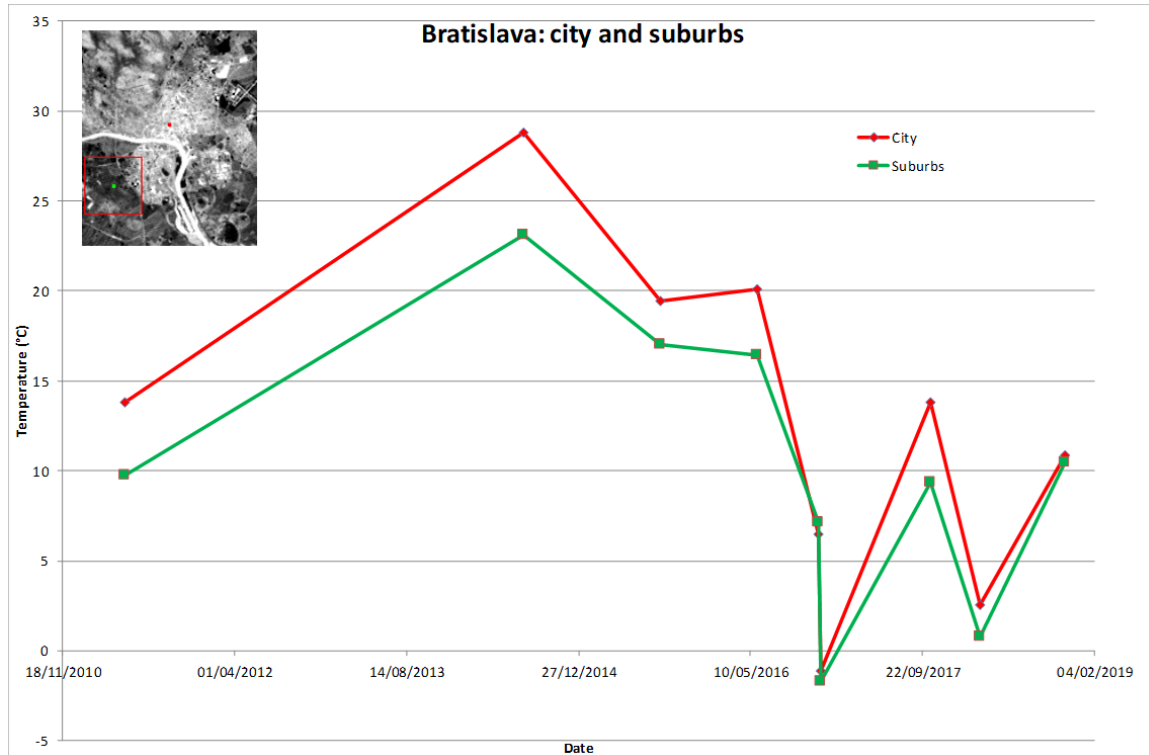


Figure 72 LST Time series on Bratislava test site

5.2.2. Comparison between LST and weather station

Historic weather data were acquired from a weather station near Valencia and Bratislava, under public access [33]. The web site offers a data archive of weather information for the same time as the satellite data.

Table 8 Comparison between temperature by weather station and LST satellite for Valencia and Bratislava

Valencia			Bratislava		
Date	Weather station temperature (°C)	Satellite temperature (°C)	Date	Weather station temperature (°C)	Satellite temperature (°C)
05/12/2005	9	9	17/05/2011	16	13.86
19/09/2015	20	21.78	19/07/2014	23	27.62
18/01/2016	10	10.2	23/08/2015	17	19.72
03/07/2016	25	25.18	30/05/2016	17	19.81
28/07/2016	26	28.42	22/11/2016	6	6.44
24/11/2016	8	7.66	29/11/2016	0	-1.33
16/03/2017	11	11.78	15/10/2017	13	13.52
26/10/2017	16	18.69	08/03/2018	2	2.12
30/01/2018	8	8.72	12/11/2018	11	10.31
23/11/2018	9	10.12			

These temperatures have been used to compare the trend of surface temperature estimated by satellite data with the local climate, as cross-comparison measurements and for representative of the soil-atmosphere interface temperature. When the satellite data were available during the analysed period, the temperatures, reported at 22:00 UTC for Valencia and 20.40 UTC for Bratislava, were compared daily with the results of the satellite-processed data, by a paired dataset. This comparison is aimed to verify if the background temperature trends, derived by satellite image processing, and validation measurements provided by the weather station near the cities, have similar behaviour (cf. Table 7), fostering the capability to extend local measurements to a wider area. For the satellite, a ROI (region of interest) including the city of Valencia and Bratislava, respectively, is considered for cross-comparison.

5.2.3. Urban Heat Islands

To refine this analysis and evaluate potential Urban Heat Islands, the Principal Component Analysis (cf. [34],[35],[36]) of the 10 LST image for Valencia and of 9 LST images for Bratislava has been done. The results are reported in Figure 73 and Figure 74.

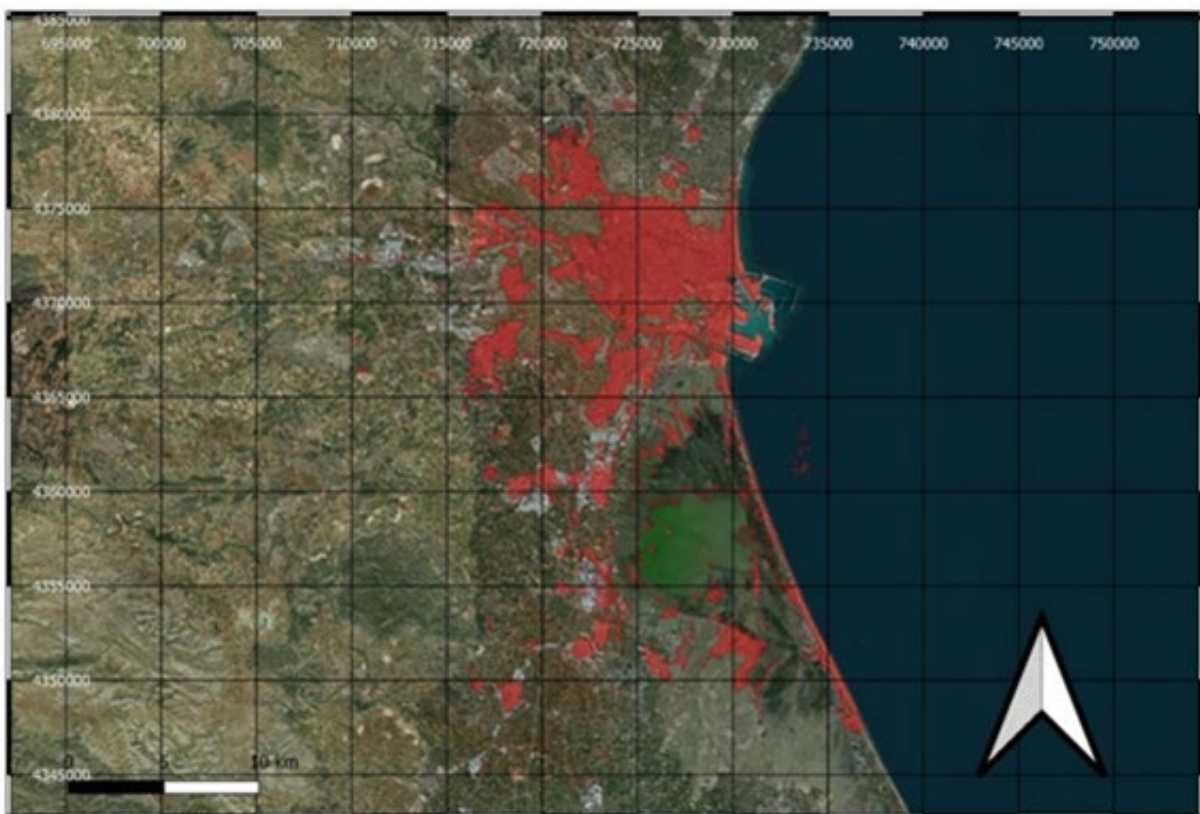


Figure 73: Valencia UHI detected with PCA

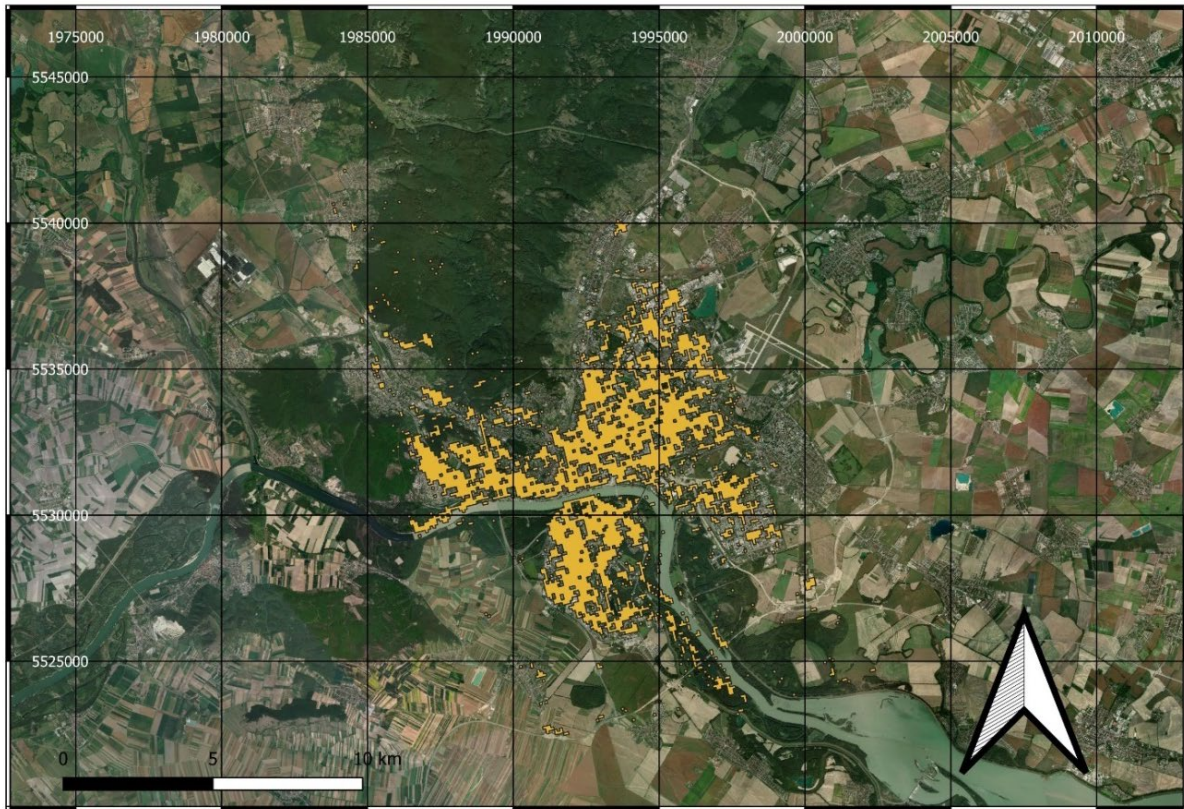


Figure 74: Bratislava UHI detected with PCA

5.3. Land classification

Urban areas are currently the most rapidly changing types of land covers. Therefore, their monitoring is one of the most relevant issues concerning the evaluation of the human impact on the environment. For such a reason EO data can provide a synoptic view of urban land covers. In ARCH, we decided to combine classification both through multispectral and hyperspectral selected images (section 5.3.1), to produce analyses on the most up-to-date data, and existing services (section 5.3.2), to obtain information about the use and coverage of large areas and their change over time. All these data can be used by the WP5 to characterise the exposed elements, also taking into account the spatial scale of the analysis.

The most common approach for classifying urban areas is the land-cover/use classifications by means of algorithms suitable to exploit the spectral characteristics of EO data. However, surface classification through remote sensed image characterization can be complicated by the heterogeneity of the outcropping material and their spatial distribution. Urban areas are heterogeneous and most pixels, at the satellite spatial resolution of 30 m/pixel, appear mixed with varying proportions of different components and/or materials, therefore individual classes are spectrally not well distinguishable. Other challenges include low sun illumination angles, which can produce atmospheric and topographic effects, as well as shadows and cloud cover. A method to reduce uncertainties and improve the quality of the classification process relies on the use of higher spatial resolution images. Italian Space Agency - Hyperspectral Precursor

of the Application Mission (ASI-PRISMA⁷³) provides datasets with both requirements: A 30 m Ground Sampling Distance (GSD) & 230 hyperspectral Very Near Infrared –Short Wave Infra-Red (VNIR-SWIR) stack and a 5 m GSD panchromatic band co-registered with the previous.

By using the combined dataset, urban land use and land cover mapping can directly benefit from the high level of detail provided by hyperspectral data and the improved spatial resolution enabling the classification at the single block scale. Indeed, applications in urban areas are mostly dedicated to the detection of surfaces (e.g. roads, rooftops, and buildings), which are the most common in an urban scene. However, it is interesting to note that urban green features such as urban forests can also benefit from the technology, despite their relatively smaller extent in an urban environment as well as the identification and classification of the waterbodies like lakes and rivers.

5.3.1. Land cover classification

In the framework of ARCH, we have focused our attention on the PRISMA data that can be downloaded by ASI catalogue⁷⁴ obtained for free and usable after the subscription license⁷⁵. This type of licence permits, to registered user, to download the EO data and, obviously, any dissemination of the product derived by the original dataset, however it's prohibited the redistribution of original data.

By querying the ASI web page, two L2D PRISMA data have been made available for Valencia and Bratislava, both collected in February 2021. From the ASI portal official reflectance L2D*.he5 file format images have been downloaded. By using an in-house code, files in PAN, VNIR and SWIR HDF format were generated. The two different VNIR and SWIR files are stacked, removing overlapping channels generating a continuous array in wavelength. PAN and VNIR-SWIR have been georeferenced by using auxiliary data contained in the original he5 file, and noisy channels are removed by applying Principal Component Analysis (PCA) forward and back (Figure 75).

The data obtained by this procedure are roughly 6 time greater than the original, indeed each 30x30 m pixel corresponds to a new matrix of 6x6 5 m GSD pixels. Starting from this new data, several training sets representative of recognizable classes were collected with the help of the PAN PRISMA channel. The selection of the training set was guided by the stacking of PAN-PRISMA channel and hyperspectral PRISMA bands (acquired simultaneously and co-registered to PAN). The training sets were restricted to the most homogeneous regions where “ground truth” was recognizable. The spectra collected are representative of material prevalently present in the scene.

⁷³ <https://www.asi.it/en/earth-science/prisma/>

⁷⁴ <http://prisma.asi.it/js-cat-client-prisma-src/>

⁷⁵ https://prismauserregistration.asi.it/LICENCE_TO_USE_PRISMA_DATA.pdf

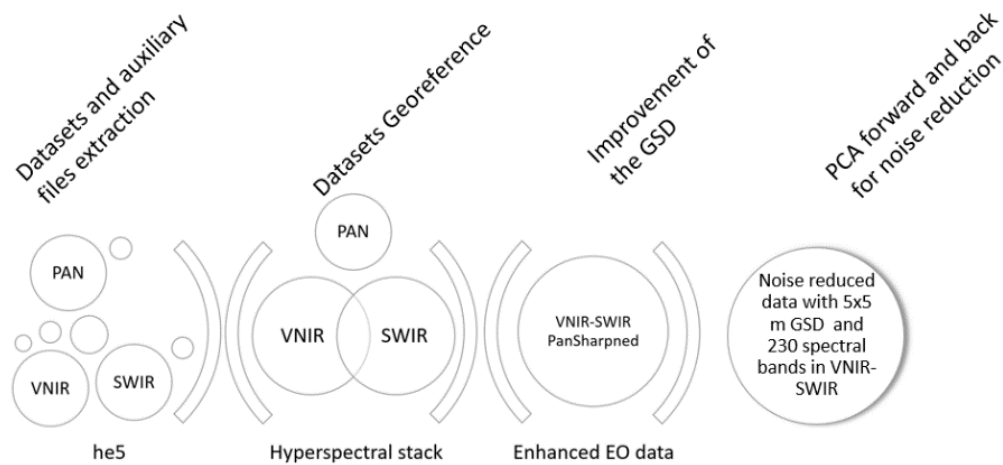


Figure 75: Logic Flow used for EO Data preparation: Processing steps used to obtain a unique hyperspectral data set; the extraction of the three dataset (VNIR, SWIR and PAN, from original ASI dataset) and their data format conversion, generation of full hyperspectral stack and noise removal by means of PCA analysis

5.3.1.1. Quality analysis

Beside the improvement of geometry, it is fundamental that the scales transformation does not infer the quality of the spectral response. Some differences can be present, in particular in the first channel of the VNIR region. Changes are attributed to the different aspect vs illumination condition, which affects the intensity of the signal but not its trend. Considering the SWIR spectral range, used to classify the image by means of Support Vector Machine (SVM) algorithm, the use of PCA generates a noise removed spectral behaviour very similar to that contained in the Pan Sharpened image.

The analysis of Bratislava and Valencia ASI-PRISMA⁷⁶ images has been based on the images listed in Table 8 where beside the technical features the weather information at the acquisition time is shown.

Table 9: Technical features and weather information about PRISMA acquisitions over ARCH sites.

City	Date	Time (UTC)	Cloud Mask	Sun Angle	Zenith	Sky conditions
Bratislava	2021/02/01	09:57	0.28	66.81		Clear sky
Valencia	2021/01/18	10:56	0.40	62.39		Clear sky

PRISMA data were downloaded as L2D products in He5 format and converted to ENVI format by means of an in house code, which also perform the processing steps described in the previous paragraph and reported in Figure 75.

It is important to remark that data sets show an error in geo-referencing characterized by different values both in term of direction and magnitude. This unpredictable misinterpreted

⁷⁶ <http://prisma-i.it/index.php/en/>

geo-registration do not interfere with the classification results, but it should be considered during the validation and publication processes.

Where the sensed scene shows a spatial homogeneity with respect to the GSD the error in geo-referencing could be neglected, otherwise for areas with significant differences at smaller scale this error becomes a key parameter in the classification processes. Concerning the radiometry, we have decided to use the data as they are delivered by ASI with the only exception of the band removal in the VNIR-SWIR limit where the two spectrometers overlap.

Given the limitations discussed earlier in the text, our work has focused on the analysis and evaluation of hyperspectral data for producing surface classification in an urban context. The objective of this activity is to use a two-step method for producing surface classification, based on spectral analysis of PRISMA space-borne hyperspectral data.

The first step involves the transformation of the hyperspectral data using a PCA algorithm and visually interpreting the obtained inverse PCA colour images. The second step requires the extraction of training areas (which represents the spectral signature of the material in the image, also known as endmember) from the PCA images and the classification of the data set using a Support Vector Machine algorithm. The first method is based on simple interpretation of enhanced imagery, whereas the second is computer assisted and uses a classification that is based on training areas for each material. The training areas were chosen where a typical spectral signature of a given surface could be clearly identified. The spectral signatures derived from these training areas were used to identify similar signatures throughout the area on the hyperspectral data using various classification techniques. However, in the present case, the training areas do not represent end members under the true definition since they do not represent unique signatures for individual material, but rather represent mixed signatures based on groups of materials.

5.3.1.2. Principal Component Analysis

The PCA transform is an effective technique for reducing a large multiband data set into a smaller number of components that contain the majority of information (spectral variance) in the data set. The PCA transform implemented in ENVI™⁷⁷ involves two cascaded PCA transformations.

The first transformation, based on an estimated noise covariance matrix, decorrelates and rescales the noise in the data. The second step is a standard PCA transformation of the noise-reduced data. There can be as many components as there are input bands; however, each component, starting from the first, describes less and less of the overall variance of the data set. Typically, only a small number of components are required to describe most of the information for the entire data set. The contribution of each band to each component is measured by an eigenvector, which can be interpreted like a correlation coefficient.

⁷⁷ https://www.l3harrisgeospatial.com/docs/using_envi_Home.html

5.3.1.3. SVM classification

The full PRISMA resolution imagery was used, where the feature space of SVMs was defined using all PRISMA bands considering the targets (Figure 76). The SVM was implemented using the radial basis function (RBF) kernel for performing the pair wise classification. We chose the RBF kernel as it generally requires defining a small number of parameters and is also known to generally produce good results ([37], [38] [39]). The input parameters required for running SVMs in ENVI include the “gamma (γ)” in the kernel function, the penalty parameter, the number of pyramid levels to use, and the classification probability threshold value. In our case, parameterization of the above RBF kernel function was based on performing a number of permutations and combinations using classification accuracy as a measure of quality. A similar approach was followed by [33], [40] and [41]. In addition, suggestions provided in the ENVI User’s Guide were also taken into account in kernel function parameterization. As a result, the γ parameter was set to a value equal to the inverse of the number of the spectral bands of the PRISMA (i.e. 0.007), whereas the penalty parameter was set to its maximum value (i.e. 100), forcing no misclassification during the training process. The pyramid parameter was set to a value of zero, forcing the PRISMA to be processed at full resolution, whereas a classification probability threshold of zero was used, thus all image pixels had to be classified into one class.

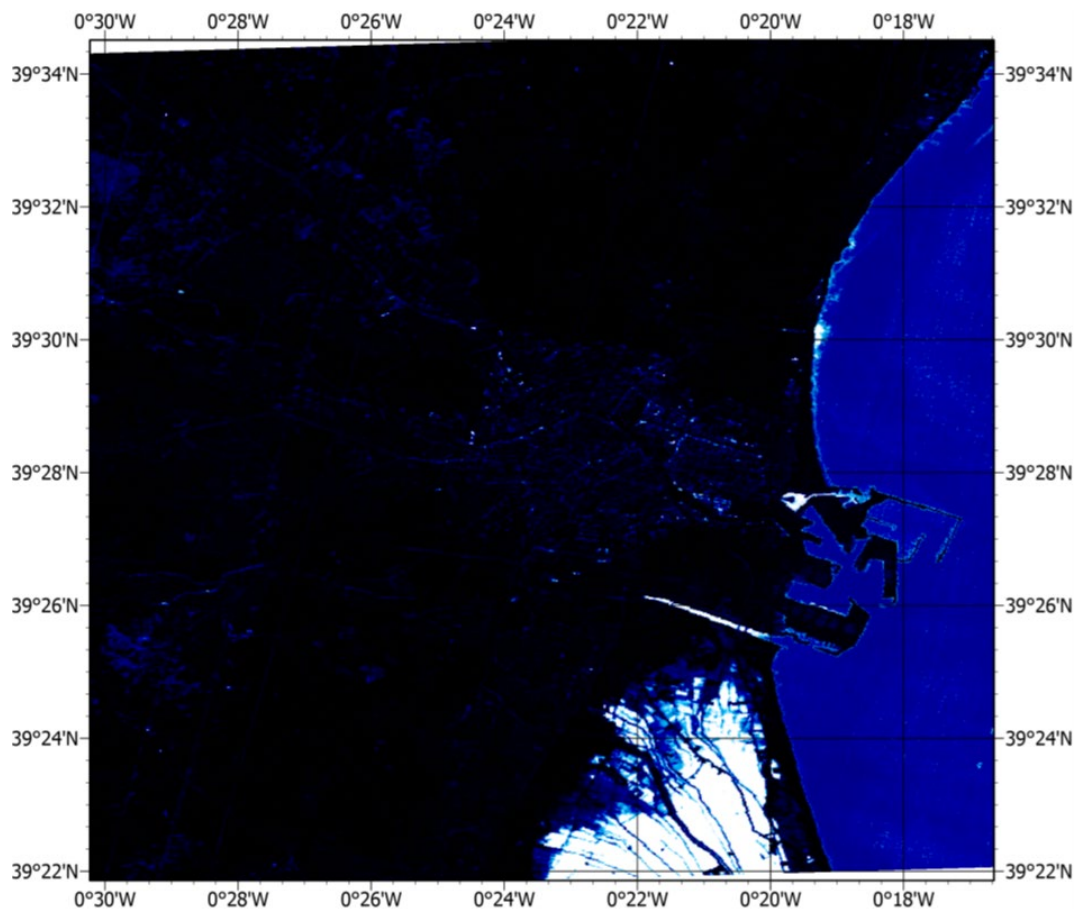


Figure 76: Support Vector Machine algorithm result applied on PRISMA data. The Albufera area is highlighted: the White Black scale indicates the accuracy of the classification with respect to the ground truth data sampled by using PRISMA data. As example, in this map: white indicates the maximum compliance between ground truth related to wetland area and all pixels of the image, whereas black is the minimum.

5.3.2. LULC by Copernicus Land Monitoring Service

The land use and land cover classification provided by CLMS was included as service in the ARCH information system, this permits to cover the ARCH pilot cities. In particular, two classification datasets were used:

- The CORINE Land Cover inventory started from 1990 and producing updates in 2000, 2006, 2012, and 2018. It consists of an inventory of land cover in 44 classes and uses a Minimum Mapping Unit (MMU) of 25 hectares for areal phenomena and a minimum width of 100 m for linear phenomena⁷⁸. The time series are complemented by change layers, which highlight changes in land cover with an MMU of 5 ha. Different MMUs mean that the change layer has higher resolution than the status layer. The classification is based on different satellite data available over time (e.g. CLC 2018 is based on Sentinel-2 and Landsat-8 for gap filling).
- The Urban Atlas inventory provides pan-European comparable land cover and land use data covering a number of Functional Urban Areas (FUA). It will be based on very high resolution imagery (2,5 x 2,5 m pixels) in combination with other available datasets (high and medium resolution images) over the pan-European area.⁷⁹ The nomenclature of this LULC product includes 17 urban classes with MMU 0.25 ha and 10 rural classes with MMU 1ha.

5.4. Digital Elevation Models by LIDAR data

Digital Elevation Models (DEM) are three-dimensional (3D) representations of the surface created from elevation data. Digital Terrain Models (DTM) are DEMs of the shape of the ground surface, whereas Digital Surface Models (DSM) are DEMs of the shape of the surface including vegetation, infrastructures, buildings, and other elements above the ground. The generation of digital models plays an important role both to define topography (cf. Figure 77), that play a key role in the most hazard analyses (e.g. slope instabilities or pluvial flooding), and to characterize geometry and elevation of the elements above the ground (cf. Figure 78) as difference between DSM and DTM (e.g. to characterize height of buildings).

Table 10 Data and providers for digital elevation models of the ARCH pilot areas

City	Type of data	Period of survey	Data-provider
Camerino	LIDAR	2014	Italian Ministry of the Environment and the Protection of the Territory and the Sea
Bratislava	LIDAR	2017-2018	Geodesy, Cartography and Cadastre Authority of the Slovak Republic (ÚGKK SR)
Valencia	Digital Elevation Model	2015-today	Centro Nacional de Información Geográfica (CNIG)

⁷⁸ <https://land.copernicus.eu/pan-european/corine-land-cover>

⁷⁹ <https://land.copernicus.eu/local>

DEMs can be derived through a variety of techniques, such as digitizing contours from existing topographic maps, topographic levelling, EDM (Electronic Distance Measurement), differential GPS measurements, (digital) photogrammetry, Radar remote sensing (InSAR), and Light Detection and Ranging (LiDAR). DSMs and DTMs have been extracted for the ARCH pilot cities directly from digital models or through processing of LiDAR data, available free or on-demand, and provided by national cartographic services (cf. Table 9).

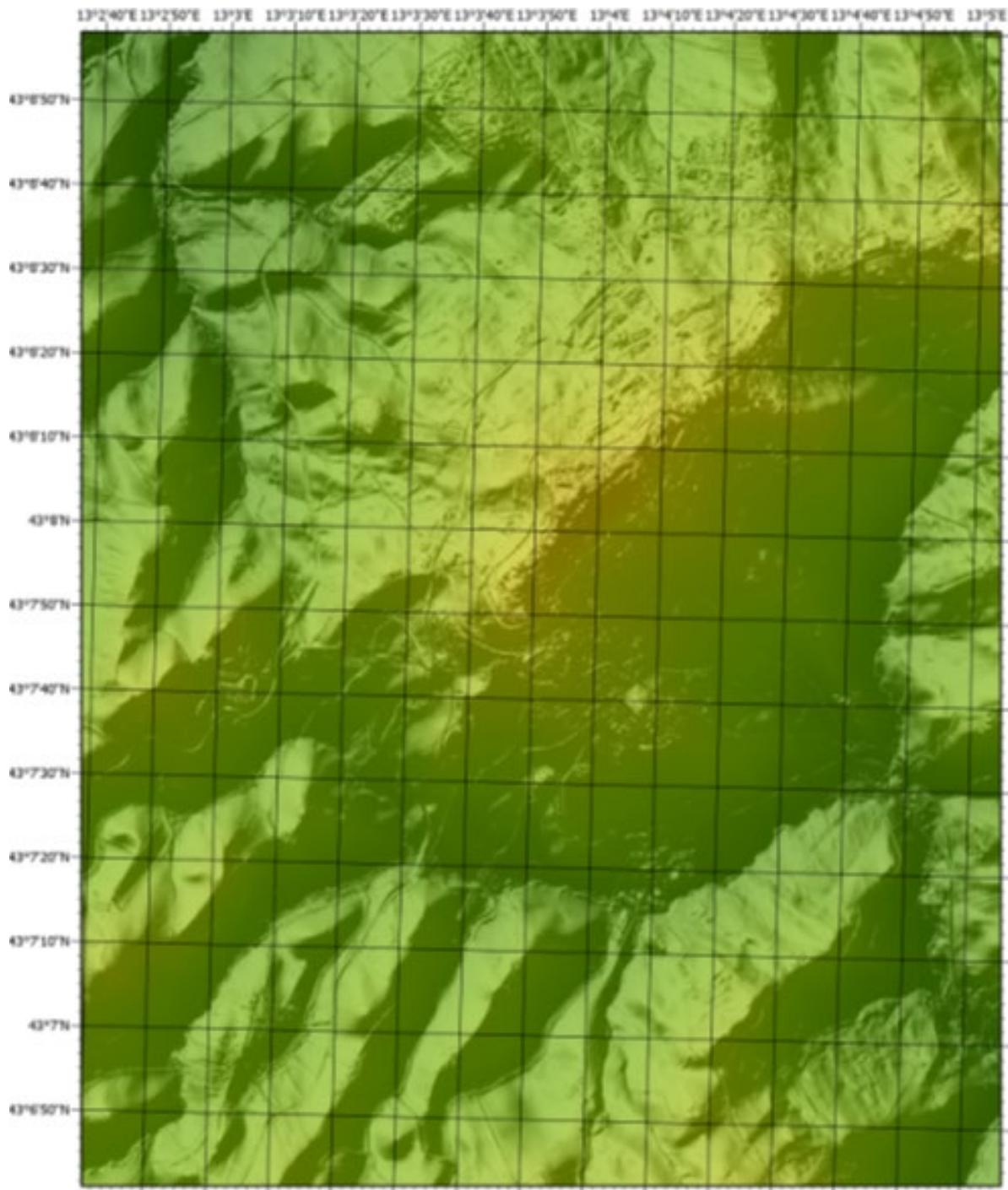


Figure 77 Digital Terrain Model of the Camerino hill (Cell size 1x1m) obtained by processing the LIDAR datasets provided by Italian Ministry of the Environment and the Protection of the Territory and the Sea.

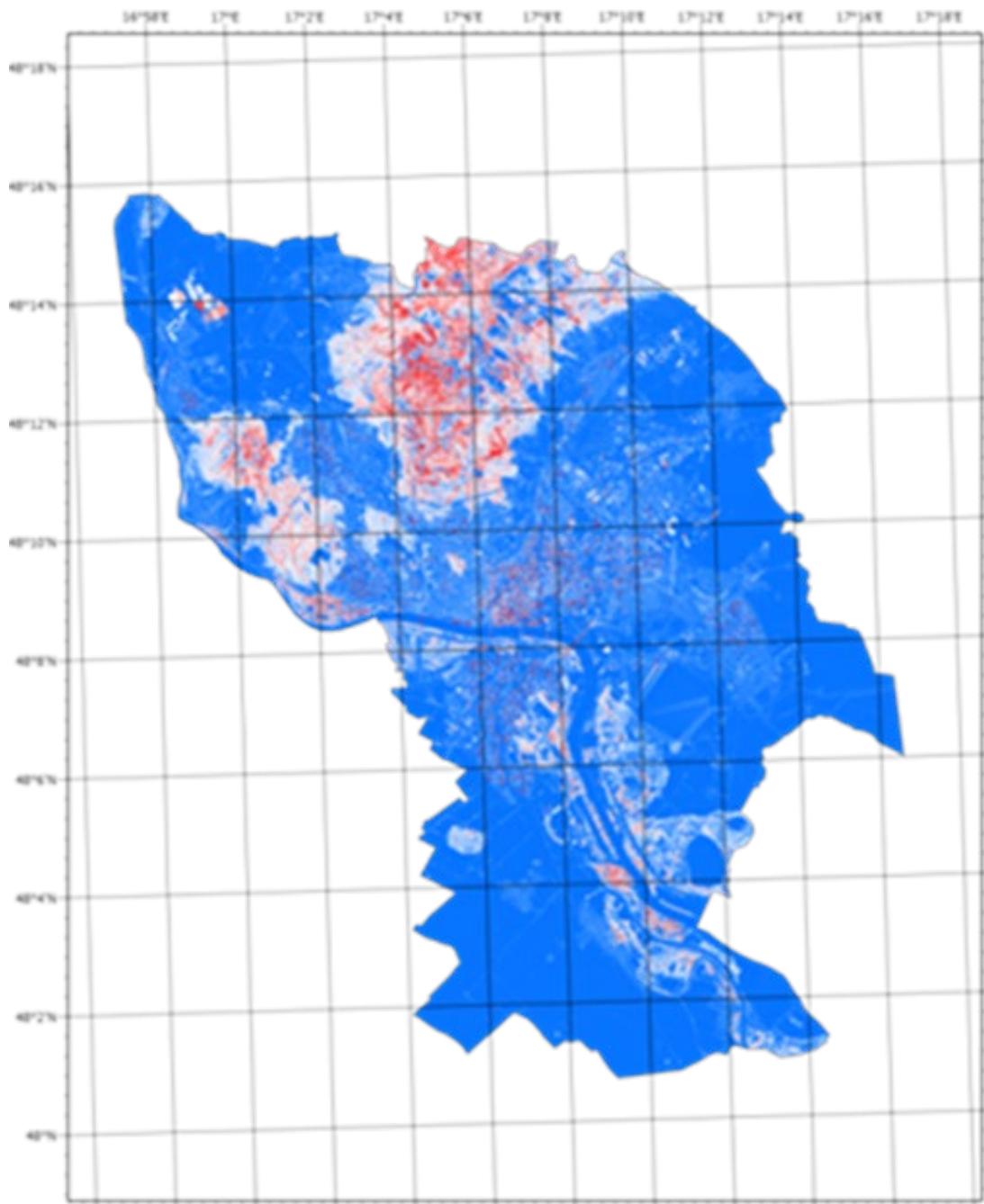


Figure 78: Difference between Digital Surface Model and Digital Terrain Model for Bratislava city (Cell size 1x1m) obtained by processing the LIDAR datasets provided by Geodesy, Cartography and Cadastre Authority of the Slovak Republic (ÚGKK SR).

5.5. Copernicus Atmosphere Monitoring Service (CAMS) integration

The work described in this section refers to activities in Task 4.3 where capturing of historical and real-time data related to environmental threats was performed from existing climate services like Copernicus Climate Change Service and Copernicus Emergency Management Service, complementing real-time sensor networks, cloud based environmental monitoring systems described in earlier sections. As part of this work, maps of environmental contaminations with their spatial and temporal evolution (e.g. satellite derived data about

atmospheric gases from Copernicus Climate Services), were overlaid at THIS with sensor data about the current condition of heritage assets. Considering its global perspective, satellite based monitoring service has been built to support all of the ARCH pilot sites.

The CAMS service offered by the European Centre for Medium-Range Weather Forecasts(ECMWF)⁸⁰ provides consistent information about the condition of the atmosphere and various air pollutants for any location on Earth. It offers both near real-time (12hrs periodicity) monitoring as well as historical data derived from satellite images for several decades back. The CAMS service uses satellite and ground-based observations with forecast models to provide added value information regarding composition of the atmosphere. The list of all available sensor types includes over 5000 parameters⁸¹, out of which only 60 are directly accessible in near real-time (every 12 hrs) via a FTP service.

The remaining ones are only available as historical data and need to be requested on one to one bases from MARS service, since much of it is on removal storage media. The added benefit is that resolution of historical data goes as low as 0.125 degrees as compared to 0.4 degrees for CAMS service. Data from CAMS is provided in both GRIB⁸² and NetCDF⁸³ formats. The list of parameters acquired from CAMS for ARCH is shown in Table 10.

Table 11. Parameters captured every 12hrs from the CAMS service

Parameter	Description
<i>Lnsp</i>	Logarithm of surface pressure
<i>aermr01</i>	Sea Salt Aerosol (0.03 - 0.5 um) Mixing Ratio [kg/kg]
<i>aermr02</i>	Sea Salt Aerosol (0.5 - 5 um) Mixing Ratio [kg/kg]
<i>aermr03</i>	Sea Salt Aerosol (5 - 20 um) Mixing Ratio [kg/kg]
<i>aermr04</i>	Dust Aerosol (0.03 - 0.55 um) Mixing Ratio [kg/kg]
<i>aermr05</i>	Dust Aerosol (0.55 - 0.9 um) Mixing Ratio [kg/kg]
<i>aermr06</i>	Dust Aerosol (0.9 - 20 um) Mixing Ratio [kg/kg]
<i>aermr07</i>	Hydrophilic Organic Matter Aerosol Mixing Ratio [kg/kg]
<i>aermr08</i>	Hydrophobic Organic Matter Aerosol Mixing Ratio [kg/kg]
<i>aermr09</i>	Hydrophilic Black Carbon Aerosol Mixing Ratio [kg/kg]
<i>aermr10</i>	Hydrophobic Black Carbon Aerosol Mixing Ratio [kg/kg]
<i>aermr11</i>	Sulphate Aerosol Mixing Ratio [kg/kg]
<i>aermr16</i>	Nitrate fine mode aerosol mass mixing ratio [kg/kg]
<i>aermr17</i>	Nitrate coarse mode aerosol mass mixing ratio [kg/kg]
<i>aermr18</i>	Ammonium aerosol mass mixing ratio [kg/kg]
<i>c2h6</i>	Ethane [kg/kg]
<i>c3h8</i>	Propane [kg/kg]
<i>c5h8</i>	Isoprene [kg/kg]
<i>ch4_c</i>	Methane (chemistry) [kg/kg]
<i>co</i>	Carbon monoxide

⁸⁰ European Centre for Medium-Range Weather Forecasts(ECMWF): <https://www.ecmwf.int/>

⁸¹ Full parameter list on CAMS: <https://apps.ecmwf.int/codes/grib/param-db/?filter=All>

⁸² GRIB format: <https://www.wmo.int/pages/prog/www/DPS/FM92-GRIB2-11-2003.pdf>

⁸³ NetCDF format: <https://www.unidata.ucar.edu/software/netcdf/>

den	Density [kg/m ³]
h2o2	Hydrogen peroxide [kg/kg]
hcho	Formaldehyde [kg/kg]
hno3	Nitric acid [kg/kg]
no	Nitric oxide [kg/kg]
no2	Nitric dioxide [kg/kg]
oh	Hydroxyl radical [kg/kg]
pan	Peroxyacetyl nitrate [kg/kg]
so2	Sulphur dioxide
amaod550	Ammonium aerosol optical depth at 550 nm [-]
aod1240	Total Aerosol Optical Depth at 1240nm [-]
aod469	Total Aerosol Optical Depth at 469nm
aod550	Total Aerosol Optical Depth at 550nm
aod670	Total Aerosol Optical Depth at 670nm
aod865	Total Aerosol Optical Depth at 865nm
bcaod550	Black Carbon Aerosol Optical Depth at 550nm
duaod55	Dust Aerosol Optical Depth at 550nm
gtco3	GEMS Total column ozone [kg/m ²]
ism	Land-sea mask (0 to 1)
niaod550	Nitrate aerosol optical depth at 550 nm
omaod550	Organic Matter Aerosol Optical Depth at 550nm
ssaod550	Sea Salt Aerosol Optical Depth at 550nm
tchcho	Total column Formaldehyde [kg/m ²]
tcno2	Total column Nitrogen dioxide [kg/m ²]
tcso2	Total column Sulphur dioxide [kg/m ²]
tc_c2h6	Total column ethane [kg/m ²]
tc_c3h8	Total column propane [kg/m ²]
tc_c5h8	Total column isoprene [kg/m ²]
tc_ch4	Total column methane [kg/m ²]
tc_h2o2	Total column hydrogen peroxide [kg/m ²]
tc_hno3	Total column nitric acid [kg/m ²]
tc_no	Total column nitrogen monoxide [kg/m ²]
tc_oh	Total column hydroxyl radical [kg/m ²]
tc_pan	Total column peroxyacetyl nitrate [kg/m ²]
z	Geopotential [m ² /s ²]
pm1	Particulate matter d < 1 um [kg/m ³]
pm10	Particulate matter d < 10 um [kg/m ³]
pm2p5	Particulate matter d < 2.5 um [kg/m ³]
uvbed	UV biologically effective dose
uvbedcs	UV biologically effective dose clear-sky

The above parameters are further converted into distribution maps at global Earth scale and overlays are produced in KMZ format for upload to the THIS server using “mapupload” WEB service from INGV. An example map produced for Sea Salt Aerosol is shown in Figure 79.

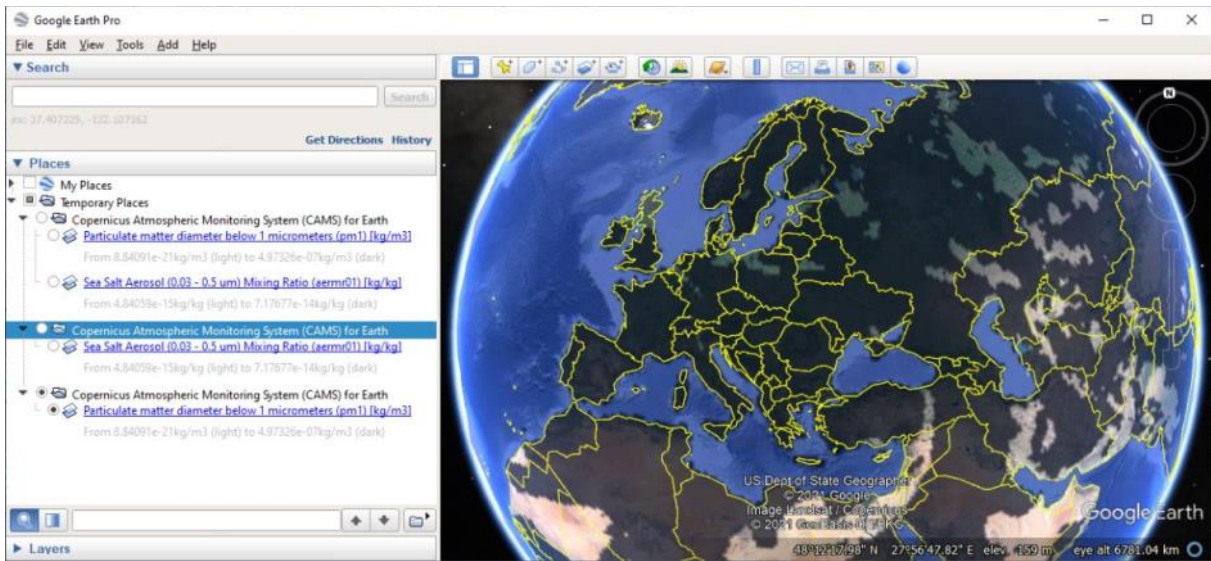


Figure 79: Example of a KMZ map generated from CAMS data

5.5.1. MapUpload WEB service from INGV

This service allows both single and multiple map overlap upload to THIS server.

The list of methods available is:

- <https://160.97.1.28/archportal/api/mapupload/uploadsinglefile>

It uploads a single map overlay file. Example use:

```
var client = new RestClient("https://160.97.1.28/archportal/api/mapupload/uploadsinglefile");
var request = new RestRequest();
request.AddFile("file", @"d:\CAMS_Earth.kmz");
var response = client.Post(request);
var content = response.Content; // Raw content as string
```

- <https://160.97.1.28/archportal/api/mapupload/uploadmultiplefile>

It uploads multiple map overlay files. Example use:

```
var client = new RestClient("https://160.97.1.28/archportal/api/mapupload/uploadmultiplefile");
var request = new RestRequest();
request.AddFile("files", @"d:\CAMS_Earth1.kmz");
request.AddFile("files", @"d:\CAMS_Earth2.kmz");
request.AddFile("files", @"d:\CAMS_Earth3.kmz");
var response = client.Post(request);
var content = response.Content; // Raw content as string
```

- <https://160.97.1.28/archportal/api/mapupload/>

It lists uploaded files.

The custom Python implementation of the upload function:

```
import requests
INGV_URL = 'http://160.97.1.28/archportal/api/mapupload/uploadsinglefile'
myHeader = {'X-Auth-Token' : ""}
myFiles = {'file': open('countries-2.kmz' , 'rb')}
myData = { 'createGroupForEachFile' : 'false' }
response = requests.post (INGV_URL, headers = myHeader, files = myFiles, data = myData)
print(response.text)
```

5.6. Conclusions

This chapter details the integration of two Copernicus services that have been flagged by end users as most important for their pilot areas, the Climate Change Service (C3S) and Atmospheric Monitoring Service (CAMS) for near real time monitoring of weather and pollution in global scales, with optional extensions to MARS service in case of a need for historical data with higher resolution (0.125°/pixel instead of 0.4°/pixel). The CAMS service currently supplies the THIS server with more than 60 air pollution parameters that are available in near real-time (i.e. at 12hrs intervals) out of more than 5000 parameters available, most of which are only available from historical MARS database considering that those require longer processing time from the satellite acquired EO imaging. Since users have been more interested in current conditions, the historical data acquisition is supported, but will be supplied on demand from specific pilots, especially that amounts of available data are likely to overload the THIS server if all available data was to be processed and sent to THIS platform.

This section also details the WEB services used for uploading satellite derived data to THIS server. Sensor data derived from satellite imaging use the same type of WEB services as for any other in-situ sensor, adding only an extra info regarding the source of the data. The proprietary WEB service that was fully developed for Copernicus services was for uploading overlay maps of pollutants produced out of CAMS data that can be overlaid on request with other maps provided already by the THIS platform.

6. Summary of outcomes

This deliverable reported on the overall achievements from research and developments performed in Task 4.1 altogether comprising the THIS repository of sensor data about heritage assets and their environmental conditions, in a form suitable for subsequent use in analysis of historic areas and hazards to the information management systems.

A range of custom sensor technologies have been developed in response to explicit needs and requirements as expressed through numerous teleconferences with city partners through a co-creative process organised by ICLEI. Considering that needs in different pilot sites have not been exactly the same, the approach adopted in ARCH was to produce a common superset of data sources for all pilot sites irrespective if they have or not been explicitly asked for by a given pilot site. This has proven beneficial, as the data begun to be available via THIS platform and pilot sites have started realising added value of data that they have not firstly requested.

Such developments included e.g. a range of weather and pollution parameters acquired from both European, National, Open Platform and proprietary sensor data providers. Since such already available data sources have not covered all required types of sensors, a range of custom wireless sensing solutions have been also developed. Those offer various levels of customisation, from indoor to outdoor deployment options, mains powered to those employing ambient energy supplies, from highly accurate and hence expensive nodes to less accurate though much more economic options. Furthermore, different Internet-of-Things (IoT) service options have been produced to ease the collection, processing and transmission of sensor information to the Threats and Hazards Information System (THIS) server deployed for ARCH.

An important infrastructure of accelerometric sensors was deployed in the framework of the Task 4.1, in order to monitor any seismic events occurring in the area of Camerino. This urban seismic network allows the recording of the ground motion in (and around) the historic centre, thus providing the shaking parameters in near real-time by means of an automatic processing of the signals, that is being developing in the Task 4.3. In addition, the monitoring of selected buildings of the cultural heritage has been performed both to take under control the dynamic behaviour of these assets, already damaged by the 2016-2017 Central Italy seismic, and to provide indications for future recovery interventions.

Another part of work in Task 4.1 that has been reported in this deliverable are also technologies related to 3D scanning of heritage assets and historical areas that due to their large sizes necessitate the use of technologies like aerial drone surveillance for capturing imaging from which 3D models can be produced, preferably with high accuracy. In many cases such models may already exist, acquired earlier by various site, though as it has proven in ARCH in various meetings with pilot cities, the available 3D models do not always cover all areas of interest or accuracy is not sufficient for performing specific types of analysis like predictive simulation of degradations. Therefore, the system developed in SCAN4RECO project has been adapted from dealing with small tangible objects to large city areas and large heritage assets. The system is soon to be fully operational, as reported in section 2. Such a system, even that operating as an autonomous one with respect to THIS and HARIS platforms, offers an ability to end users to perform custom scans with option to upload results directly to THIS. Developed originally with aerial scanning in mind to specifically address the needs of Bratislava to monitor a bedrock under Devin castle, Camerino in assessing post-seismic damages to heritage

assets, the 3D scanning system is also being adapted to underwater scanning thus fitting the specific needs of Hamburg to analyse long term damage caused by varying canal water levels to safety of structures around canals

An important part of the work that has been requested by pilot sites quite late in the project was the collection and processing of Earth Observation data (primarily from Copernicus CAMS and C3S services) for providing climate and pollution data for all ARCH pilot areas required for assessing immediate and long-term risks. In addition, CMLS services have also been integrated into THIS to provide information about land use and land cover in the urban areas. Moreover, EO data - including optical, thermal and radar images from middle to high resolution – were processed to produce specific land use/land cover maps, information on the thermal distribution and the ground level change. These products have been stored in the THIS repository and will be available through the GIS platform. Following different needs expressed by pilot sites regarding selection of parameters and distribution maps, ultimately all available (near) real time parameters are now being acquired from CAMS as well as current and near future forecasts regarding weather conditions, all at global scales.

It is worth pointing out that the demonstrators developed in the framework of the task support a dynamic system, and therefore can be updated even after the drafting of this document, as well as new datasets and information collected in the framework of the ARCH project will be included in the information systems.

7. References

- [1] Artur Krukowski and Emmanouela Vogiatzaki, “*High Resolution 3D Modelling of Cultural Heritage*”, 12th International Conference on non-destructive investigations and microanalysis for the diagnostics and conservation of cultural and environmental heritage (ART’17), Politecnico di Torino, 22-24th of November 2017, Torino, Italy.
- [2] Krukowski, A. and E. Vogiatzaki, “*Aerial Detection of Forest Fires with Automated 3D Fuel Volume Estimation*”, Proceedings of the 6th International Fire Behaviour and Fuels Conference, Marseille (France), 29th of April to 3rd of May 2019 (<http://albuquerque.firebehaviorandfuelsconference.com/conference-proceedings>)
- [3] Krukowski, A. and E. Vogiatzaki, “*Autonomous Aerial Systems in Service of Cultural Heritage Protection from Climate Change Effects*”, International Conference on Cultural Heritage (EUROMED’2020), Cyprus, 2-5th of November 2020 (<http://euromed2020.eu>). Proceedings: <https://www.cut.ac.cy/euromed2020proceedings/projectPapers.html> and https://www.cut.ac.cy/euromed2020proceedings/pdf/Euromed2020_BOOKLET.pdf
- [4] Book: “*Digital Heritage. Progress in Cultural Heritage: Documentation, Preservation, and Protection*”, Springer International Publishing, eBook ISBN: 978-3-030-73043-7, DOI: 10.1007/978-3-030-73043-7, Softcover ISBN: 978-3-030-73042-0, Edition: 1, 2021 (<https://www.springer.com/us/book/9783030730420>).
- [5] Krukowski, A. and E. Vogiatzaki, “*Application of UAS in Forest Firefighting for Detecting Ignitions and 3D Fuel Volume Estimation*”, International Conference on Forest Fire Disaster Management (ICFFDM’2020), Rome (Italy), 10-11th of December 2020 (<https://panel.waset.org/conference/2020/12/rome/ICFFDM>), ZENODO: <https://zenodo.org/record/4291150>, DOI: 10.5281/zenodo.4291150, Open AIRE: https://explore.openaire.eu/search/publication?articleId=od_2659::bcf01959eb668dc1a396defc1b7f371c
- [6] Krukowski, A. and E. Vogiatzaki, “*Protection of Cultural Heritage against the Effects of Climate Change using Autonomous Aerial Systems combined with Automated Decision Support*”, International Conference on Heritage Tourism, Cultural Heritage and Preservation (ICHTCHP’2021), Amsterdam, (The Netherlands), 21-22nd of January 2021 (<https://panel.waset.org/conference/2021/01/amsterdam/ICHTCHP>). Published in the International Journal of Social and Business Sciences of the World Academy of Science, Engineering & Technology, Vol:15, No:1, 2021 (<https://panel.waset.org/abstracts/128755>).
- [7] D’Alessandro, A., Costanzo, A., Ladina, C., Buongiorno, F., Cattaneo, M., Falcone, S., La Piana, C., Marzorati, S., Scudero, S., Vitale, G., Stramondo, S., Doglioni, C. “Urban Seismic Networks, Structural Health and Cultural Heritage Monitoring: The National Earthquakes Observatory (INGV, Italy) Experience”. (2019) *Frontiers in Built Environment*, 5, art. no. 127, . DOI: 10.3389/fbuil.2019.00127.
- [8] D’Alessandro, A., Greco, L., Scudero, S., Siino, M., Vitale, G., D’Anna, R., Di Gangi, F., Nicolosi, D., Passa_ume, G., Speciale, S., et al.: Sviluppo di una stazione sismica low-cost basata su tecnologia mems. *Quaderni di Geofisica* (2019).
- [9] Antonino D’Alessandro, Giovanni Vitale, and Salvatore Scudero MEMS-based system for structural health monitoring and earthquake observation in Sicily”. *European Workshop on Structural Health Monitoring, EWSHM2020*.
- [10] D’Alessandro, A., Vitale, G., Scudero, S., D’Anna, R., Costanza, A., Fagiolini, A., Greco, L.: Characterization of mems accelerometer self-noise by means of psd and allan variance analysis. In: 2017 7th IEEE International workshop on advances in sensors and interfaces (IWASI). pp. 159{164. IEEE (2017).

- [11] D'Alessandro, A., Greco, L., Scudero, S., Siino, M., Vitale, G., D'Anna, R., et al. Sviluppo di una stazione sismica low-cost basata su tecnologiaMEMS. Quaderni di Geofisica 153, 1–60. Available online at: <http://editoria.rm.ingv.it/quaderni/2019/quaderno153/> (2019).
- [12] D'Alessandro, A., Scudero, S., Vitale, G., Di Benedetto, A., Bosco, G.L. "Optimization of Low-Cost Monitoring Systems for On-Site Earthquake Early-Warning of Critical Infrastructures". (2020) Lecture Notes in Computer Science (including subseries Lecture Notes in Artificial Intelligence and Lecture Notes in Bioinformatics), 12250 LNCS, pp. 963-975. DOI: 10.1007/978-3-030-58802-1_69.
- [13] Ahern, T., Casey, R., Barnes, D., Benson, R., Knight, T.: Seed standard for the exchange of earthquake data reference manual format version 2.4. Incorporated Research Institutions for Seismology (IRIS), Seattle (2007).
- [14] Eric S. Raymond gpsmon: real-time GPS packet monitor and control utility - Linux Man Pages (1) (systutorials.com).
- [15] Chad Trabant: Ringserver manual - ringserver - IRIS SeisCode ([washington.edu](http://www.washington.edu)) IRIS Data Management Center (2015).
- [16] D'Alessandro, A., Greco, L., Scudero, S., Siino, M., Vitale, G., D'Anna, R., et al. Sviluppo di una stazione sismica low-cost basata su tecnologiaMEMS. Quaderni di Geofisica 153, 1–60. Available online at: <http://editoria.rm.ingv.it/quaderni/2019/quaderno153/> (2019).
- [17] D'alessandro, A., Greco, L., Scudero, S., Vitale, G., Patanè, D. "Real-time networks for earthquake observation and structural health monitoring in sicily". (2019) Earthquake Geotechnical Engineering for Protection and Development of Environment and Constructions- Proceedings of the 7th International Conference on Earthquake Geotechnical Engineering, 2019, pp. 1919-1926.
- [18] Helmholtz Centre Potsdam GFZ German Research Centre for Geosciences and gempa GmbH (2008). The SeisComP seismological software package. GFZ Data Services. doi:10.5880/GFZ.2.4.2020.003.
- [19] Ferretti, A., Prati, C., Rocca, F., 2001. Permanent scatterers in SAR interferometry. IEEE Transactions on Geoscience and Remote Sensing 39, 8–20. <https://doi.org/10.1109/36.898661>
- [20] Berardino, P., Fornaro, G., Lanari, R., Sansosti, E., 2002. A new algorithm for surface deformation monitoring based on small baseline differential SAR interferograms. IEEE Transactions on Geoscience and Remote Sensing 40, 2375–2383. <https://doi.org/10.1109/TGRS.2002.803792>
- [21] Yamaguchi, Y., Kahle, A. B., Tsu, H., Kawakami, T., & Pniel, M. (1998). Overview of advanced spaceborne thermal emission and reflection radiometer (ASTER). IEEE Transactions on geoscience and remote sensing, 36(4), 1062-1071.
- [22] Kahle, A. B., Palluconi, F. D., Hook, S. J., Realmuto, V. J., & Bothwell, G. (1991). The advanced spaceborne thermal emission and reflectance radiometer (ASTER). International Journal of Imaging Systems and Technology, 3(2), 144-156.
- [23] Roy, D. P., Wulder, M. A., Loveland, T. R., Woodcock, C. E., Allen, R. G., Anderson, M. C., ... & Scambos, T. A. (2014). Landsat-8: Science and product vision for terrestrial global change research. Remote sensing of Environment, 145, 154-172.
- [24] Landsat 8. Available online <https://landsat.gsfc.nasa.gov/landsat-8/> (accessed on 29 April 2021)
- [25] Fisher, J. B., Hook, S., Allen, R., Anderson, M. C., French, A. N., Hain, C., ... & Wood, E. F. (2015, December). ECOSTRESS: NASA's next-generation mission to measure evapotranspiration from the International Space Station. In AGU Fall Meeting Abstracts; AGU: Washington, DC, USA.

- [26] Qin, Z.; Karnieli, A.; Berliner, P. A mono-window algorithm for retrieving land surface temperature from Landsat TM data and its application to the Israel-Egypt border region. *Int. J. Remote Sens.* 2001, 22, 3719–3746.
- [27] Sun, D.; Pinker, R.T. Estimation of land surface temperature from a Geostationary Operational Environmental Satellite (GOES-8). *J. Geophys. Res. Atmos.* 2003, 108
- [28] Sun, D.; Pinker, R.T. Retrieval of surface temperature from the MSG-SEVIRI observations: Part I. Methodology. *Int. J. Remote Sens.* 2007, 28, 5255–5272.
- [29] Yamamoto, Y.; Ishikawa, H.; Oku, Y.; Hu, Z. An Algorithm for Land Surface Temperature Retrieval Using Three Thermal Infrared Bands of Himawari-8. *J. Meteorol. Soc. Jpn. Ser. II* 2018, 96, 59–76.
- [30] Sobrino, J.A.; Caselles, V.; Coll, C. Theoretical split-window algorithms for determining the actual surface temperature. *Il Nuovo Cim. C* 1993, 16, 219–236.
- [31] Gillespie, A., Rokugawa, S., Matsunaga, T., Cothorn, J. S., Hook, S., & Kahle, A. B. (1998). A temperature and emissivity separation algorithm for advanced spaceborne thermal emission and reflection radiometer (ASTER) images. *IEEE Transactions on Geoscience and Remote Sensing*, 36(4), 1113-1126.
- [32] USGS. Landsat 8 OLI and TIRS Calibration Notices. Available online: <https://www.usgs.gov/land-resources/nli/landsat/landsat-8-oli-and-tirs-calibration-notices> (accessed on 24 July 2020).
- [33] Fauvel, M., Chanussot, J., & Benediktsson, J.A. (2006, May). Evaluation of kernels for multiclass classification of hyperspectral remote sensing data. In *ICASSP 2006, Proceedings of the IEEE International Conference on Acoustics, Speech and Signal Processing*, 14–19 May 2006, Toulouse, France. IEEE, New York. Vol. 2, pp. 813–816
- [34] Fernández, F., Montávez, J. P., González-Rouco, J. F., & Valero, F. (2003, September). A PCA Analysis of the UHI Form of Madrid. In *Proceedings of Fifth International Conference on Urban Climate* (pp. 1-5).
- [35] Ruiz, M. A., Sosa, M. B., Cantaloube, E. N. C., & Cantón, M. A. (2015). Suitable configurations for forested urban canyons to mitigate the UHI in the city of Mendoza, Argentina. *Urban Climate*, 14, 197-212.
- [36] Müller, B., Bernhardt, M., & Schulz, K. (2014). Identification of catchment functional units by time series of thermal remote sensing images. *Hydrology and Earth System Sciences*, 18(12), 5345-5359.
- [37] Huang, C., L.S. Davis, J.R.G. Townshend, 2002. An assessment of support vector machines for land cover classification. *International Journal of Remote Sensing*, 23; 725–749 Pal, M., & Mather, P. (2005). Support vector machines for classification in remote sensing. *International Journal of Remote Sensing*, 26, 1007–1011.
- [38] Petropoulos, G., W. Knorr, M. Scholze, L. Boschetti, G. Karantounias, 2010. Combining ASTER multispectral imagery analysis and support vector machines for rapid and cost-effective post-fire assessment: a case study from the Greek wildland fires of 2007. *Natural Hazards Earth System Sciences*, 10; 305–317.
- [39] Petropoulos GP, Vadrevu KP, Xanthopoulos G, Karantounias G, Scholze M (2010) A comparison of spectral angle mapper and artificial neural network classifiers combined with Landsat TM imagery analysis for obtaining burnt area mapping. *Sensors* 10(3):1967–1985
- [40] Kuemmerle, T., Chaskovskyy, O., Knorn, J., Radeloff, V.C., & Kruhlov, I. (2009). Forest cover change and illegal logging in the Ukrainian Carpathians in the transition period from 1988 to 2007. *Remote Sensing of Environment*, 113, 1194–1207.
- [41] Pal M., Mather P.M. (2005) Support vector machines for classification in remote sensing *International Journal of Remote Sensing* Vol. 26, No. 5, 10 March 2005, 1007–1011.

- [42] Shafaei, Jalil & Hosseini, Abdollah & Marefat, Mohammd & Khanmohammadi, Mohammad. (2013). Seismic retrofitting of non-seismic detailing external RC beam-column joints by joint enlargement using steel angles. 10.13140/2.1.5026.8169.
- [43] Izzet Kale, Richard C.S. Morling and Artur Krukowski, "A high-fidelity decimator chip for the measurement of Sigma - Delta modulator performance", IEEE Transactions on Instrumentation and Measurement, Vol. 44, No. 5, October 1995.
- [44] Chang, P.C., Flatau, A., Liu, S.C., 2003. Review Paper: Health Monitoring of Civil Infrastructure. Structural Health Monitoring; 2(3): p. 257–267.
- [45] ICOMOS/ISCARSAH 2005. Recommendations for the Analysis, Conservation and Structural Restoration of Architectural Heritage.
- [46] De Stefano, A., Matta, E., Clemente, P., 2016. Structural health monitoring of historical heritage in Italy: some relevant experiences. J Civil Struct Health Monit 6, 83–106.
- [47] Housner, G.W., Bergman, L.A., Caughey, T.K., Chassiakos, A.G., Claus, R.O., Masri, S.F., Skelton, R.E., Soong, T.T., Spencer, B.F., Yao, J.T.P., 1997. Structural Control: Past, Present, and Future. Journal of Engineering Mechanics 123, 897–971.
- [48] Farrar, C.R., Worden, K., 2007. An introduction to structural health monitoring. Phil. Trans. R. Soc. A. 365, 303–315.
- [49] Deraemaeker, A., Worden, K., 2010. New trends in vibration based structural health monitoring, Courses and lectures / International Centre for Mechanical Sciences. Springer, Wien New York.
- [50] Bisby, L.A., 2006, ISIS Canada Educational Module No. 5: An Introduction to Structural Health Monitoring, ISIS Canada, www.isiscanada.com.
- [51] Das, S., Saha, P., Patro, S., 2016. Vibration-based damage detection techniques used for health monitoring of structures: a review. Journal of Civil Structural Health Monitoring, vol. 6, no. 3, p. 477–507.
- [52] Bandara, R.P., Chan, T.H., Thambiratnam D.P., 2014. Structural damage detection method using
- [53] Moradipour, P., Chan, T.H., Gallage, C., 2015. An improved modal strain energy method for structural damage. Structural Engineering and Mechanics, vol. 54, no. 1, pp. 105-119.
- [54] Zona, A., 2020. Vision-Based Vibration Monitoring of Structures and Infrastructures: An Overview of Recent Applications. Infrastructures 6, 4. <https://doi.org/10.3390/infrastructures6010004>
- [55] Glisic, B., Inaudi, D., 2007. Fibre Optic Methods for Structural Health Monitoring, John Wiley & Sons, Inc., Chichester, UK (ISBN: 978-0-470-06142-8), 2007 (Europe) / 2008 (USA).
- [56] Glisic, B., D. Inaudi, D., Posenato, A., Figini., 2007. Monitoring of heritage structures and historical monuments using long-gage fiber optic interferometric sensors – an overview. The 3rd International Conference on Structural Health Monitoring of Intelligent Infrastructure Vancouver, British Columbia, Canada November 13-16, 2007.
- [57] Farrar, C.R., Worden, K., 2013. Structural Health Monitoring, A Machine Learning Perspective, Wiley.
- [58] Diez, A., Khoa, N.L.D., Alamdari, M.M., Wang, Y., Chen, F., 2016. A clustering approach for structural health monitoring on bridges. Journal of Civil Structural Health Monitoring, pp. 1-17.
- [59] Zhou, Q., Zhou, H., Zhou, Q., Yang, F., Luo, L., Li, T., 2015. Structural damage detection based on posteriori probability support vector machine and Dempster–Shafer evidence theory. Applied Soft Computing, vol. 36, p. 368–374.

- [60] Santos, J.P., Cremona, C., Orcesi, A.D., Silveira, P., Calado, L., 2014. Static-based early-damage detection using symbolic data analysis and unsupervised learning methods. *Frontiers of Structural and Civil Engineering*, vol. 9, no. 1, pp. 1-16.
- [61] Zheng, W., Shen, J., 2015. Adjustable hybrid resampling approach to computationally efficient probabilistic inference of structural damage based on vibration measurements. *Journal of Civil Structural Health Monitoring*, vol. 6, no. 1, pp. 153-173.
- [62] Rao, A.R.M., Lakshmi, K., 2015. Damage diagnostic technique combining POD with timefrequency analysis and dynamic quantum PSO. *Meccanica*, vol. 50, no. 6, pp. 1551-1578.
- [63] Alamdari, M.M., Samali B., Li, J., 2015. Damage localization based on symbolic time series analysis," *Structural Control and Health Monitoring*, vol. 22, no. 2, pp. 374-393.
- [64] Cucci, C., 2009. Sensori di impatto per l'ambiente museale. IFAC-TSRR-TR-07-3-009 (64-7)
- [65] Despotaki, V., Silva, V., Lagomarsino, S., Pavlova, I., Torres, J., 2018. Evaluation of Seismic Risk on UNESCO Cultural Heritage sites in Europe. *International Journal of Architectural Heritage*, 12, 1231–1244.
- [66] Canuti, C., Carbonari, S., Dall'Asta, A., Dezi, L., Gara, F., Leoni, G., Morici, M., Petrucci, E., Prota, A., Zona, A., 2019. Post-Earthquake Damage and Vulnerability Assessment of Churches in the Marche Region Struck by the 2016 Central Italy Seismic Sequence. *International Journal of Architectural Heritage* 1–22.
- [67] Dall'Asta A., Leoni G., Meschini A., Petrucci E., Zona A., 2019. Integrated approach for seismic vulnerability analysis of historic massive defensive structures. *Journal of Cultural Heritage*, 35(1):86-98. DOI: 10.1016/j.culher.2018.07.004
- [68] Wriggers, P., 2008. *Nonlinear finite element methods*. Springer, Berlin.
- [69] Aras, F., Krstevska, L., Tashkov L., 2011. Experimental and numerical modal analyses of a historical masonry palace. *Constr Build Mater*, 25(1): 81-91.
- [70] Benedetti, D., Gentile, C., 1994. Identification of modal quantities from two earthquake responses. *Earthquake Eng Struct Dynam*, 23(4): 447-462.
- [71] Gentile, C., Ruccolo, A., Canali, F., 2019. Continuous monitoring of the Milan Cathedral: dynamic characteristics and vibration-based SHM. *Journal of Civil Structural Health Monitoring*, 9(5), 671-688.
- [72] Brincker, R., Ventura, C., 2015. *Introduction to operational modal analysis*. John Wiley & Sons.
- [73] Peeters B., De Roeck, G., 1999. Reference-based stochastic subspace identification for output-only modal analysis. *Mechanical systems and signal processing*, 13(6), 855-878.
- [74] Bitter, R., Mohiuddin, T., & Nawrocki, M. (2006). *LabVIEW: Advanced programming techniques*. Crc Press.
- [75] *MATLAB and Signal Processing Toolbox Release 2020b*, The MathWorks, Inc., Natick, Massachusetts, United States.

8. Annex

8.1. Installation report of the accelerometric stations of the RUSN

In this annex the installation detail is reported after the deployment of the MEMS accelerometric stations.

The following characteristics are indicated:

- network identification code;
- station name;
- code of the channels;
- location (latitude and longitude);
- Roll (cf. Figure 80);
- Pitch (cf. Figure 80);
- Yaw (cf. Figure 80).

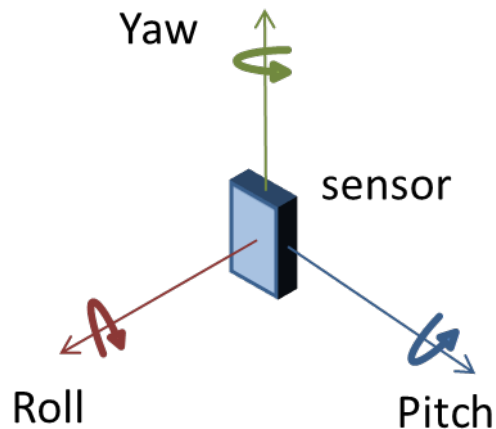


Figure 80: Rotation of the sensor in three dimensions

In addition, the report sheet includes the map with the position of the station superimposed on the local geological setting and two pictures of the installation.

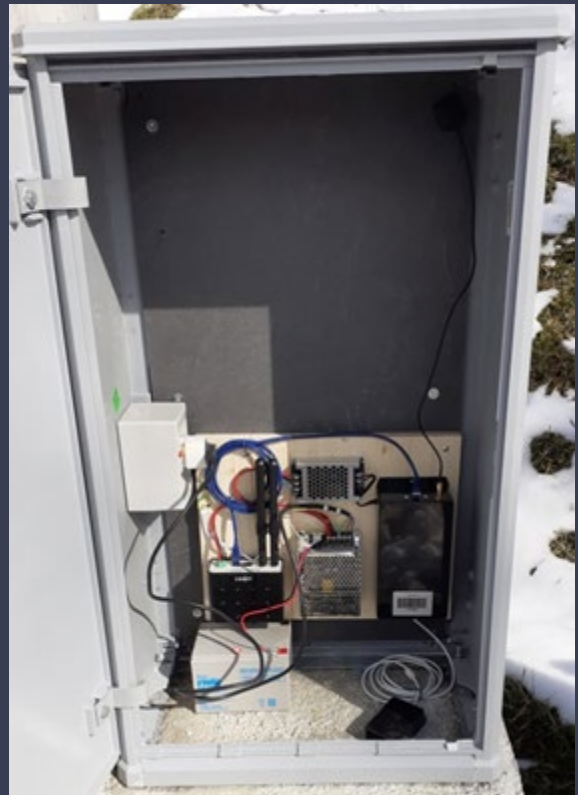
8.1.1. Accelerometric station CAM00

Network	Name	Channels	Lat.	Long.	Roll	Pitch	Yaw
XX	CAM00	HNN/E/Z	43.131421	13.057169	0	0	180

The screenshot shows the ARCH website interface for the Camerino site. The main map displays geological data overlaid on an aerial view. The legend on the left includes categories such as Geology (Soil with debris of anthropogenic activity, Silty gravels, gravel mixture, etc.) and Administrative Borders (Camerino). Three station locations are marked: CAM00 (red dot), CAM04 (red triangle), and CAM08 (red triangle). The footer of the website includes logos for ARCH, INGV, and the European Union, along with a copyright notice for 2020-2021 INGV.

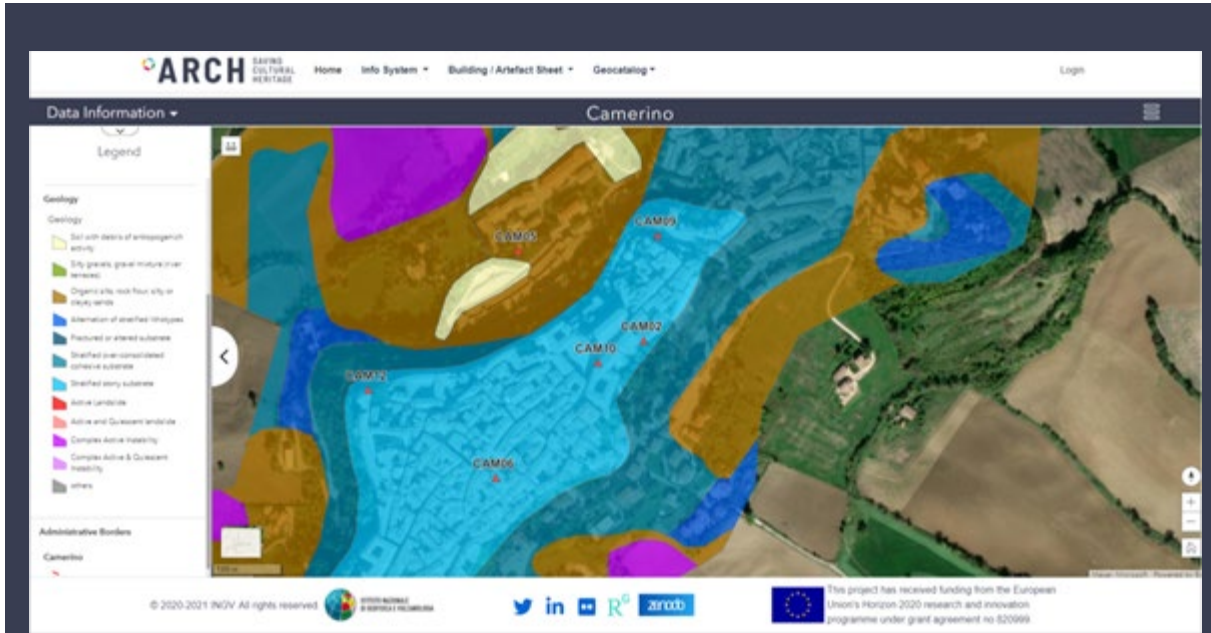
8.1.2. Accelerometric station CAM01

Network	Name	Channels	Lat.	Long.	Roll	Pitch	Yaw
XX	CAM01	HNN/E/Z	43.127175	13.068692	0	0	180



8.1.3. Accelerometric station CAM02

Network	Name	Channels	Lat.	Long.	Roll	Pitch	Yaw
XX	CAM02	HNN/E/Z	43.135997	13.069378	0	0	180



8.1.4. Accelerometric station CAM03

Network	Name	Channels	Lat.	Long.	Roll	Pitch	Yaw
XX	CAM03	HNN/E/Z	43.138821	13.072184	0	0	180



8.1.5. Accelerometric station CAM04

Network	Name	Channels	Latitude	Longitude	Roll	Pitch	Yaw
XX	CAM04	HNN/E/Z	43.132593	13.065209	0	0	180



8.1.6. Accelerometric station CAM05

Network	Name	Channels	Lat.	Long.	Roll	Pitch	Yaw
XX	CAM05	HNN/E/Z	43.137144	13.067184	0	0	180



8.1.7. Accelerometric station CAM06

Network	Name	Channels	Lat.	Long.	Roll	Pitch	Yaw
XX	CAM06	HNN/E/Z	43.134250	13.066801	0	0	180



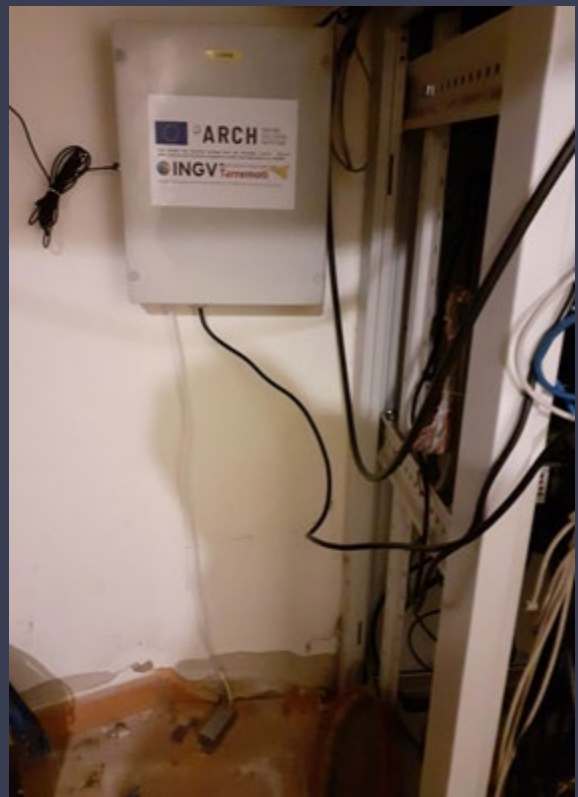
8.1.8. Accelerometric station CAM07

Network	Name	Channels	Lat.	Long.	Roll	Pitch	Yaw
XX	CAM07	HNN/E/Z	43.146846	13.063849	0	0	180



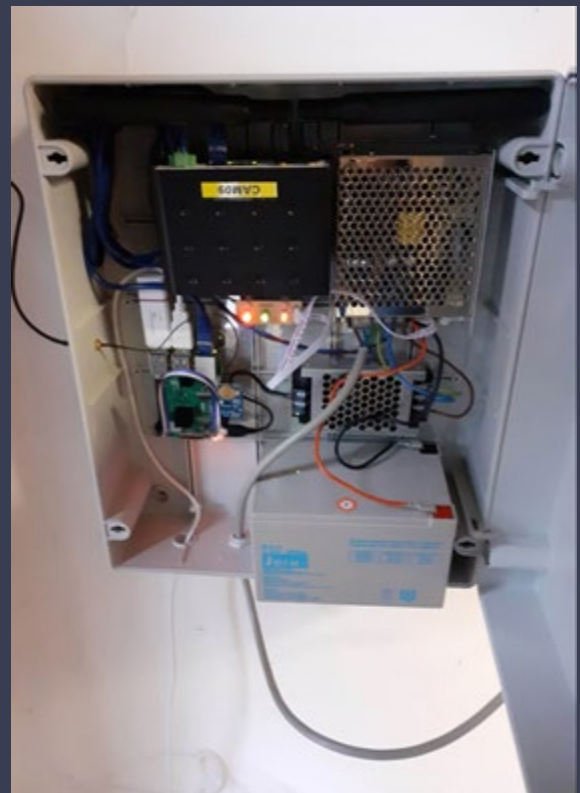
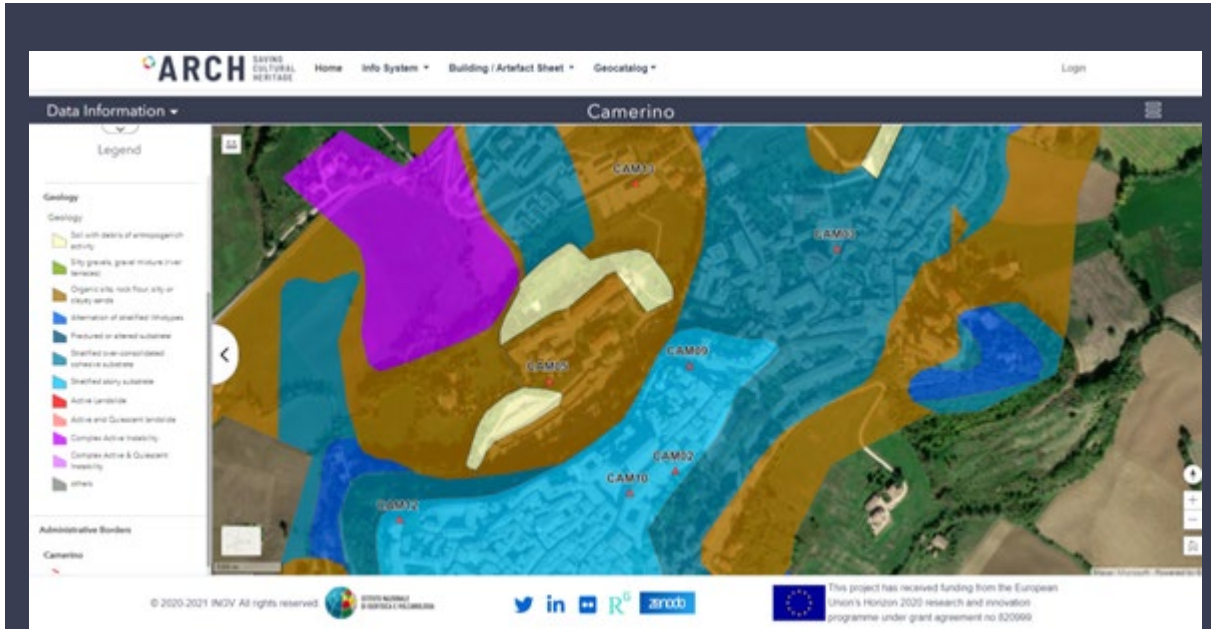
8.1.9. Accelerometric station CAM08

Network	Name	Channels	Lat.	Long.	Roll	Pitch	Yaw
XX	CAM08	HNN/E/Z	43.132157	13.064066	0	0	180



8.1.10. Accelerometric station CAM09

Network	Name	Channels	Lat.	Long.	Roll	Pitch	Yaw
XX	CAM09	HNN/E/Z	43.137334	13.069624	0	0	180



8.1.11. Accelerometric station CAM10

Network	Name	Channels	Lat.	Long.	Roll	Pitch	Yaw
XX	CAM10	HNN/E/Z	43.135718	13.068584	0	0	180



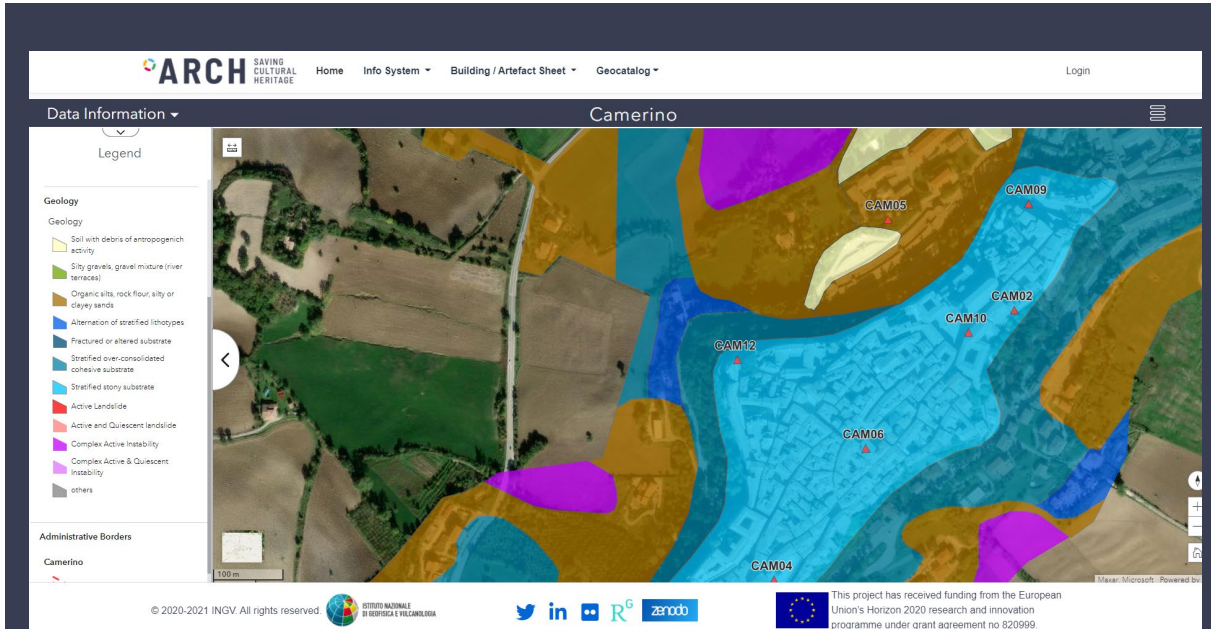
8.1.12. Accelerometric station CAM11

Network	Name	Channels	Lat.	Long.	Roll	Pitch	Yaw
XX	CAM11	HNN/E/Z	43.144749	13.08285	0	0	180



8.1.13. Accelerometric station CAM12

Network	Name	Channels	Lat.	Long.	Roll	Pitch	Yaw
XX	CAM12	HNN/E/Z	43.135557	13.064632	0	0	180



8.1.14. Accelerometric station CAM13

Network	Name	Channels	Lat.	Long.	Roll	Pitch	Yaw
XX	CAM13	HNN/E/Z	43.139657	13.068688	-44	85	54

